Unconfined Compression Tests on Basalt Rocks from Hawaii

A THESIS SUBMITTED TO THE GRADUATE DIVISION OF THE UNIVERSITY OF HAWAII AT MANOA IN PARTIAL FULFILLMENT OF THE REQUIREMENTS FOR THE DEGREE OF

MASTER OF SCIENCE

IN

CIVIL ENGINEERING

March 31, 2016

Prepared by:

Miles Toshimi Yamada

Thesis Committee:

Horst Brandes, Chairperson

Phillip Ooi

Gaur Johnson

ACKNOWLEDGEMENTS

The author would like to thank Dr. Horst Brandes, Dr. Philip Ooi, and Dr. Gaur Johnson for reviewing this thesis. Dr. Brandes advised and helped the author throughout his research and in preparation of this thesis. The author also acknowledges Dr. Adrian Archilla for his permission to use his CoreLok machine and weight scales as well as providing instructions on how to use it. Dr. Ian Robertson gave permission and instruction on use of the loading frames, extensometer, and computer software, and also provided advice throughout the testing. Dr. Johnson also helped with the testing and interpretation of results. Mitchell Pinkerton assisted with sawing and preparing the rock samples for testing. Lastly, the author acknowledges Shinsato Engineering, Inc. for performing the boring.

ABSTRACT

Unconfined compression tests were performed on 66 basalt samples to obtain index properties and elastic constants. The samples were obtained from a boring drilled at the University of Hawaii at Manoa. These values were compared to results obtained from other studies to determine correlations and observe vertical trends at the site. Properties obtained from nondestructive tests on the basalt rocks included unit weight (oven-dried, saturated-surface-dry, and apparent), unit weight through the use of a CoreLok machine, absorption, RQD, and percent recovered. Properties obtained from compression tests included unconfined compressive strength, Young's Modulus, axial strain at failure or at 50% of ultimate load, failure type, and failure plane angle to horizontal.

The results indicate that there appears to be two different layers of rock at the location of the boring. There is an upper layer of rock characterized by lower unit weights, higher absorption and lower strength and stiffness, compared to the lower layer of rock. This points to significantly different rock types, probably from different lava flows with somewhat different original magma composition and viscosity. It is worth noting that RQD, percent recovery and axial strain do not show discernible distinctions between these two rock units and thus appear to be less useful as indicators of distinct rock units, at least as encountered at the site.

Strong correlations were observed between absorption and unit weight, as expected. Strong correlations were also noted between the various unit weights and the results of the unconfined compression tests. In particular, there are reasonably strong correlations between index properties in terms of unit weight and absorption, and test results in terms of unconfined compression strength and stiffness. No discernible correspondence was observed between field parameters in terms of RQD, percent recovery or axial strain versus index parameters and strength test results.

Table of Contents

ACKNOWLEDGEMENTS i
ABSTRACT ii
1. BACKGROUND 1
1.1 Geology and Project Site 1
1.2 Types of Rock Strength Tests 10
1.3 Reported Rock Strength Parameters 12
2. TEST PROGRAM AND METHOD 17
2.1 Introduction 17
2.2 Tolerance Checks 18
2.3 Unit Weights and Sulfur Caps 20
2.4 Strength Testing 24
3. TEST RESULTS AND DISCUSSION 29
3.1 Unit Weights and Strengths 29
3.2 Trends with Depth 37
3.3 Correlations among Parameters 50
3.3.1 Absorption 50
3.3.2 Unconfined Compressive Strength 53
3.3.3 Young's Modulus 56
3.3.4 RQD, Percent Recovery, Axial Strain at Failure and Axial Strain at 50% Strength 60
3.4 Failure Patterns 60
4. CONCLUSIONS 66
5. REFERENCES 68
APPENDIX 72

List of Figures

Figure 1: Honolulu Volcanic Series Lava Flows at Project Site (Macdonald 1983) 4
Figure 2: Project Site 5
Figure 3: Boring B4 Log 6
Figure 4: Straightness Tolerance Check 19
Figure 5: Flatness Tolerance Check 19
Figure 6: Perpendicularity Tolerance Check 20
Figure 7: CoreLok Machine 22
Figure 8: Sulfur Cap Block 23
Figure 9: Sample with Sulfur Caps 23
Figure 10: Screenshot of Station Manager Software used on 50-kip Test Frame 26
Figure 11: 50-kip Test Frame 26
Figure 12: User Interface of 50-kip Test Frame 27
Figure 13: 300-kip Test Frame 27
Figure 14: 300-kip Test Frame Readings 28
Figure 15: User Interface for 300-kip Test Frame 28
Figure 16: Example of shatter-type failure mode (STF) 29
Figure 17: Example of multiple fracture failure mode (MFF) 30
Figure 18: Example of dominant plane failure mode (DPF) 30
Figure 19: Oven-Dried Unit Weight versus Depth 39
Figure 20: Saturated-Surface-Dry Unit Weight versus Depth 40
Figure 21: Apparent Unit Weight versus Depth 41
Figure 22: CoreLok Unit Weight versus Depth 42
Figure 23: Absorption versus Depth 43
Figure 24: Unconfined Compressive Strength versus Depth 44
Figure 25: Young's Modulus versus Depth 45
Figure 26: Axial Strain at 50% Strength versus Depth 46
Figure 27: Axial Strain at Failure versus Depth 47
Figure 28: RQD versus Depth 48
Figure 29: Percent Recovered versus Depth 49
Figure 30: Oven-Dried Unit Weight versus Absorption 51
Figure 31: Saturated-Surface-Dry Unit Weight versus Absorption 51
Figure 32: Apparent Unit Weight versus Absorption 52
Figure 33: CoreLok Unit Weight versus Absorption 52
Figure 34: Oven-Dried Unit Weight versus Unconfined Compressive Strength 54
Figure 35: Saturated-Surface-Dry Unit Weight versus Unconfined Compressive Strength 54
Figure 36: Apparent Unit Weight versus Unconfined Compressive Strength 55
Figure 37: CoreLok Unit Weight versus Unconfined Compressive Strength 55
Figure 38: Absorption versus Unconfined Compressive Strength 56

Figure 39: Oven-Dried Unit Weight versus Young's Modulus 57
Figure 40: Saturated-Surface-Dry Unit Weight versus Young's Modulus 57
Figure 41: Apparent Unit Weight versus Young's Modulus..... 58
Figure 42: CoreLok Unit Weight versus Young's Modulus 58
Figure 43: Absorption versus Young's Modulus 59
Figure 44: Unconfined Compressive Strength versus Young's Modulus 59
Figure 45: Failure Type versus Oven-Dried Unit Weight 61
Figure 46: Failure Type versus Saturated-Surface-Dry Unit Weight 62
Figure 47: Failure Type versus Apparent Unit Weight 62
Figure 48: Failure Type versus CoreLok Unit Weight 63
Figure 49: Failure Type versus Absorption 63
Figure 50: Failure Type versus Unconfined Compressive Strength 64
Figure 51: Failure Type versus Young's Modulus 64
Figure 52: Failure Type versus Depth 65

List of Tables

Table 1: Light-Colored Igneous Rocks (Macdonald 1983) 2
Table 2: Dark-Colored Igneous Rocks (Macdonald 1983) 3
Table 3: List of Rock Mass Rating Systems (Edelbro 2004) 11
Table 4: Rock Strengths Reported in the Literature 16
Table 5: Rock Core Samples 17
Table 6: Number of Strength Tests 18
Table 7: Apparent Gravity of Small CoreLok Bags 24
Table 8: Physical Properties of Test Specimens 31
Table 9: CoreLok Calculations 33
Table 10: Strength and Stiffness Parameters of Basalt Samples 35

1. BACKGROUND

The strength of rocks varies even within rocks of the same classification. For example, all rocks classified as basalt do not necessarily have the same compressive strength. Tests have been performed on various rock types from various locations around the world and correlations have been derived between index parameters and strength parameters. However, little data is available on the strength of rocks from Hawaii. Due to unique processes of formation and weathering under tropical conditions, Hawaiian rocks may well behave differently.

In this study, unconfined compression tests were performed on basalt rocks from Hawaii. This thesis aims to provide characterization of local basalt type that is currently unavailable but necessary for many engineering projects.

1.1 Geology and Project Site

The Hawaiian Islands are located in the middle of the Pacific tectonic plate. A hot spot lies underneath the island of Hawaii and the plate slowly moves northwest. This hot spot creates magma and fuels the volcanoes on the island of Hawaii, also known as the "Big Island". The volcanoes on the other islands in the archipelago are believed to be either dormant or extinct.

Lava seen in Hawaii are labeled as one of two types; pahoehoe or a'a. Pahoehoe is smooth, billowy and ropy, while a'a is rough, spiny and rubbly. Lava flows are more likely to erupt from the volcanoes as pahoehoe and can change into a'a downslope. The more viscous the lava is, the more likely it will change into a'a as it flows downslope. However, a'a will never change into pahoehoe. (Stearns, 1965).

One characteristic of Hawaiian volcanic activity that differs from eruptions typically seen anywhere else is exactly how the lava erupts and flows. Hawaiian lava flows are generally very smooth and not explosive compared to eruptions in other parts of the world. These smooth lava flows will layer on top of previous lava flows. Eventually these lava flows will form shield volcanoes, named as such because their appearance in plan view is similar to a shield. In contrast, most other volcanoes around the world are composite volcanoes, as they are comprised of interbedded lava flows and layers of pyroclastic material formed by explosive eruptions of viscous magma with high amounts of silica (Macdonald et al., 1983). Composite volcanoes are conical in shape.

The lava flows in Hawaii are smooth because the magma has low viscosity, which is controlled by its chemical composition, temperature, and amount of gas. In low viscosity magma, the gas in the volcano can escape relatively easily. In high viscosity magma, the gases get trapped underneath the magma until they build up to a high pressure which will cause the magma to

explode out of the volcano. Viscosity in magma increases with increasing silica content, decreasing temperature, and decreasing gas content.

Basalt is an igneous rock composed almost wholly of calcic plagioclase feldspar and pyroxene (Macdonald et al, 1983). It is one of many types of igneous rocks, which are usually classified according to Table 1. They are fine grained and usually dark colored. In Hawaii, there are two general types of basalt; tholeiite, sometimes known as tholeiitic basalt, and alkalic basalt. They are differentiated by the amount of silica and alkali present and by the content of pyroxene in the basalt. Tholeittic basalt has a relatively high silica content and lower alkalies content, and the pyroxene is largely pigeonite containing little calcium or aluminum. Alkalic basalt has little silica and contains more alkalies, and the pyroxene is largely augite containing calcium and aluminum. Both types of basalt usually contain olivine and may contain phenocrysts of plagioclase feldspar or pyroxene. Tables 1 and 2 describe various types of igneous rocks (Macdonald et al., 1983).

Basalt rocks in Hawaii are greatly affected by weathering. Weathering can be mechanical or chemical. Mechanical weathering occurs when a rock is broken into smaller pieces without change in its chemical or mineral composition. Chemical weathering is when the chemical or mineral composition in a rock changes and the rock breaks down into soil. The two forms of weathering are often seen together since significant chemical weathering does not normally take place without mechanical weathering. Hawaiian rocks endure significant chemical weathering since the islands are located in the tropical zone (Stearns, 1965).

Table 1: Light-Colored Igneous Rocks (Macdonald 1983)

	Potassium feldspar dominant			Plagioclase feldspar dominant	
	Quartz present	Quartz and nepheline absent	Nepheline present	Quartz present	Quartz and nepheline absent
Fine-grained	Rhyolite	Trachyte	Phonolite	Dacite Rhyodacite	Andesite Hawaiite Icelandite Mugearite
Coarse-grained	Granite	Syenite	Nepheline syenite	Quartz diorite Granodiorite	Diorite

Table 2: Dark-Colored Igneous Rocks (Macdonald 1983)

	Plagioclase feldspar dominant	Feldspar essentially absent	
	Quartz and nepheline absent	Nepheline present	Quartz and nepheline absent
Fine-grained	Tholeiitic basalt Alkalic basalt Olivine basalt Oceanite Ankaramite Basanite	Nephelinite	-
Coarse-grained	Gabbro	-	Peridotite Dunite

The island of Oahu was formed by two major volcanoes; the Waianae volcano on the west and the Koolau volcano on the east. These volcanoes are referred to as ranges due to the fact that erosion and landslides have turned these shield volcanoes into long, narrow ridges. The Waianae volcano became active around 3 million years ago and remained so for about half a million years before becoming dormant. The Koolau volcano became active around the time the Waianae volcano became dormant and then became dormant itself about half a million years later.

A new period of volcanic activity began hundreds of thousands of years ago in the southeastern end of the Koolau range. These series of eruptions are known as the Honolulu Volcanic Series. The lava flows from these eruptions were notably different in composition compared to the older rocks as these eruptions contained cinder, spatter, and ash. These recent eruptions created distinct landmarks such as Diamond Head, Koko Head, Hanauma Bay, Punchbowl, Tantalus, and Salt Lake. It is believed that the Waianae volcano also had eruptions after it was assumed to be dormant, but they were fewer in number compared to the Koolau volcano and occurred earlier.

More than 30 eruptions were part of the Honolulu Volcanic Series. Figure 1 shows the Sugarloaf eruption, which occurred approximately 67,000 years ago. The a'a lava flow was roughly 12 meters thick and traveled down Manoa Valley and over the land of area now occupied by the University of Hawaii at Manoa. Most of the lava flow ended north of Lunalilo freeway but a narrow path continued half a kilometer through Moiliili. The old Moiliili Quarry was excavated in the center of the lava flow and the rock in the quarry walls was coarse grained and contained veinlets of pegmatoid. The openings are generally lined with crystals of nepheline, augite, apatite, and zeolite. Macdonald (1983) determined that the lava was rich in gas.

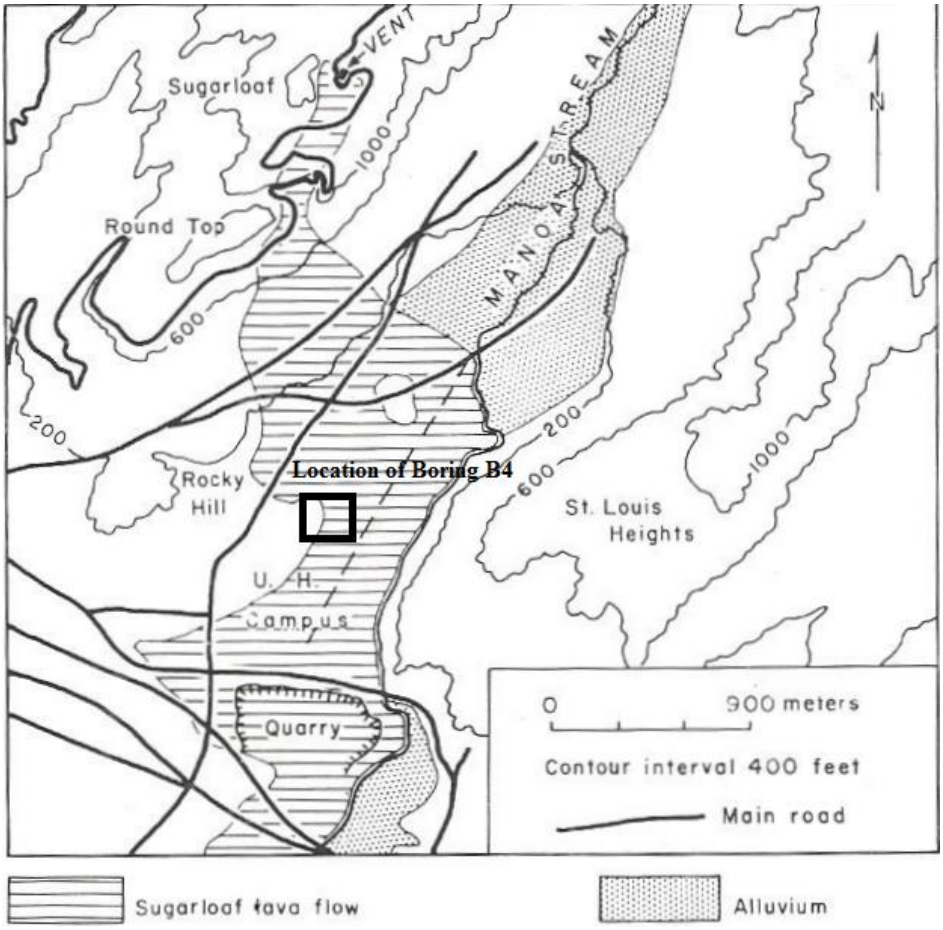

Figure 1: Honolulu Volcanic Series Lava Flows at Project Site (Macdonald 1983)

Rock coring requires a rotary drilling machine, drill rods, cutting bit, and core barrel. The core barrel is rotated using the drill rig while water is circulated through the hole. Generally the initial core runs when rock is encountered are short because the rock layer could be soft and fractured. If the rock is strong the core runs become longer. The core barrel's spin rate depends on the bit diameter and rock quality; high speeds are used for hard rocks while slow speeds are used in soft or highly fractured rocks. The bit pressure and the type of coring bit used also depend on the rock quality, with higher pressures and stronger bits required for strong rocks. Water is also necessary to return the cuttings to the surface to avoid erosion of borehole walls and to avoid overheating the bit. (Hunt, 2005).

Core barrels range between 2 feet and 20 feet long, but 5 feet and 10 feet are the most common. The barrel used is based on the rock quality and the amount of rock required. The core is retrieved from the barrel and laid in wooden boxes exactly as recovered. The core runs are divided by wooden spacers and the depths are recorded.

Two variables recorded for a rock coring are percent recovered and rock quality designation (RQD). RQD is calculated by summing the length of core recovered that are at least 4 inches in length divided by the length of the core run. RQD requires that the core is at least 50 mm in diameter. Percent recovered is calculated as the total length recovered divided by the length of the core run.

Rock samples for the study were collected from a soil and rock boring conducted adjacent to Hawaii Hall on the University of Hawaii at Manoa campus (Figures 1 and 2). This boring was part of a larger project throughout the university. The drilling included a split-barrel sampler and thin-walled undisturbed sampler for soils. When rock was encountered, a rock corer was used instead. The boring log (Figure 3) indicates that the soil in front of Hawaii Hall had brown silt topsoil to a depth of 3 feet, underlain by dark gray gravel and sand to a depth of 5 feet. Underlain by that layer is olive gray clay to a depth of 10 feet, then a layer of fractured cinder gravel and sand to a depth of 17.5 ft. After that, sampling recovered dark gray basalt, essentially unweathered but with varying degrees of fracturing. The boring was terminated at a depth of 95 feet. Pictures of the rock cores were taken before they were cut and prepared. The core barrel had an inside diameter of 2.5 inches. The RQD was recorded during sampling.

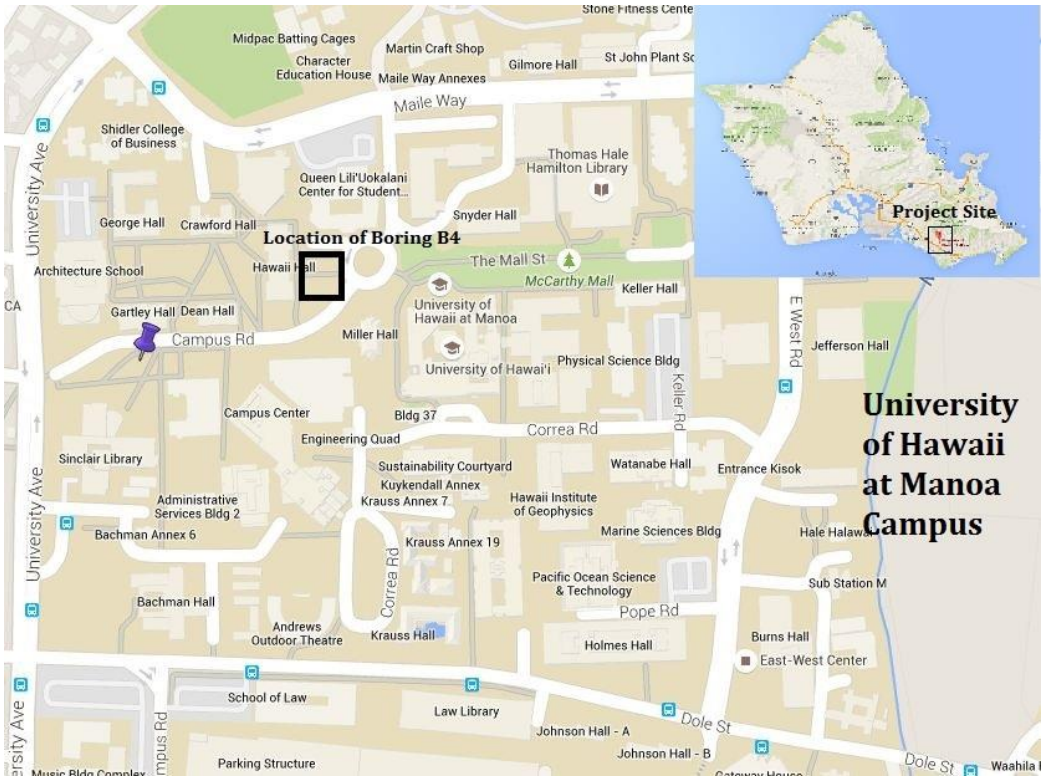

Figure 2: Project Site

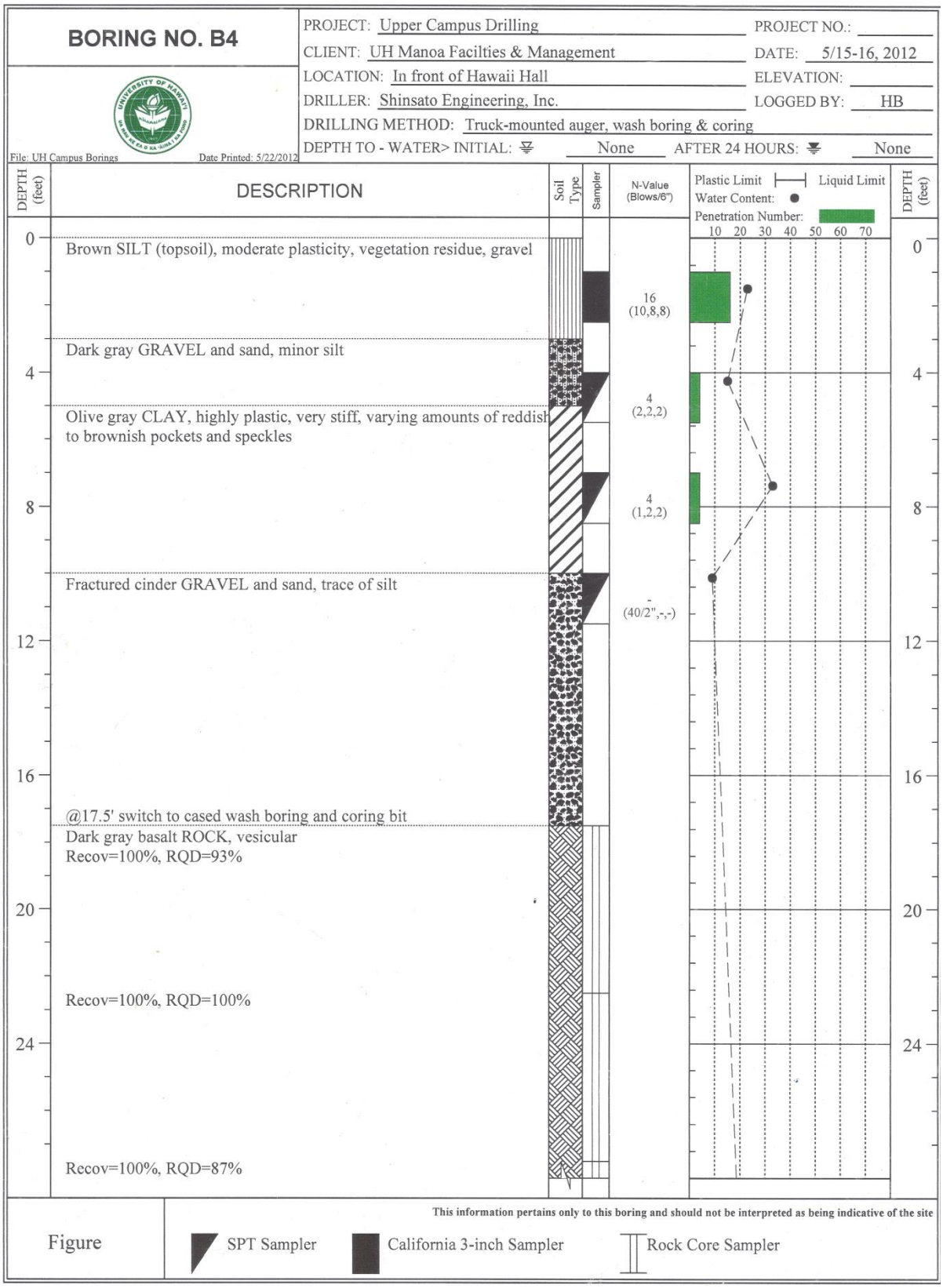

Figure 3: Boring B4 Log

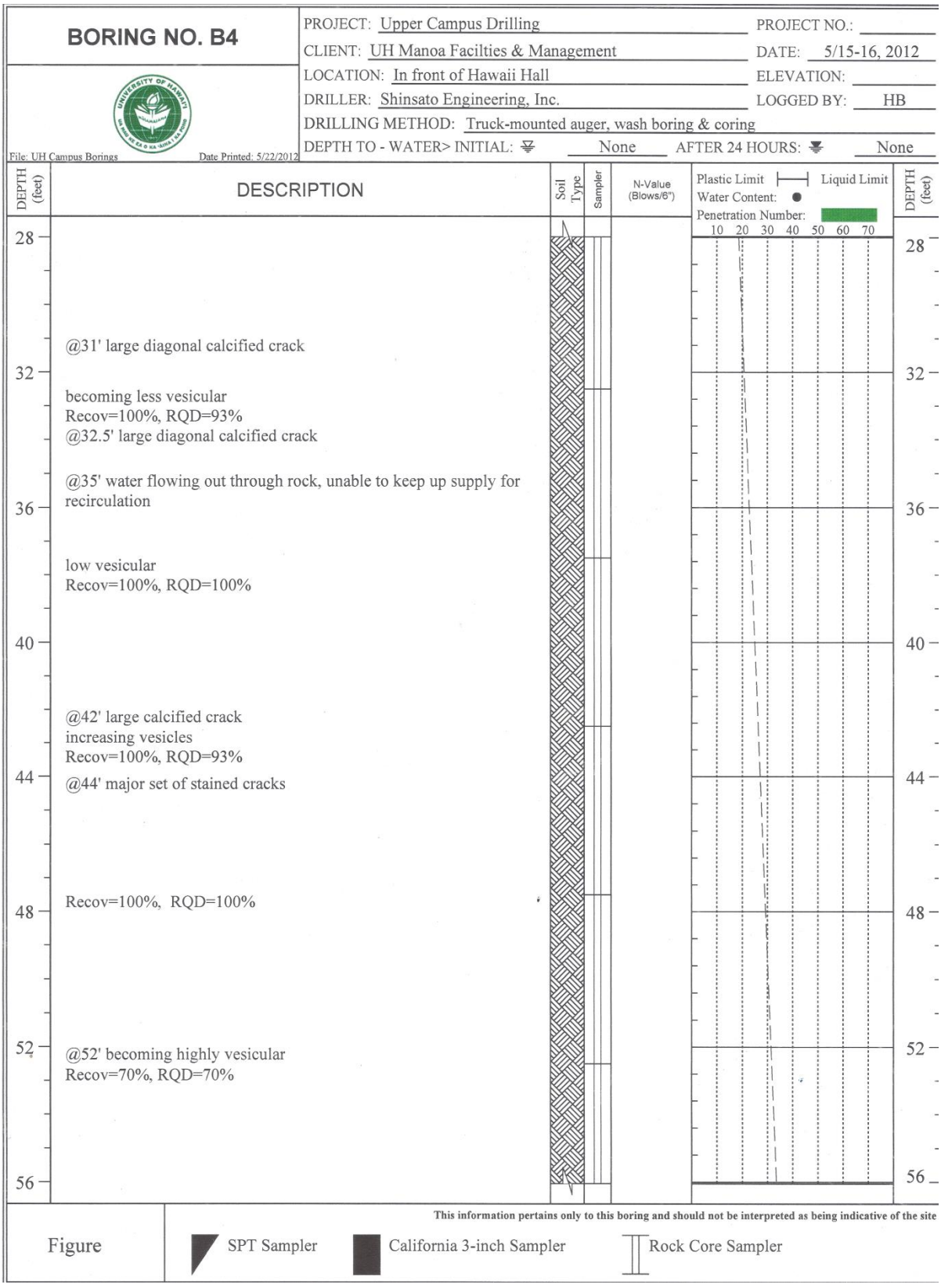

Figure 3: Boring B4 Log (continued)

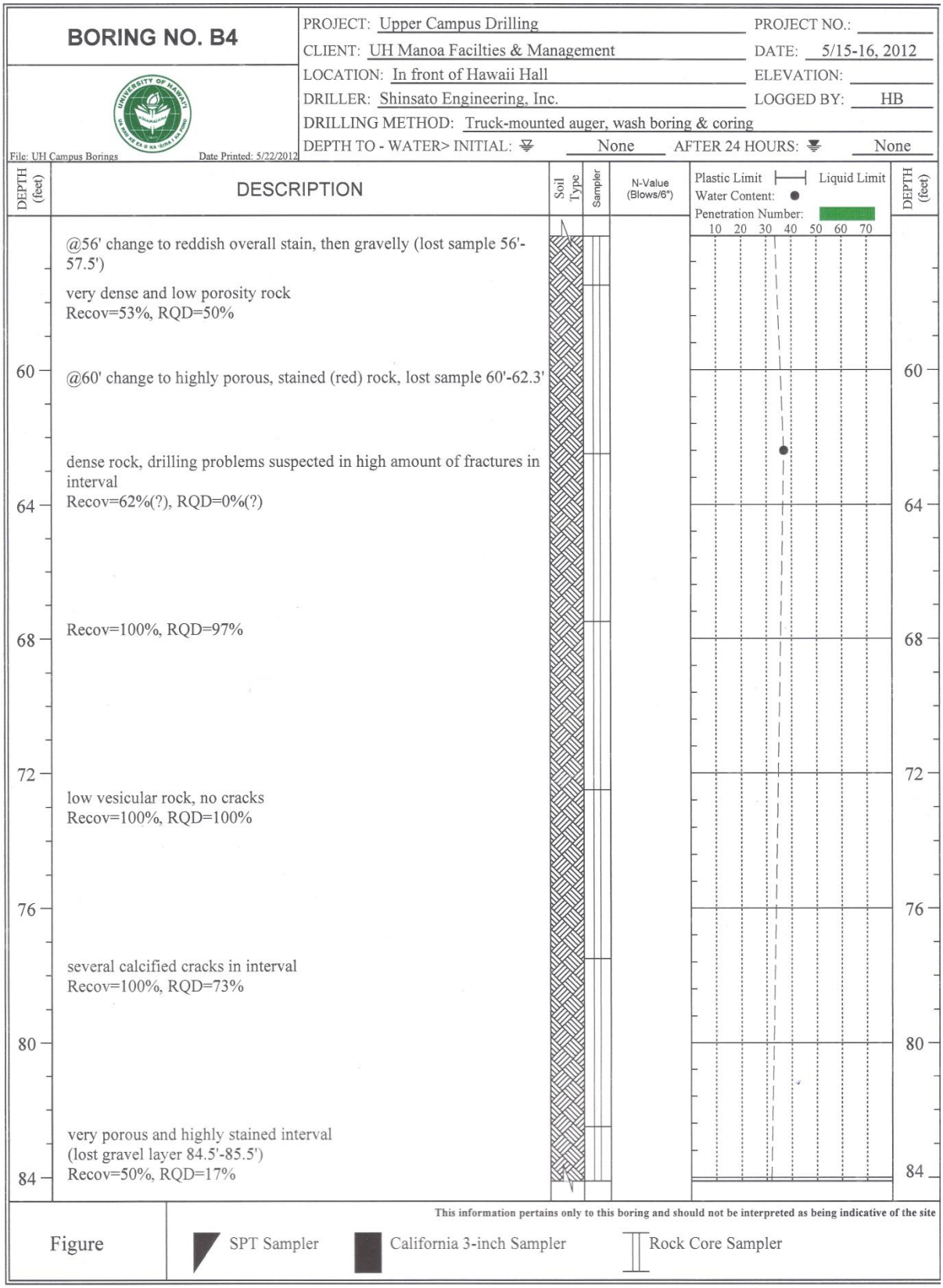

Figure 3: Boring B4 Log (continued)

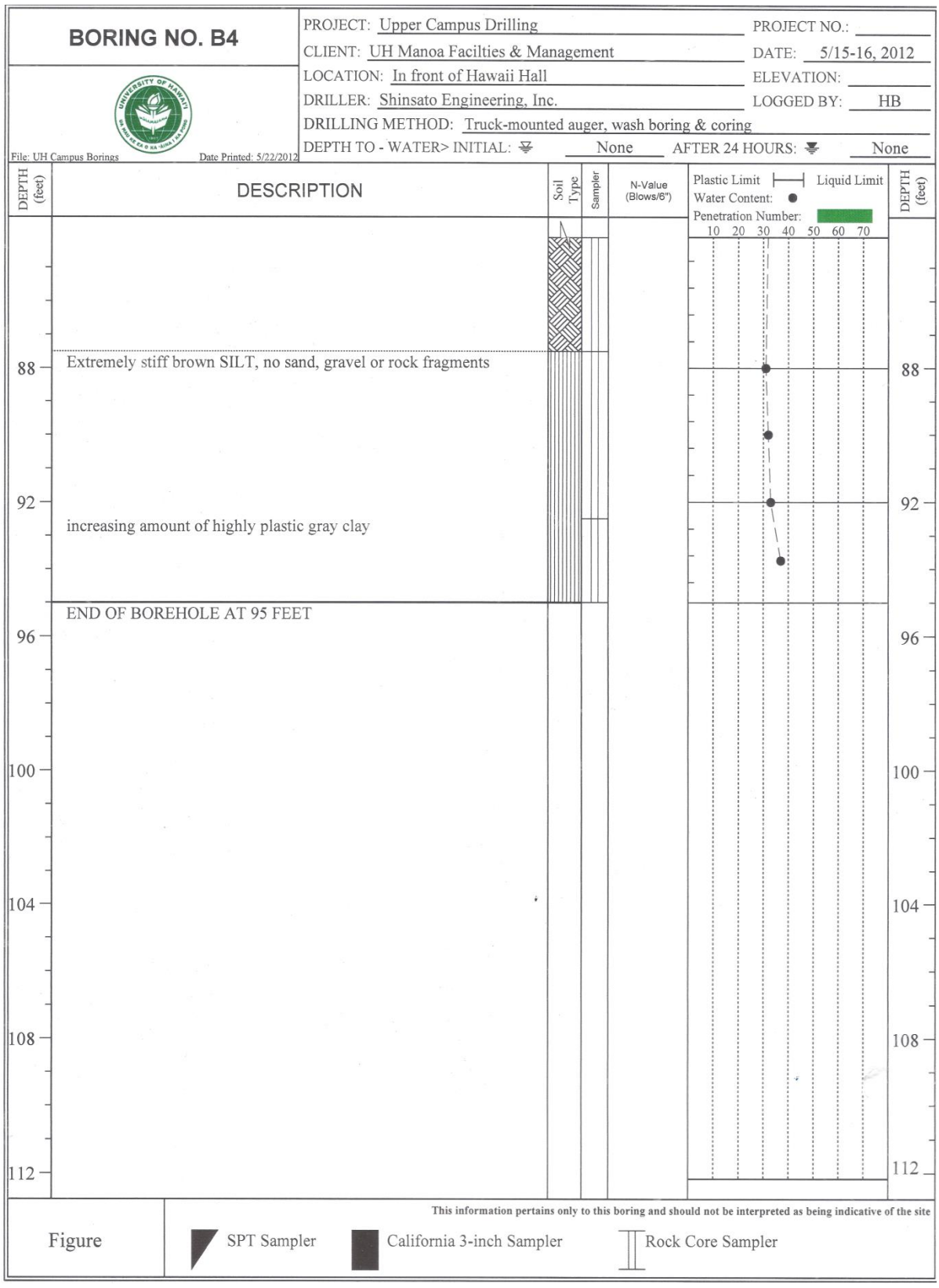

Figure 3: Boring B4 Log (continued)

1.2 Types of Rock Strength Tests

The two most common types of rock strength tests are the point load test and the triaxial test, sometimes known as the multiaxial test. Other tests such as the Schmidt hammer test and the tensile splitting test are also common in the literature. These tests will be discussed briefly.

The point load test is given its name due to how the test is run. ASTM D5731 explains the process of the point load test. A load is applied through two spherically truncated, conical platens onto the midpoint of the sample until it fails. The load at failure and the core diameter can then be used to calculate the Uncorrected Point Load Index. This can be used to find the size-corrected point load strength index. Researchers such as Guidicini et al. (1973) and Raj and Pedram (2015) have attempted to determine correlations between the results of the point load strength Index to compressive strength.

The advantages of the point load test compared to the unconfined compression test are its speed and simplicity. The equipment required to perform the point load test is smaller and simpler than the equipment required to perform the unconfined compressive test, and it can be performed in the field. The disadvantage is its reliability. The sample fails under induced tension and there's a higher variability in the mode of failure and higher chances of unintuitive and misleading results. A large number of tests, generally over 100, need to be performed in order to obtain useful data (Brady and Brown, 2004).

The multiaxial compressive test is very similar to the unconfined compressive test. The unconfined compressive test, also known as the uniaxial compressive test, is given that name because the forces applied to the sample are only along its axial axis. The multiaxial compressive test has forces applied along multiple axes. The most common multiaxial test is the triaxial test. In the triaxial test, the specimen is placed inside a pressure vessel and a fluid applies a confining pressure to the sample's surface. The specimen is wrapped in a rubber jacket to separate it from the fluid. An axial load is applied to the sample at a given strain rate until failure occurs.

The advantage of the triaxial test over the uniaxial test is accuracy of the results compared to the point load test or the unconfined compression test. The triaxial test is more likely to represent conditions in the field and can account for pore pressure variations, if any. The disadvantages are that it is cumbersome and slow to carry out. The equipment required to run a triaxial test is more advanced and time consuming.

Rock strength can also be estimated by examining the rock as a large mass. Rock masses have joints and discontinuities which cause them to act as multiple blocky structures and not as a single entity. Rock mass classification systems have been developed by many researchers in order to empirically determine the strength of a rock mass. Edelbro (2004) summarized various types of these systems (Table 3), which include those by Terzaghi (1946), Lauffer (1958), Deere (1967), Wickham et al. (1972), Bieniawski (1973) and Barton et al. (1974). These systems can

provide preliminary information about the rocks encountered at a site, although they should be supported with laboratory tests and analytical results.

The Schmidt hammer test, which is a type of rebound hammer test, is a quick nondestructive test that can be used to classify a rock in the field. The test involves a spring-loaded mass hitting the surface of the rock and measuring the amount of energy reflected back. Because the rebound value is dependent on the surface hardness of the sample, a chart can be used to convert the rebound value into an appropriate compressive strength. The conversion chart used depends on the type of hammer. The method is described in ASTM D5873.

The tensile splitting test, sometimes known as the splitting tensile test or the Brazilian test, measures the tensile strength of the sample. The sample dimensions are similar to those used in the unconfined compressive test. The sample is placed on its side and then compressed in a machine to force the sample to fail through shearing. Because the compressive strength cannot be calculated from this test, it is of limited usefulness. The method is explained in ASTM D3967.

Table 3: List of Rock Mass Rating Systems (Edelbro 2004)

Name of Classification	Author
Rock Load Theory	Terzaghi (1946)
Stand up time	Lauffer (1958)
New Austrian Tunnelling Method	Rabcewicz (1964)
Rock Quality Designation	Deere et al. (1966)
Rock Structure Rating	Wickham et al. (1972)
Rock Mass Rating	Bieniawski (1974)
Q-system	Barton et al. (1974)
Mining RMR	Laubscher (1975)
The typological classification	Matula and Holzer (1978)
Unified Rock Classification System	Williamson (1980)
Basic geotechnical description	ISRM (1981)
Rock mass strength	Stille et al. (1982)
Simplified rock mass rating	Brook and Dharmaratne (1985)
Slope mass rating	Romana (1985)
Ramamurthy/Arora	Ramamurthy and Arora (1993)
Geological Strength Index	Hoek et al. (1995)
Rock Mass Number	Goel et al. (1995)
Rock mass index	Palmstrom (1995)

1.3 Reported Rock Strength Parameters

Farmer (1968) listed bulk density, compressive strength, and Young's modulus of basalt rocks taken from other references; among those listed were those of Hosking (1955), Blair (1955, 1956), Nicholls (1961), Coates and Parsons (1966), and Windes (1949, 1950), along with his own observations. He included rock types such as granite and sandstone and listed other parameters like Poisson's ratio and porosity as well. For basalt rocks, he reported a bulk density of 2.80 to 2.90 g/cm^3, a compressive strength of 21.3 to 42.7 ksi, and a Young's modulus of 8,530 to 14,200 ksi (Table 4). Values for granite, gabbro, limestone, and marble are included in Table 4, along with the values taken from other studies referenced in this paper. He does not go in-depth about the tests behind the values.

Four types of rocks were tested by Stowe (1969). These rocks were collected from the Atomic Energy Commission's Nevada test site in Mercury, Nevada. He tested granite, basalt, limestone, and tuff under various rates of loading. The types of tests performed were unconfined compression, tensile splitting and triaxial compression with confining pressures ranging from 250 to 5,000 psi. Nondestructive tests such as specific gravity, porosity and compressional wave velocity were also performed on the specimens. The nondestructive tests showed that within each rock type, the specimens were fairly uniform. The unconfined compression tests showed that as the loading rate increased, the ultimate strength, total axial strain, and Young's Modulus all increased while the total diametral strain decreased. For basalt rocks tested under unconfined compression, he calculated a mean bulk dry specific gravity of 2.69, a mean compressive strength of 21.5 ksi, and a mean Young's modulus of 5,060 ksi.

Guidicini et al. (1973) performed point load tests on various types of rocks with irregular shapes. The authors wanted to reanalyze the work of Protodiakonov performed in the 1950s. They determined that unconfined compressive or tensile strength of rocks using data obtained from the point load test can lead to scattered results.

Jumikis (1979) listed values taken from other references as well as his own observations. He referred to many sources throughout his book, including those of Birch (1972), Griffith (1937), Johnson (1970), Szechy (1966), and the US Bureau of Reclamation (1954). He also cited Farmer (1968) as a reference. He does not explain the testing or methodology behind the values he obtained. For this study, his findings for basalt, granite, gabbro, and marble were noted. He listed the bulk specific gravity of basalt rocks ranging from 2.21 to 2.77, the compressive strength from 11.4 to 59.7 ksi and the Young's modulus from 2,840 to 16,200 ksi.

Basalt rocks in Deer Park, Melbourne, Victoria, Australia from a quarry were tested by Cole (1982). He performed dynamic triaxial tests on three basalt samples. The samples were pure green, pure grey, and a quarry mixture of roughly one third green and two thirds grey. The quarry mixture was rated as the best of the three samples, with the pure green basalt rated the worst, and this was the reverse order given in the Western Australian modified accelerated Texas-triaxial compression test.

Panek and Fannon (1992) performed point-load tests on three rocks from near Lake Superior, Michigan; iron formation, metadiabase, and ophitic basalt. The authors wanted to determine the effects of the size and shape of rocks and see if there is a correlation with strength values. Unconfined compression tests and Brazilian tests were also performed on the metadiabase and basalt to help determine the effects of size. The results were analyzed by multiple regression techniques. They determined that the effects of the size of the samples were dependent on the rock type, which matched the authors' previous findings. The effects of the shape of the samples were constant over all three rock types.

Al-Harthi et al. (1999) performed unconfined compressive and sonic pulse velocity tests on basalt rocks from western Saudi Arabia. They measured the porosity and density of the samples and compared them to the compressive strength, modulus of elasticity, Poisson's ratio, and sonic velocities. They also used an image analysis technique in order to measure the porosity of the samples. They determined that there is a strong correlation between porosity and the strength values obtained in the unconfined compressive test, but there is a weaker correlation between porosity and dynamic properties.

Dincer et al. (2004) performed tests on basalt, andesite, and tuff rocks located in the western part of the Mugla Province of the Bodrum Peninsula in Turkey. The site largely consists of volcanic rocks and the tests performed were the unconfined compression test and the Schmidt hammer test. The authors wanted to determine if there was a correlation between the Schmidt hammer rebound value and the properties of rocks, namely volcanic rocks. The properties they measured were unit weight, unconfined compressive strength, Young's Modulus, and Schmidt hammer rebound value. For basalt rocks, they measured a unit weight of 25.35 to 25.74 kN/m^3 which can be converted to a density of 2.58 to 2.70 g/cm^3, a compressive strength of 9.43 to 15.7 ksi and a Young's modulus of 1,680 to 3,070 ksi. The empirical correlations they determined were notably different compared to correlations determined from other studies and these correlations should only be used on basalt, andesite, and tuff rocks with similar levels of weathering and mineral composition. They also determined that using only the Schmidt hammer test would give less accurate results than multiple tests done in a laboratory.

Alemdag et al. (2007) performed tests on basalt rocks for the Atasu Dam located in Turkey. The tests were run to determine the bearing capacity of the basalt rocks. The authors were primarily interested in observing how the basalt would behave as a rock mass rather than as individual pieces and used the Hoek-Brown criterion in their modeling. No unconfined compression tests were performed; instead the authors performed triaxial tests to obtain a dynamic elasticity modulus, compressive strength, and other parameters related to triaxial tests. The numerical code ANSYS was used to determine the stress distribution of the basalt rocks mass. The authors drew from various empirical correlations and references to estimate the bearing capacity of the basalt rocks. The authors determined that it was safe to construct a dam at the site, but further analysis would be required for any structures that were to be added on later.

Brandes et al. (2011) performed tests on basalt rocks from the island of Hawaii. Several bridges located north of Hilo were to be replaced because they were deemed to be susceptible to earthquakes. The authors performed p-wave and s-wave velocity tests along with the point load test, but also performed triaxial tests with confining pressures of 1,500 kPa (0.22 ksi). The authors determined multiple types of densities – oven-dried, saturated-surface-dry, apparent unit weight, and CoreLok unit weight – and determined absorption, Young's modulus, triaxial compressive strength, and Poisson's ratio. They calculated an oven-dried unit weight of 14.5 to 26.9 kN/m^3, which translates to a density of 1.48 to 2.74 g/cm^3, a compressive strength of 2.80 to 13.4 ksi, and a Young's modulus of 1,770 to 9,180 ksi. They determined that the basalt rocks had lower strength values compared to strength values reported elsewhere and attribute this to the existence of vesicles in the samples.

Tests were performed on basalt and tuff rocks for the Baihetan Hydropower Station located in western China. These tests were conducted by Yan et al. (2011). They performed the split Hopkinson pressure bar test. These tests would determine the dynamic tensile strength properties of the basalt rock, the tuff rock, and the basalt plus tuff interface. The authors determined the elastic modulus, Poisson's ratio, static tensile strength and static compression strength of the three rocks. They determined that the basalt rock had the highest dynamic tensile strength of the three while tuff had the lowest. The basalt and tuff rocks had typical sensitivity to loading rate, but the dynamic tensile strength of the basalt plus tuff interface was largely dependent on its geometric structure rather than the loading rate.

Mendoza-Chavez et al (2012) performed tests on rocks in southern Mexico. These tests were performed because several bridges in southern Mexico were built using stone masonry during the middle of the twentieth century and there was no evidence of any testing done on the material to determine if the bridges were safe. The authors assumed that the bridges were constructed with rock obtained in the general vicinity of the bridges. The authors performed direct shear, point load, tensile strength, and unconfined compression tests. The unconfined compression tests were performed on masonry prisms and not pure basalt. They measured the internal friction angle, cohesion, compressive strength via point load and unconfined compression tests, Young's modulus, Poisson's ratio, density, and tensile strength.

Tests were also performed on Termaber basalt rocks located in Central Ethiopia near the town of Debre Birhan. These tests were conducted by Engidasew and Barbieri (2013). These tests were performed to determine the suitability of the rocks as construction materials, either as aggregate for concrete or as a block of stone. The authors determined the uniaxial compressive strength, ultrasonic pulse velocity, dynamic elasticity modulus, bulk density, absorption, specific gravity, porosity, aggregate impact value, petrographic examination and XRF, aggregate crushing value, Los Angeles abrasion value, sodium sulfate soundness, X-ray diffraction and alkali silica reactivity. A bulk density of 2.80 to 3.03 g/cm^3 and a compressive strength of 18.9 to 50.9 ksi for basalt rocks were determined. They concluded that the basalt had high strength values and was suitable for construction.

Oliveira and Zuquette (2014) performed pH, electrical conductivity, and point-load tests on several types of basalt rocks from the Itaipu Dam region on the border between Brazil and Paraguay. The types of basalts they examined were dense basalts, vesicular-amygdaloidal basalts, and basaltic breccias. They wanted to determine if there was a correlation between pH, electrical conductivity, and point load strength to the degree of weathering in the rocks. They concluded that pH increases with increasing degrees of weathering while the point load strength decreases. Electrical conductivity appeared to have no correlation with any of the calculated values.

Jiang et al. (2014) performed tests on columnar jointed basalts located at the Baihetan hydropower station in China. They wanted to examine properties of the anisotropic rock mass and performed in situ p-wave velocity, point load, and unconfined compression tests. Insufficient data on the unconfined compression tests in the paper makes it difficult to analyze their findings. They determined that the anisotropic coefficients obtained for its deformability and strength are similar for all testing methods they used.

Raj and Pedram (2015) performed tests on basalt and rhyolite rocks from a Nevada gold mine. The tests were performed to determine a correlation between indirect and direct compression test methods on these rock types. The tests they performed included point load index, splitting tensile strength, block punch index, uniaxial compression test, Schmidt hammer test, and ultrasonic pulse velocity test. They calculated a density of 1.96 to 2.55 (units were not specified), a compressive strength of 2.67 to 54.5 ksi, and a Young's modulus of 2,520 to 9,030 ksi. They determined that of the correlations that they examined, the uniaxial compression test compared to the splitting tensile strength had the strongest correlation, while the Poisson's ratio had no correlation to any value they determined.

Of all these studies, only the one by Brandes et al. (2011) involved basalt rocks from Hawaii. Compared to Farmer (1968), Stowe (1969), Jumikis (1979), Dincer et al. (2004), Engidasew and Barbieri (2013) and Raj and Pedram (2015), Brandes et al. (2011) reports the lowest mean density, minimum density and Young's modulus. The maximum density and maximum Young's modulus are in line with other reported values. Brandes et al. (2011) reports a lower mean, minimum, and maximum compressive strength than all of the other references.

The objectives of this study are to determine the soil profile of the University of Hawaii at Manoa and compare the results to that of Brandes et al. (2011) to determine any correlations among Hawaiian basalt rocks.

Table 4: Rock Strengths Reported in the Literature

CLASS	ROCK TYPE	REFERENCE	Density (g/cm^3)* or Specific Gravity				Compressive Strength (ksi)				Young's Modulus (E) (ksi)			
			mean	min	max	**STDEV	mean	min	max	STDEV	mean	min	max	STDEV
IGNEOUS	BASALT	Farmer (1968)	-	2.80	2.90	-	-	21.3	42.7	-	-	8530	14200	-
		Stowe (1969)	2.69	2.65	2.77	0.0208	21.5	20.0	22.7	0.908	5060	3430	5370	582
		Jumikis (1979)	-	2.21	2.77	-	-	11.4 21.3	59.7 42.7	-	-	2840 7030	14200 16200	-
		Dincer et al. (2004)	2.62	2.58	2.70	0.0520	12.5	9.43	15.7	3.04	2320	1680	3070	645
		Brandes et al. (2011)	2.21	1.48	2.74	0.505	6.0	2.80	13.4	3.84	4510	1770	9180	1820
		Engidasew and Barbieri (2013)	2.90	2.80	3.03	0.0654	36.1	18.9	50.9	10.3	-	-	-	-
		Raj and Pedram (2015)	2.29	1.96	2.55	0.276	21.3	2.67	54.5	18.7	5610	2520	9030	2910
	GRANITE	Farmer (1968)	-	2.60	2.70	-	-	14.2	35.6	-	-	2850	8530	-
		Stowe (1969)	2.70	2.68	2.72	0.0126	11.2	9.50	12.8	1.63	11200	10420	12000	791
		Jumikis (1979)	-	2.53	2.62	-	-	17.1 14.2	39.8 35.6	-	-	3700 3090	9950 10200	-
	GABBRO	Farmer (1968)		3.00	3.10			25.6	42.7			9960	15600	
		Jumikis (1979)	-	2.72	3.00	-	-	21.3 25.6	28.4 42.7	-	-	8530 8470	15600 12600	-
SEDIMENTARY	LIMESTONE	Farmer (1968)	-	2.20	2.60	-	-	4.27	35.6	-	-	1420	11400	-
		Stowe (1969)	2.70	2.68	2.72	0.0126	11.18	9.50	12.8	1.628	11200	10420	12000	791
METAMORPHIC	MARBLE	Farmer (1968)	-	2.60	2.70	-	-	14.2	35.6	-	-	-	-	-
		Jumikis (1969)	-	2.51	2.86	-	-	7.11 14.2 -	25.6 28.4 -	-	-	8530 7150 4060	12800 12600 14500	-

*Farmer (1968) reported bulk density. Stowe (1969) reported bulk dry specific gravity. Jumikis (1979) listed bulk specific gravity. Dincer et al. (2004) stated unit weight but did not specify the units. Brandes et al. (2011) measured multiple types of unit weight, but the one reported is oven-dried. Engidasew and Barbieri (2013) measured bulk density. Raj and Pedram (2015) stated density but did not specify the units.

**STDEV = standard deviation

2. TEST PROGRAM AND METHOD

2.1 Introduction

A total of 66 samples were tested in this report under unconfined compression in accordance with ASTM D2938-1 (Table 5). All samples were cut from 5-foot core runs obtained from boring B4. The samples ranged from a depth of 25 feet to 81 feet. First, each sample was cut to a length of 5 inches with a diameter of 2.5 inches. The oven-dried density, saturated-surface-dry density, apparent density, and bulk density obtained via CoreLok were obtained in accordance with ASTM D127-04. Then the tolerance checks for each sample were determined in accordance with ASTM 4543, followed by placing sulfur caps on the ends of each sample to help reduce the effects of imperfect sample ends.

Unconfined compression testing required the use of two different test frames; one that had a load capacity of 50 kips (*Material Test System* or MTS) and one that had a load capacity of 300 kips (*Riehle)*. Of the 66 samples that were tested, 41 did not fail on the 50-kip test frame (Table 6). Those samples had to be re-tested on the 300-kip test frame. The 50-kip test frame was connected to a computer and the software *Station Manager* was used to record the stress-strain response of each sample. Load data from the 300-kip machine was read from a dial and recorded by hand. An extensometer was used with the 50-kip load frame to measure axial strain during loading. No such extensometer was used with the 300-kip frame, hence only the failure load could be determined.

Table 5: Rock Core Samples

Rock Core Sample Interval ft	RQD %	Recov %	Intact Specimens Recovered and Tested
17.5-22.5	93	100	-
22.5-27.5	100	100	1, 2, 3, 4
27.5-32.5	87	100	5, 6, 7, 8, 9
32.5-37.5	93	100	10, 11, 12, 13, 14, 15, 16, 17
37.5-42.5	100	100	18, 19, 20, 21, 22, 23, 24, 25, 26
42.5-47.5	93	100	27, 28
47.5-52.5	100	100	29, 30, 31, 32, 33, 34
52.5-56	70	70	35, 36, 37, 38, 39
57.5-60	50	53	40, 41, 42, 43
62.3-67.5	0?	62	-
67.5-72.5	97	100	44, 45, 46, 47, 48, 49, 50, 51
72.5-77.5	100	100	52, 53, 54, 55, 56, 57, 58, 59
77.5-82.5	73	100	60, 61, 62, 63, 64, 65, 66
82.5-87.5	17	50	-

Table 6: Number of Strength Tests

Test Type	Test Frame	Number of Tests
UC	50 kip max	66
UC	300 kip max*	41

* Samples that did not fail at 50 kips were tested again on the 300-kip frame

2.2 Tolerance Checks

Rock samples were prepared in accordance with ASTM D4543-01, which describes how the samples should be cut and how tolerance checks should be conducted. The samples required a length to diameter ratio between 2 to 2.5. Since the inside diameter of the rock core sampler was 2.5 inches, the length of each sample was cut to be approximately 5 inches. The diameter and length of each sample were measured with a caliper. The diameter was measured twice and averaged. The length was measured once.

Each test sample required three tolerance checks; the straightness of the cylindrical surface, the flatness of each end face, and the perpendicularity of the end face with the axis of the core (Figure 4 through 6). The straightness of the cylindrical surface was checked following Procedure A in ASTM D 4543, where the specimen was rolled on a smooth, flat surface, and the height of the maximum gap between the specimen and the flat surface was measured with a feeler gage (Figure 4). The straightness would be acceptable if the deviation was less than 0.02 inches.

The flatness of each end face was checked following Procedure B in ASTM D4543, but a feeler gage was used in place of a dial gage. The specimen was placed upright on a smooth, flat surface, and a feeler gage was used to determine the maximum height between the specimen and the flat surface Figure 5. The flatness would be acceptable if the deviation was less than 0.0015 inches.

The perpendicularity of the end face with the axis of the core was also checked following Procedure B in ASTM D4543, where the specimen was placed upright on a smooth flat surface and a true square was placed next to it. The specimen would be rotated until the maximum gap between the true square and the top of the specimen was found and measured with a feeler gage (Figure 6). The perpendicularity would be acceptable if the deviation was less than H/230 inches, where H is the height of the sample in inches.

No test sample satisfied all three tolerance checks simultaneously. However, the samples were not discarded for failing any of the tolerance checks since that would leave no specimens for

further testing. Table A1 in the Appendix shows the results of the tolerance checks for each of the specimens.

Figure 4: Straightness Tolerance Check

Figure 5: Flatness Tolerance Check

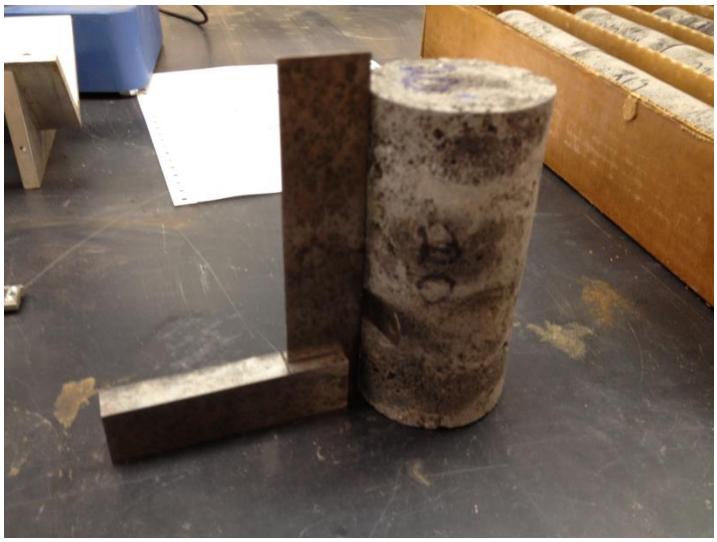

Figure 6: Perpendicularity Tolerance Check

2.3 Unit Weights and Sulfur Caps

Weights of the rock samples were determined in various moisture states in accordance with ASTM D127-04. First, each rock sample was placed fully submerged in a bucket of water for at least 24 hours to allow all the voids to become fully saturated. Each rock sample was dried with a towel and weighed in a saturated-surface-dry condition (SSD). Then each rock sample was placed in a large tub of water connected to a scale to obtain the submerged weight, or apparent weight, of the sample. Finally, each rock sample was oven-dried for 24 hours and weighed to determine the oven-dried mass (OD).

Each rock sample was weighed using the CoreLok machine. This machine was developed by Instrotek Inc. and its purpose is to seal rock and asphalt samples into an air tight bag so the densities of the sample can be measured by water displacement methods. The procedures performed were in accordance with the manual from the manufacturer. First, each sample was oven dried and weighed. The weight of the bag used for the CoreLok machine was also weighed. Then the sample was placed into the empty bag used for the CoreLok machine shown in Figure 7 and sealed air tight. Next, the rock sample in the bag was placed in the same large tub of water to obtain the submerged weight. After submersion, the sample was taken out of the bag and immediately weighed again to determine if any water leaked into the bag. The bulk gravity of the rock sample could be determined from these weights (see equations in Chapter 3).

At the start of testing, each sample's diameter (*D*) was measured twice and averaged, and each sample's height (*H*) was measured once. Each measurement was taken with a caliper. The

sample's area (A) and volume (V) were calculated. Each sample had a diameter of 2.5 +/- 0.01 inches, and a height of 5.0 +/- 0.10 inches.

The oven dried density (γ_{OD}), taken from ASTM D127-04, is calculated as:

$$\gamma_{OD} = \frac{W_{OD}}{W_{SSD} - W_{SUB}} * g \quad (1)$$

where W_{OD} is the oven-dried weight, W_{SSD} is the saturated-surface-dry weight, and W_{SUB} is the submerged weight.

The saturated-surface-dry density (γ_{SSD}) is given by:

$$\gamma_{SSD} = \frac{W_{SSD}}{W_{SSD} - W_{SUB}} * g \quad (2)$$

The apparent density (γ_{APP}) can be derived as:

$$\gamma_{APP} = \frac{W_{OD}}{W_{OD} - W_{SUB}} * g \quad (3)$$

The absorption can be found using the following equation:

$$Absorption\ (\%) = \frac{W_{SSD} - W_{OD}}{W_{OD}} * 100 \quad (4)$$

The CoreLok machine was used to determine the bulk density (γ_{CL}). It required that the following values be obtained:

C_A = Bag weight

C_B = Oven-dried weight = W_{OD}

C_C = Sealed sample submerged weight

C_D = Dry weight after submersion

C_E = C_B/C_A

C_F = Apparent gravity of bag

C_F = Value determined from Table 7, which is based on C_E.

The bulk density can be defined as:

$$\gamma_{CL} = \frac{C_B}{C_I} * g \tag{5}$$

$$C_I = C_G - C_H \tag{6}$$

$$C_H = \frac{C_A}{C_F} \tag{7}$$

$$C_G = C_A + C_D - C_C \tag{8}$$

Here C_G is the total volume, C_H is the volume of the bag, and C_I is the volume of the sample.

Sulfur caps were placed on each end of each sample to make them flat and perpendicular to the sides in accordance with ASTM C617. The sulfur was heated until it reached a liquid state. A thin layer of oil was sprayed onto the metal block so the sample could be removed more easily after the sulfur cap is placed on. Then the rock sample was placed in the metal block (Figure 8) and the sulfur was poured into the void. The sulfur would cool after approximately 10 seconds and the sample could be flipped over to have a cap melted onto the other end (Figure 9).

Figure 7: CoreLok Machine

Figure 8: Sulfur Cap Block

Figure 9: Sample with Sulfur Caps

Table 7: Apparent Gravity of Small CoreLok Bags

C_E	Apparent gravity
20	0.801
30	0.795
40	0.789
50	0.784

2.4 Strength Testing

Rock samples were tested in unconfined compression in accordance with ASTM D2938-95, with certain deviations as noted below. The samples were tested using an 810 Material Test System machine. This test frame had a load capacity of 50 kips. The strain rate used was 0.02 inches per minute. Each sample was outfitted with an extensometer that measured axial deformation. No horizontal deformation was measured. The extensometer had four rubber bands to wrap around the sample and keep the extensometer together. Pins were used to keep the extensometers from slipping while assembling the test. The pins were removed before the test started to prevent them from being sheared during the test.

The software interface used for the 50-kip machine is shown in Figure 10. Every half a second during the test, the software would log the displacement of the swivel head in inches, the displacement of the extensometer in inches, and the load in kips. The data was saved to a DAT file, which can be opened in Excel.

The 50-kip machine is shown in Figure 11 and the user interface for the 50-kip machine is shown in Figure 12. The button labeled “Station Stop” would automatically shut down the machine in case of emergency. The manual control knob, when enabled, would allow the user to manually control the top swivel head, and had to be disabled in order to run the test. The screen displayed the load, displacement of the top swivel and the strain in real time.

If the sample did not fail in the 50-kip test frame, it was tested again using a 300-kip test frame (Figure 13). For a given sample, the test area would first be cleaned of any fragments. Since the samples were small, metal blocks were used to elevate them up to the top swivel head on the test frame. The dial readings also had two needles (Figure 14). The larger one would note the maximum load measured during the test and the smaller needle would note the current load. The knob “range selector” (Figure 12) would be set to an appropriate load range. The load pacer knob would control the loading rate.

The test on the 300-kip machine was started by moving the swivel head so that it would make contact with the sample, and the main knob would be used to close the rest of the gap between the swivel head and the sample by switching it to “load” and then turning it to “hold” until the

user was ready. Once the swivel head made firm contact with the sample and loading was applied, the two needles would move together. The main knob would control the loading rate. Once the sample failed, the larger needle would record the maximum strength while the smaller needle would automatically move back to zero. Once the maximum strength was noted, the large needle could be moved back to zero. Thereafter the test area would be cleaned for the next test.

Only the maximum strength was obtained on samples that had to be tested on the 300-kip frame. For these samples, the strain at 50-kip load was noted, but the strain beyond 50 kips was not obtained.

Slight deviations to the ASTM standards were needed. ASTM D2938-95 requires that the water content of the sample be preserved until testing in order to get results representative of the conditions present on the field. However, in this study the samples were instead tested at zero moisture content.

The unconfined compressive stress at failure was calculated as:

$$q_u(ksi) = \frac{f_{max}}{A} \tag{9}$$

where f_{max} is the load at failure and A is the cross-sectional area of the sample.

Young's modulus (E) is defined as the initial tangential, or secant, modulus measured from the point of origin to 25 percent of the sample's maximum unconfined compressive strength in accordance with ASTM D7012-14. Due to the slack in the apparatus at the start of the test, a sufficient amount of time was needed in order to obtain reliable readings of stress and strain. For all tests, E appeared to stabilize at around 25 percent of a given sample's failure load. The following equation was used to determine E:

$$E = \frac{\sigma_{25}}{\varepsilon_{25}} \tag{10}$$

where σ_{25} is the stress at 25 percent of the ultimate strength and ε_{25} is the strain at 25 percent of the ultimate strength.

The strain at any time t could be determined by:

$$\varepsilon_t = \frac{\Delta_t - \Delta_0}{2 + \Delta_0} \tag{11}$$

where Δ_t is the displacement of extensometer at time t and Δ_0 is the displacement of extensometer at time 0.

The extensometer had an initial displacement of 2 inches plus the value the extensometer read at the start of the test, so the strain was measured over the distance that the extensometer covered.

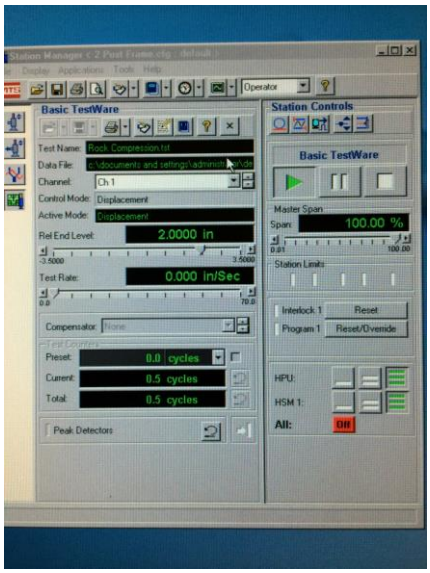

Figure 10: Screenshot of Station Manager Software used on 50-kip Test Frame

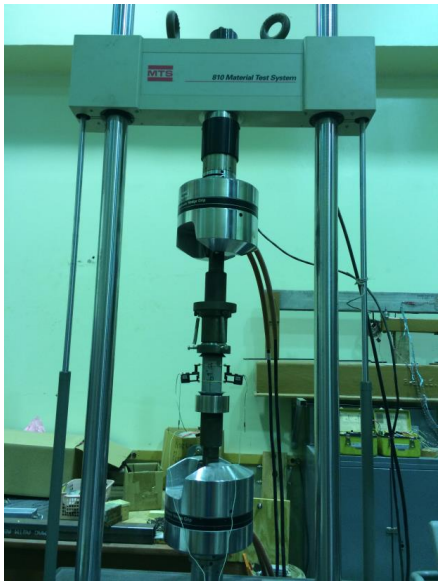

Figure 11: 50-kip Test Frame

Figure 12: User Interface of 50-kip Test Frame

Figure 13: 300-kip Test Frame

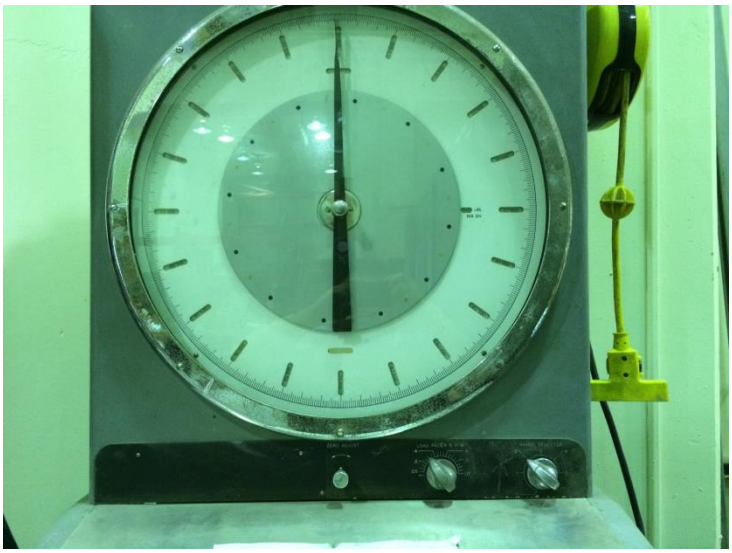

Figure 14: 300-kip Test Frame Readings

Figure 15: User Interface for 300-kip Test Frame

3. TEST RESULTS AND DISCUSSION

3.1 Unit Weights and Strengths

Unit weights and index properties for all specimens tested are listed in Table 8. In-depth CoreLok calculations are listed in Table 9. Strength test results are tabulated in Table 10.

Detailed results from all 66 unconfined compression tests are shown in the Appendix. In most cases, the stress-strain behavior up to about 0.1% axial strain is relatively linear. Young's Modulus was determined as the slope of this initial response.

Failure mode was characterized as one of three types. The first was shatter-type failure mode (STF, Figure 16). Samples that failed in this way had no discernible failure plane and often shattered into small fragments. The second was multiple fracture failure mode (MFF, Figure 17). Samples that failed in this way formed multiple cracks within the sample but without the specimen falling apart. There were generally no discernible patterns to the cracks. The third was dominant plane failure mode (DPF, Figure 18). Samples that failed in this way had one major discernible failure plane with the specimen splitting into two parts. The smaller portion in some cases detached from the larger one and in other cases it did not. The angle the failure plane made to the horizontal (α) was also noted.

Figure 16: Example of shatter-type failure mode (STF)

Test No. 1, Sample Depth = 25 ft

Figure 17: Example of multiple fracture failure mode (MFF)

Test No. 7, Sample Depth = 31 ft

Figure 18: Example of dominant plane failure mode (DPF)

Test No. 4, Sample Depth = 27 ft

Table 8: Physical Properties of Test Specimens

Test No.	Sample Depth (ft)	Oven-Dried Unit Weight (lb/ft^3) γ_{OD}	Saturated-Surface-Dry Unit Weight (lb/ft^3) γ_{SSD}	Apparent Unit Weight (lb/ft^3) γ_{APP}	CoreLok Unit Weight (lb/ft^3) γ_{CL}	Absorption (%)	RQD (%)	Percent Recovered
1	25	161.46	166.45	175.48	152.48	3.09	100	100
2	26	154.27	160.42	171.15	152.93	3.99	100	100
3	26	150.37	157.17	168.76	149.75	4.52	100	100
4	27	161.95	167.34	177.27	157.43	3.33	87	100
5	29	160.23	165.40	174.72	159.10	3.23	87	100
6	29	160.99	166.27	175.88	158.46	3.28	87	100
7	31	149.48	156.14	167.34	147.11	4.46	87	100
8	31	156.52	162.11	171.91	154.29	3.57	87	100
9	32	151.70	158.63	170.66	149.26	4.57	87	100
10	32	156.63	162.93	174.24	152.01	4.03	87	100
11	33	158.24	162.96	171.19	160.43	2.98	93	100
12	34	161.41	166.08	174.47	163.31	2.89	93	100
13	35	160.15	165.15	174.11	162.11	3.12	93	100
14	35	161.14	165.75	173.99	162.95	2.86	93	100
15	36	162.82	167.92	177.31	161.77	3.13	93	100
16	36	151.30	158.65	171.49	152.92	4.86	93	100
17	37	154.37	161.39	173.94	155.65	4.55	93	100
18	37	147.36	155.45	169.31	148.92	5.49	93	100
19	38	162.05	167.00	176.03	164.48	3.06	100	100
20	38	160.42	166.38	177.38	161.74	3.72	100	100
21	39	160.82	166.94	178.31	162.09	3.81	100	100
22	39	156.28	163.67	177.27	156.06	4.73	100	100
23	40	148.04	156.31	170.68	150.73	5.59	100	100
24	40	159.99	165.59	175.77	161.08	3.50	100	100
25	41	159.13	164.83	175.13	161.56	3.58	100	100
26	42	157.22	164.23	177.12	157.07	4.46	100	100
27	45	151.06	159.27	173.95	150.76	5.44	93	100
28	45	141.50	151.56	168.71	140.00	7.11	93	100
29	48	154.73	161.74	174.32	156.80	4.53	100	100
30	48	143.27	153.48	171.31	152.07	7.13	100	100
31	49	149.25	157.64	172.43	151.28	5.62	100	100
32	49	157.98	164.18	175.39	160.30	3.92	100	100
33	50	137.69	147.91	164.64	138.38	7.42	100	100
34	51	134.37	145.15	162.43	134.82	8.02	100	100
35	53	131.47	143.14	161.73	132.00	8.88	70	70
36	53	126.15	138.85	158.38	126.91	10.06	70	70
37	54	128.25	140.66	160.07	129.05	9.67	70	70

Table 8: Physical Properties of Test Specimens (continued)

Test No.	Sample Depth (ft)	Oven-Dried Unit Weight (lb/ft^3) γ_{OD}	Saturated-Surface-Dry Unit Weight (lb/ft^3) γ_{SSD}	Apparent Unit Weight (lb/ft^3) γ_{APP}	CoreLok Unit Weight (lb/ft^3) γ_{CL}	Absorption (%)	RQD (%)	Percent Recovered
38	55	122.95	137.98	161.95	122.70	12.22	70.00	70.00
39	55	128.69	142.19	164.22	128.56	10.49	70.00	70.00
40	57	180.77	183.19	188.06	182.27	1.34	70.00	70.00
41	58	177.43	180.81	187.59	178.60	1.91	50.00	53.00
42	58	177.73	181.86	190.33	173.71	2.32	50.00	53.00
43	59	182.18	184.36	188.78	140.16	1.20	50.00	53.00
44	68	181.25	184.88	192.45	180.50	2.00	97.00	100.00
45	68	179.12	182.54	189.51	180.40	1.91	97.00	100.00
46	69	178.70	182.35	189.79	179.77	2.04	97.00	100.00
47	69	178.79	182.42	189.82	179.88	2.03	97.00	100.00
48	70	181.98	184.84	190.71	183.36	1.57	97.00	100.00
49	71	179.56	183.22	190.74	181.18	2.04	97.00	100.00
50	71	180.08	183.85	191.63	180.32	2.09	97.00	100.00
51	72	182.51	185.36	191.24	183.53	1.56	97.00	100.00
52	73	180.77	184.16	191.16	180.84	1.88	100.00	100.00
53	73	180.34	183.65	190.45	182.10	1.84	100.00	100.00
54	74	181.89	184.90	191.09	182.46	1.65	100.00	100.00
55	74	182.88	185.90	192.18	183.60	1.65	100.00	100.00
56	75	184.06	187.20	193.82	182.97	1.71	100.00	100.00
57	75	183.12	186.20	192.62	183.28	1.68	100.00	100.00
58	76	182.56	185.59	191.89	182.50	1.66	100.00	100.00
59	76	182.67	185.93	192.73	182.50	1.78	100.00	100.00
60	77	180.06	183.64	191.01	181.09	1.99	100.00	100.00
61	78	179.84	182.93	189.21	181.63	1.72	73.00	100.00
62	78	181.25	184.39	190.84	181.26	1.73	73.00	100.00
63	79	179.28	183.18	191.23	180.73	2.18	73.00	100.00
64	79	180.72	184.38	191.99	181.56	2.03	73.00	100.00
65	80	184.40	187.31	193.42	184.63	1.58	73.00	100.00
66	81	185.57	188.46	194.57	184.44	1.56	73.00	100.00

Table 9: CoreLok Calculations

Test No.	Depth	Bag Weight	Dry Sample Weight Before Sealing	Sealed Sample Weight in Water	Dry Sample Weight After Water Submersion	Ratio of C_B/C_A	Bag Apparent Gravity	Total Volume	Volume of Bag	Volume of Sample	CoreLok Unit Weight
	ft	g	g	g	g						pcf
		C_A	C_B	C_C	C_D	C_E	C_F	C_G	C_H	C_I	γ_{CL}
1	25	26.8	1027.0	599.7	1027.1	38.3	0.790	454.2	33.9	420.3	152.5
2	26	26.9	964.9	564.0	964.8	35.9	0.791	427.7	34.0	393.7	152.9
3	26	27.0	939.8	541.1	939.8	34.8	0.792	425.7	34.1	391.6	149.7
4	27	26.7	981.8	585.6	981.8	36.8	0.791	422.9	33.8	389.1	157.4
5	29	27.0	1024.8	615.6	1024.7	38.0	0.790	436.1	34.2	401.9	159.1
6	29	27.2	1005.4	602.2	1005.3	37.0	0.791	430.3	34.4	395.9	158.5
7	31	27.2	944.8	536.8	944.7	34.7	0.792	435.1	34.3	400.8	147.1
8	31	27.2	991.8	583.6	991.9	36.5	0.791	435.5	34.4	401.1	154.3
9	32	27.0	953.7	547.9	953.7	35.3	0.792	432.8	34.1	398.7	149.3
10	32	26.9	975.9	568.2	975.9	36.3	0.791	434.6	34.0	400.6	152.0
11	33	26.7	1018.9	615.5	1018.9	38.2	0.790	430.1	33.8	396.3	160.4
12	34	26.8	1030.3	629.4	1030.2	38.4	0.790	427.6	33.9	393.7	163.3
13	35	26.5	1030.7	626.7	1030.5	38.9	0.790	430.3	33.6	396.7	162.1
14	35	26.5	1042.0	636.0	1042.1	39.3	0.789	432.6	33.6	399.0	162.9
15	36	26.7	1038.0	630.5	1038.0	38.9	0.790	434.2	33.8	400.4	161.8
16	36	27.2	976.2	570.7	976.2	35.9	0.791	432.7	34.4	398.3	152.9
17	37	26.5	1004.9	595.1	1005.0	37.9	0.790	436.4	33.5	402.9	155.6
18	37	26.6	952.9	546.6	952.9	35.8	0.792	432.9	33.6	399.3	148.9
19	38	26.4	1046.3	642.2	1046.2	39.6	0.789	430.4	33.5	396.9	164.5
20	38	26.7	1037.3	630.0	1037.3	38.9	0.790	434.0	33.8	400.2	161.7
21	39	26.4	1027.0	624.6	1027.0	38.9	0.790	428.8	33.4	395.4	162.1
22	39	26.5	1002.8	594.8	1002.8	37.8	0.790	434.5	33.5	401.0	156.1
23	40	27.2	963.9	557.3	963.5	35.4	0.792	433.4	34.4	399.0	150.7
24	40	26.8	1033.5	626.0	1033.5	38.6	0.790	434.3	33.9	400.4	161.1
25	41	27.3	1024.4	621.5	1024.4	37.5	0.790	430.2	34.5	395.7	161.6
26	42	27.4	1000.0	595.5	1000.0	36.5	0.791	431.9	34.6	397.3	157.1
27	45	27.0	958.4	554.6	958.4	35.5	0.792	430.8	34.1	396.7	150.8
28	45	26.6	880.3	481.0	880.3	33.1	0.793	425.9	33.5	392.4	140.0
29	48	26.6	1001.5	595.9	1001.5	37.7	0.790	432.2	33.7	398.5	156.8
30	48	26.7	962.5	560.6	962.6	36.0	0.791	428.7	33.7	395.0	152.1
31	49	26.6	946.7	549.1	946.6	35.6	0.792	424.1	33.6	390.5	151.3
32	49	26.9	1023.1	617.7	1023.1	38.0	0.790	432.3	34.0	398.3	160.3
33	50	26.8	883.1	477.7	882.9	33.0	0.793	432.0	33.8	398.2	138.4
34	51	26.6	860.3	455.2	860.3	32.3	0.794	431.7	33.5	398.2	134.8
35	53	26.2	842.1	437.1	842.0	32.1	0.794	431.1	33.0	398.1	132.0

Table 9: CoreLok Calculations (continued)

Test No.	Depth	Bag Weight	Dry Sample Weight Before Sealing	Sealed Sample Weight in Water	Dry Sample Weight After Water Submersion	Ratio of C_B/C_A	Bag Apparent Gravity	Total Volume	Volume of Bag	Volume of Sample	CoreLok Unit Weight
	ft	g	g	g	g						pcf
		C_A	C_B	C_C	C_D	C_E	C_F	C_G	C_H	C_I	γ_{CL}
36	53	26.7	802.8	401.0	802.6	30.1	0.795	428.3	33.6	394.7	126.9
37	54	26.9	817.0	415.0	817.0	30.4	0.795	428.9	33.8	395.1	129.0
38	55	26.6	751.1	362.0	750.8	28.2	0.796	415.4	33.4	382.0	122.7
39	55	26.8	807.4	408.6	807.4	30.1	0.795	425.6	33.7	391.9	128.6
40	57	27.0	1157.9	754.1	1157.8	42.9	0.788	430.7	34.3	396.4	182.3
41	58	26.5	1154.4	744.1	1154.6	43.6	0.787	437.0	33.7	403.3	178.6
42	58	27.3	1149.0	728.7	1148.8	42.1	0.788	447.4	34.6	412.8	173.7
43	59	27.3	1160.5	636.6	1160.6	42.5	0.788	551.3	34.7	516.6	140.2
44	68	26.8	1163.0	753.6	1162.9	43.4	0.787	436.1	34.0	402.1	180.5
45	68	27.3	1157.7	750.0	1157.8	42.4	0.788	435.1	34.7	400.4	180.4
46	69	27.1	1156.7	747.8	1156.6	42.7	0.788	435.9	34.4	401.5	179.8
47	69	26.8	1159.3	750.0	1159.4	43.3	0.787	436.2	34.0	402.2	179.9
48	70	27.1	1179.4	770.5	1179.2	43.5	0.787	435.8	34.4	401.4	183.4
49	71	26.7	1163.1	755.2	1163.0	43.6	0.787	434.5	33.9	400.6	181.2
50	71	27.2	1154.1	747.1	1153.8	42.4	0.788	433.9	34.5	399.4	180.3
51	72	26.8	1178.4	770.4	1178.3	44.0	0.787	434.7	34.1	400.6	183.5
52	73	26.8	1167.2	757.3	1167.3	43.6	0.787	436.8	34.0	402.8	180.8
53	73	26.9	1154.3	751.5	1154.3	42.9	0.788	429.7	34.2	395.5	182.1
54	74	27.2	1168.6	761.5	1168.5	43.0	0.788	434.2	34.5	399.7	182.5
55	74	26.9	1181.4	772.5	1181.3	43.9	0.787	435.7	34.2	401.5	183.6
56	75	26.7	1177.5	768.5	1177.3	44.1	0.787	435.5	33.9	401.6	183.0
57	75	26.4	1184.4	773.9	1184.3	44.9	0.787	436.8	33.6	403.2	183.3
58	76	26.9	1179.3	768.7	1179.2	43.8	0.787	437.4	34.2	403.2	182.5
59	76	26.7	1177.7	767.8	1177.7	44.1	0.787	436.6	33.9	402.7	182.5
60	77	26.6	1157.4	751.3	1157.3	43.5	0.787	432.6	33.8	398.8	181.1
61	78	27.1	1169.8	760.5	1169.7	43.2	0.787	436.3	34.4	401.9	181.6
62	78	27.1	1173.8	762.4	1173.8	43.3	0.787	438.5	34.4	404.1	181.3
63	79	26.9	1167.3	757.1	1167.4	43.4	0.787	437.2	34.2	403.0	180.7
64	79	26.5	1179.0	766.5	1178.9	44.5	0.787	438.9	33.7	405.2	181.6
65	80	27.4	1203.6	789.1	1203.3	43.9	0.787	441.6	34.8	406.8	184.6
66	81	26.7	1195.8	784.0	1195.8	44.8	0.787	438.5	33.9	404.6	184.4

Table 10: Strength and Stiffness Parameters of Basalt Samples

Test No.	Sample Depth	Unconfined Compressive Strength	Young's Modulus	Axial Strain at Failure	Axial Strain at 50% Strength	Failure Type	Failure Plane Angle to Horizontal
	(ft)	(ksi)	(ksi)	(%)	(%)		(Degrees)
		q_u	E	ε_{af}	ε_{a50}		α
1	25	10.01	8100	N/D	0.07	STF	N/A
2	26	6.55	6600	0.46	0.05	MFF	N/A
3	26	8.98	6800	0.13	0.07	MFF	N/A
4	27	9.82	7200	0.16	0.07	DPF	75
5	29	13.89	7600	N/D	0.09	DPF	75
6	29	12.77	7000	N/D	0.09	DPF	70
7	31	4.42	4400	0.22	0.05	MFF	N/A
8	31	9.69	7400	0.13	0.07	MFF	N/A
9	32	5.27	5200	0.21	0.05	MFF	N/A
10	32	4.92	4700	0.16	0.05	MFF	N/A
11	33	10.32	7700	N/D	0.07	MFF	N/A
12	34	9.55	7500	N/D	0.06	MFF	N/A
13	35	9.50	8500	N/D	0.06	DPF	75
14	35	15.84	7900	N/D	0.10	DPF	70
15	36	14.92	6600	N/D	0.11	DPF	65
16	36	3.59	1900	0.18	0.09	DPF	10
17	37	8.05	7500	0.06	0.05	DPF	70
18	37	5.22	4700	0.33	0.10	MFF	N/A
19	38	9.65	10000	0.12	0.05	DPF	70
20	38	15.78	5800	N/D	0.13	STF	N/A
21	39	21.75	6300	N/D	N/D	STF	N/A
22	39	13.43	7100	N/D	0.10	DPF	90
23	40	2.55	2000	0.43	0.07	DPF	40
24	40	18.70	8600	N/D	0.11	DPF	90
25	41	8.21	7000	0.13	0.06	DPF	70
26	42	9.40	6300	0.17	0.08	DPF	60
27	45	7.83	5800	0.58	0.07	MFF	N/A
28	45	2.16	1900	0.23	0.06	MFF	N/A
29	48	11.81	6700	N/D	0.09	DPF	80
30	48	9.77	6100	N/D	0.08	MFF	N/A
31	49	6.05	4700	0.29	0.07	DPF	60
32	49	10.99	6500	N/D	0.09	DPF	80
33	50	5.94	4900	0.15	0.06	DPF	80
34	51	5.00	4500	0.16	0.06	DPF	50
35	53	2.36	4600	0.05	0.03	DPF	5
36	53	4.11	3200	0.17	0.07	DPF	55
37	54	4.55	3300	0.21	0.07	DPF	70

Table 10: Strength and Stiffness Parameters of Basalt Samples (continued)

Test No.	Sample Depth (ft)	Unconfined Compressive Strength (ksi) q_u	Young's Modulus (ksi) E	Axial Strain at Failure (%) ε_{af}	Axial Strain at 50% Strength (%) ε_{a50}	Failure Type	Failure Plane Angle to Horizontal (Degrees) α
38	55	2.44	2200	0.15	0.06	DPF	70
39	55	3.37	3500	0.15	0.05	DPF	60
40	57	10.20	9700	N/D	0.06	N/A	N/A
41	58	29.99	11900	N/D	N/D	STF	N/A
42	58	40.50	10600	N/D	N/D	STF	N/A
43	59	33.98	13300	N/D	N/D	STF	N/A
44	68	23.47	10000	N/D	N/D	STF	N/A
45	68	26.91	10600	N/D	N/D	STF	N/A
46	69	21.21	10000	N/D	N/D	STF	N/A
47	69	26.72	9800	N/D	N/D	STF	N/A
48	70	32.55	10900	N/D	N/D	STF	N/A
49	71	25.29	10500	N/D	N/D	STF	N/A
50	71	21.42	9400	N/D	N/D	STF	N/A
51	72	15.09	7800	N/D	0.10	DPF	90
52	73	22.02	9700	N/D	N/D	DPF	75
53	73	24.88	10100	N/D	N/D	STF	N/A
54	74	30.70	11000	N/D	N/D	DPF	60
55	74	30.59	10700	N/D	N/D	STF	N/A
56	75	28.85	10800	N/D	N/D	DPF	60
57	75	28.96	9500	N/D	N/D	DPF	60
58	76	23.25	9900	N/D	N/D	MFF	N/A
59	76	24.47	9400	N/D	N/D	STF	N/A
60	77	22.42	9000	N/D	N/D	STF	N/A
61	78	25.49	10700	N/D	N/D	DPF	75
62	78	29.56	10800	N/D	N/D	STF	N/A
63	79	24.47	9500	N/D	N/D	DPF	60
64	79	23.04	10000	N/D	N/D	STF	N/A
65	80	34.69	12600	N/D	N/D	STF	N/A
66	81	33.86	12000	N/D	N/D	STF	N/A

N/D – Not determined N/A – Not applicable

3.2 Trends with Depth

From a depth of 25 feet to a depth of 49 feet, the OD unit weight stayed fairly constant, ranging between 142 pcf and 163 pcf (Figure 19). Between 50 and 55 feet, there is a noticeable drop in OD unit weight to between 123 and 138 pcf, while between 57 feet and 81 feet the OD unit weight increases to 172 to 186 pcf. There were no samples tested between 60 and 68 feet depth. Similar trends can be seen with the SSD and apparent unit weights (Figures 20 and 21), as well as the weight derived from the CoreLok (Figure 22). The absorption between 25 and 49 feet depth ranged between 3 to 7 percent, while it ranged between 8 to 12 percent between 50 and 55 feet depth (Figure 23). From 57 to 81 feet the absorption ranged between 1 to 2 percent.

Variations in unit weight are accompanied by similar variations in unconfined compressive strength and stiffness. From a depth of 25 feet to a depth of 49 feet, the unconfined compressive strength ranged between 1 ksi to 11 ksi (Figure 24). Between 50 and 57 feet the strength was calculated to be between 1 ksi to 5 ksi, and between 58 and 81 feet the strength increases to roughly 7.5 ksi to 20 ksi. Notable differences in the Young's Modulus occurred between these depth intervals as well. From a depth of 25 feet to a depth of 55 feet the Young's Modulus fell between 2,000 to 10,000 ksi, whereas between 57 feet to 81 feet the Young's Modulus was calculated to be between 7,800 to 13,500 ksi (Figure 25). Roughly one-third of the samples between 25 feet to 55 feet depth did not fail on the 50-kip test frame, whereas no samples between 57 feet depth to 81 feet depth failed on the 50-kip test frame. Samples that failed on the 50-kip test frame had an axial strain between 0.05 and 0.46 percent at failure. Samples had an axial strain at 50% strength between 0.03 and 0.13 percent (Figures 26 and 27).

The RQD ranged between 87.5 and 100 percent between 25 to 51 feet, 50 to 70 percent between 53 to 59 feet, 97 to 100 percent between 68 and 77 feet, and 73 percent between 78 to 81 feet (Figure 28). The percent recovered was 100 percent for all samples except between 53 and 59 feet where it ranged between 53 and 70 percent (Figure 29).

There is a clear pattern in depth trends for the various unit weights, absorption, strength and stiffness. There is an upper unit of rock, between 25 and 55 feet characterized by lower unit weights, higher absorption and lower strength and stiffness, compared to the layer from 55 feet to 81 feet. This points to significantly different rock types, probably from different lava flows with somewhat different magma composition and viscosity. On the other hand, RQD, percent recovery and axial strain do not show discernible distinctions between these two rock units. These parameters appear to be less useful as indicators of rock types, at least as encountered in Boring B4.

Interestingly, some of the unit weights drop off considerably toward the 55-foot depth, whereas absorption increases markedly. If the upper layer indeed represents a separate later lava flow, it is possible that the bottom of this newer flow would have been of lower density and higher absorption than the upper portion. Either the fluid lava interacted with the cooled lower flow in unknown ways, or it had a different composition and viscosity.

The most likely explanation is that there are two different lava flows. The one from the Sugarloaf eruption, which was part of the Honolulu Volcanic Series, was a'a and was roughly 12 meters (39.4 feet) thick (Macdonald, 1983). Rock was encountered at 17.5 feet depth and a change in rock was noted at 55 to 60 feet. This would coincide with this separate lava flow. A'a rock has many vesicles, which would explain the lower unit weight, higher absorption, and lower strength relative to the rock that exists between 60 to 80 feet depth.

However, the time period between the Sugarloaf eruption and the last eruptions from the Koolau volcano was roughly two million years. If the Sugarloaf eruption was the only lava flow from the Honolulu Volcanic Series that flowed through Manoa, there would likely be a layer of soil between the two layers of rock between 55 and 60 feet depth, which is not present in the boring log. It is likely that both flows belong to the Honolulu Volcanic Series. Either both belong to the Sugarloaf vent or perhaps one belongs to the Tantalus vent. The soil profile from 87.5 feet depth to 95 feet depth, where the borehole was terminated, consisted of silts and clays, which appears to indicate a layer of topsoil that could have existed before the Honolulu Volcanic Series occurred.

Another explanation for the change in rock strength is that the rock has been weathered up to a depth of about 55 to 60 feet. Weathering can extend up to 30 meters (98.4 feet) below the ground surface (Brandes 2011) but it is possible that for this scenario it merely reached a depth of 55 or 60 feet. However this seems to be a weaker reason than assuming it was a different lava flow. If the rock layer from 17.5 feet depth to 81 feet depth was treated as a single lava flow, it would be roughly 20 meters thick, which does not match the 12 meter thick lava flow that Macdonald (1983) reported.

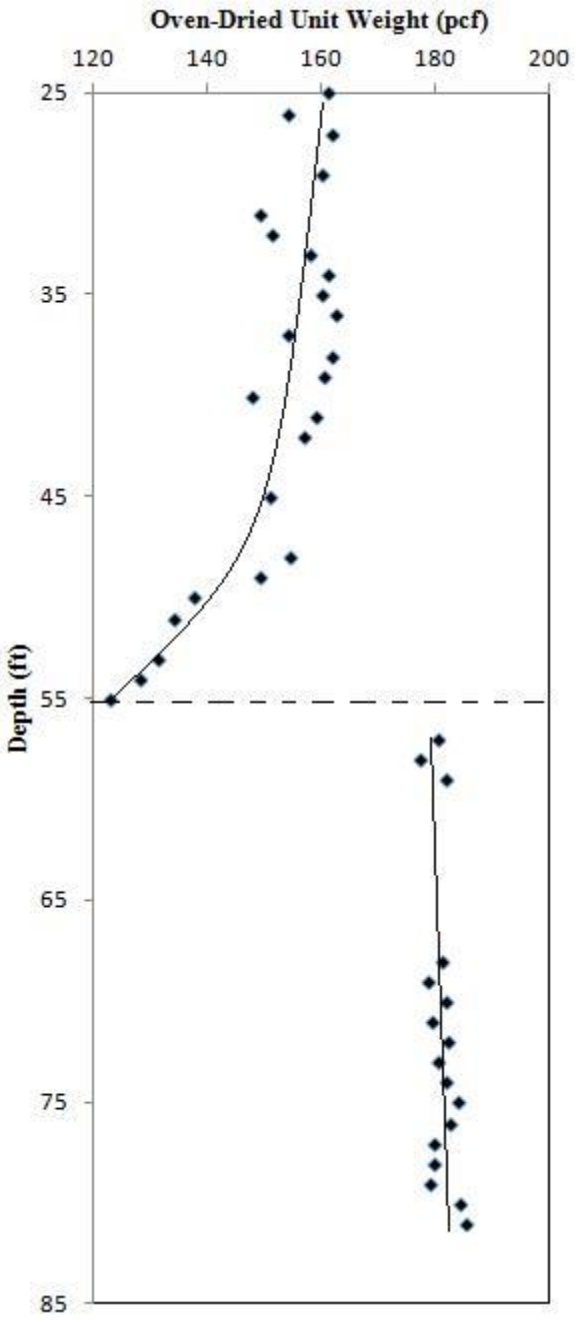

Figure 19: Oven-Dried Unit Weight versus Depth

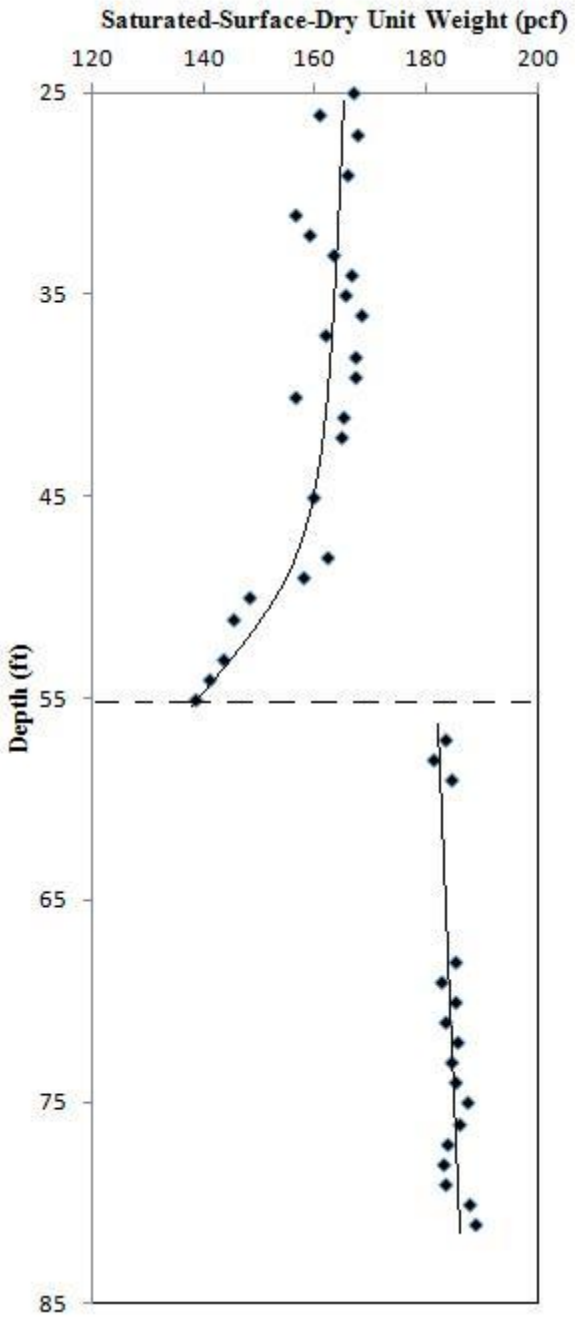

Figure 20: Saturated-Surface-Dry Unit Weight versus Depth

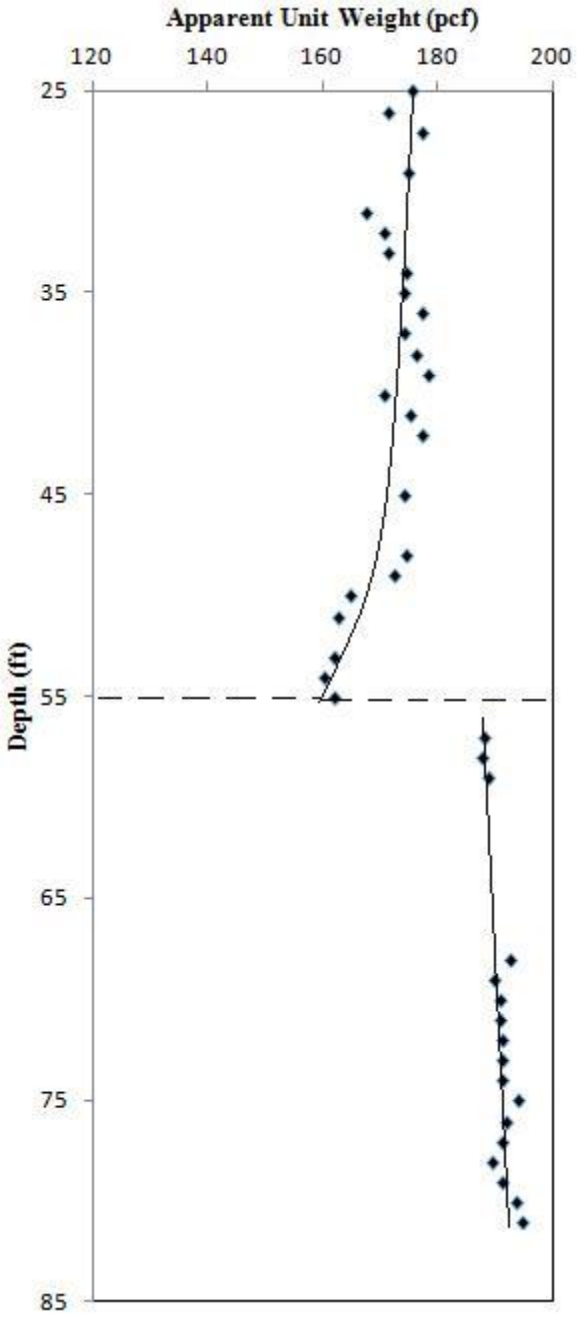

Figure 21: Apparent Unit Weight versus Depth

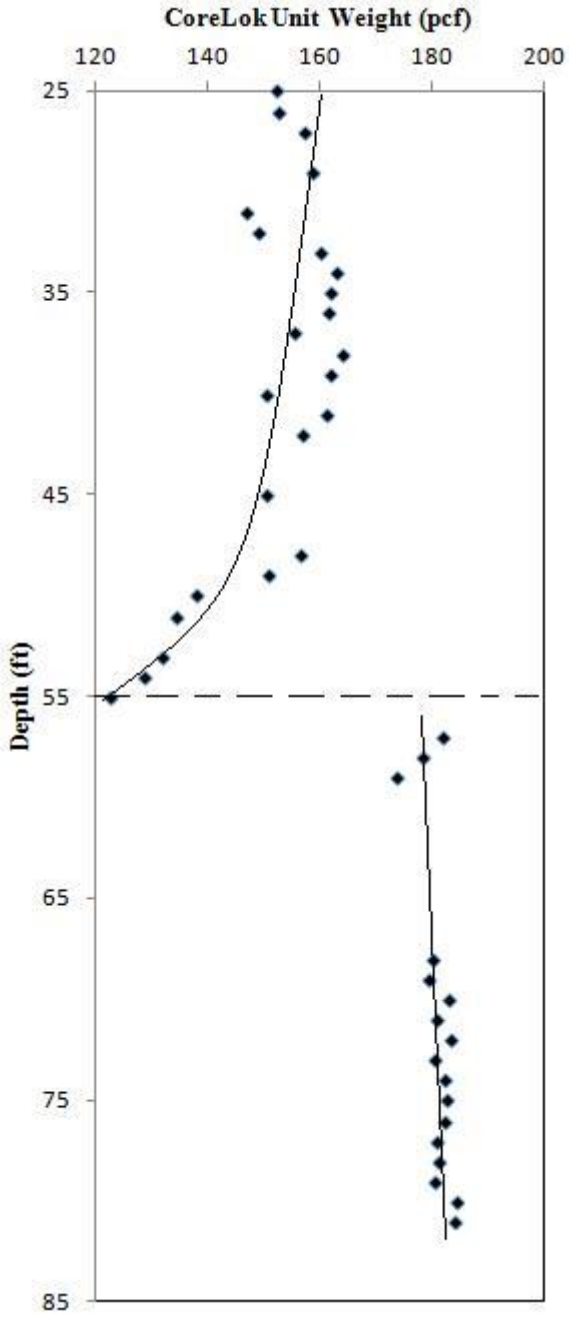

Figure 22: CoreLok Unit Weight versus Depth

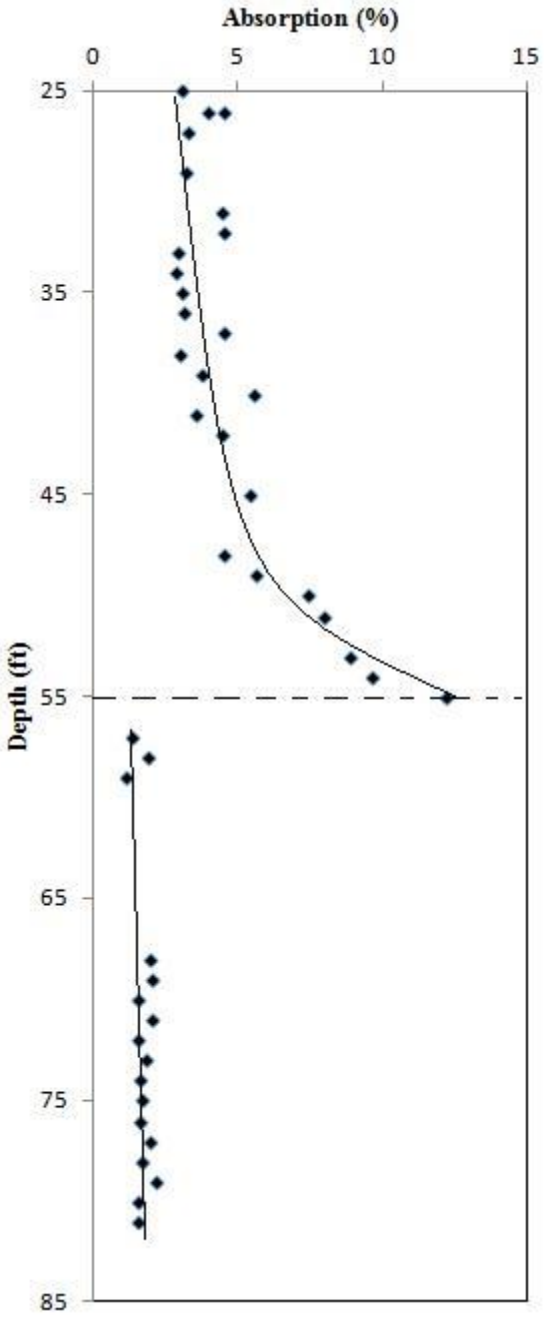

Figure 23: Absorption versus Depth

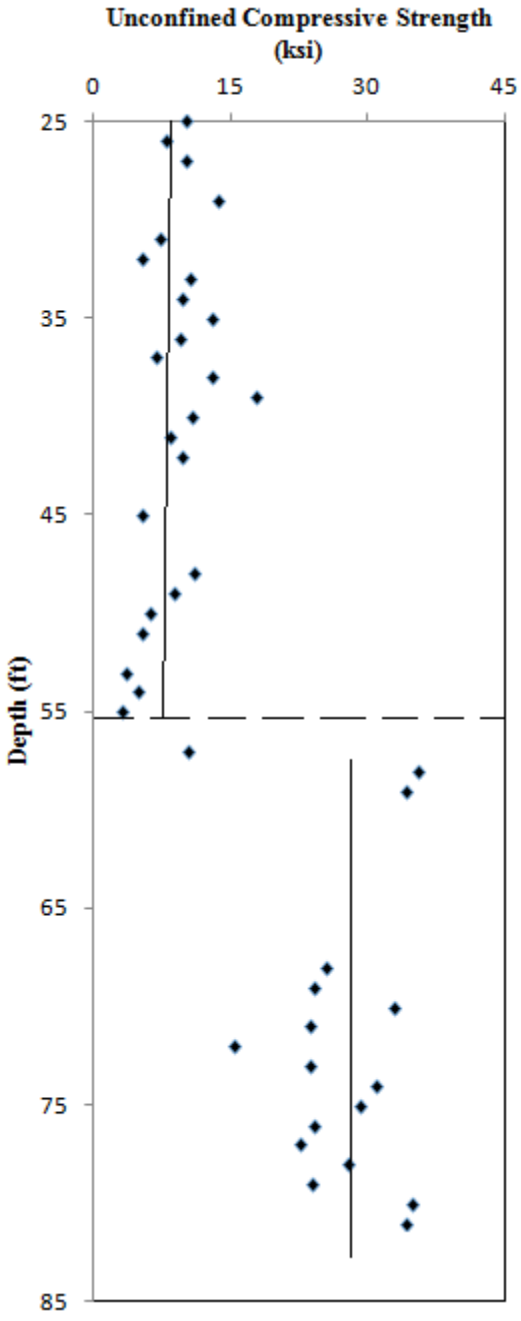

Figure 24: Unconfined Compressive Strength versus Depth

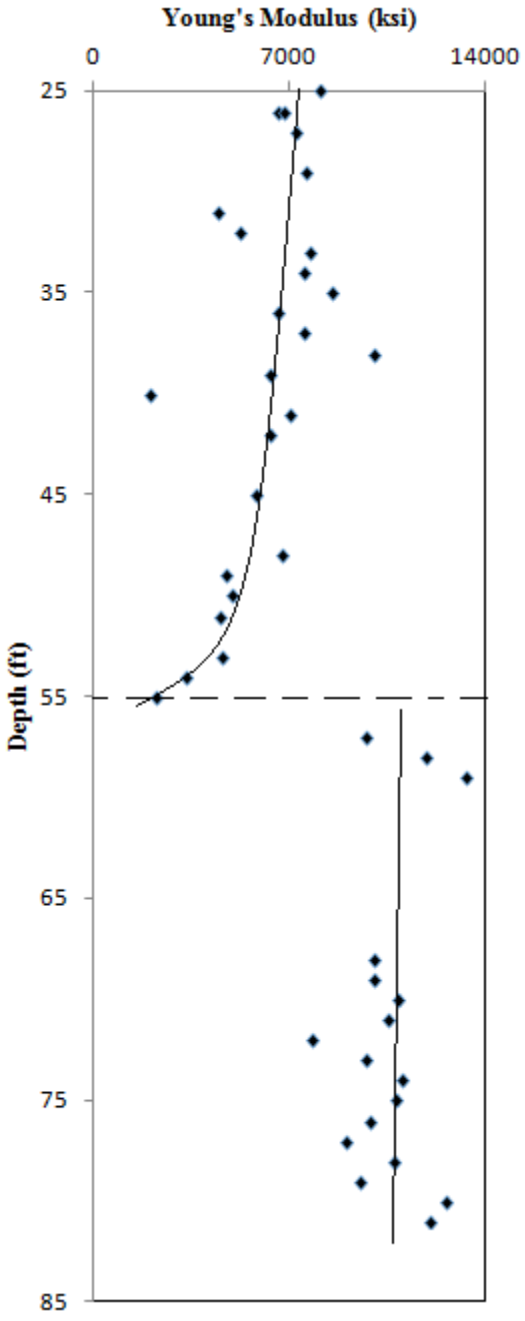

Figure 25: Young's Modulus versus Depth

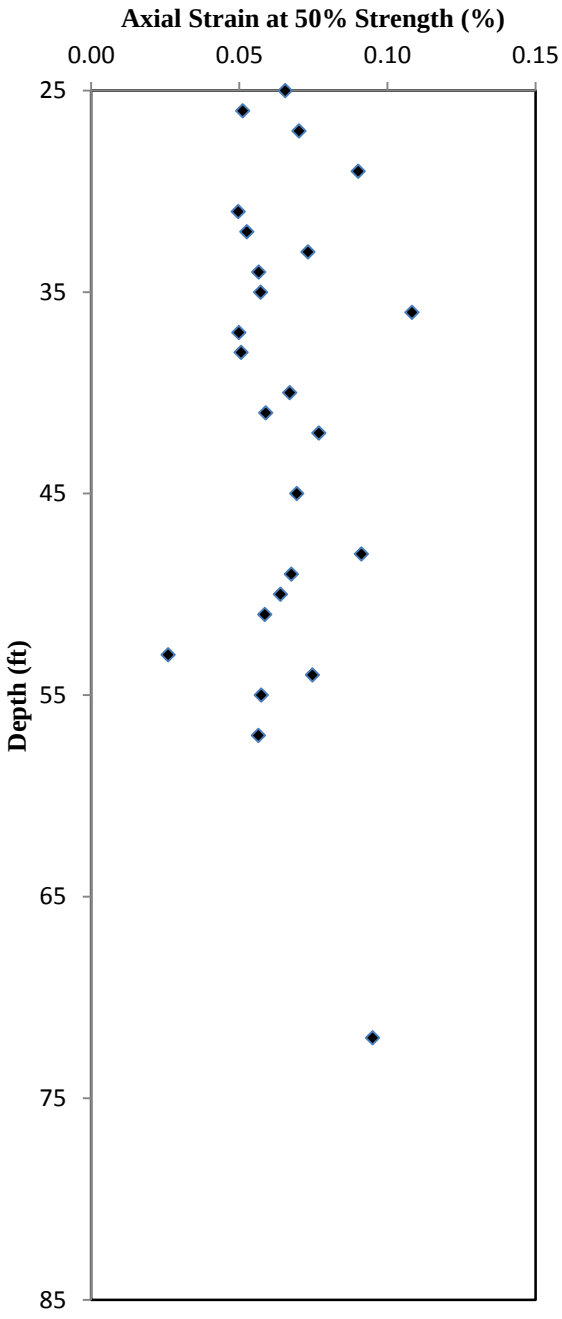

Figure 26: Axial Strain at 50% Strength versus Depth

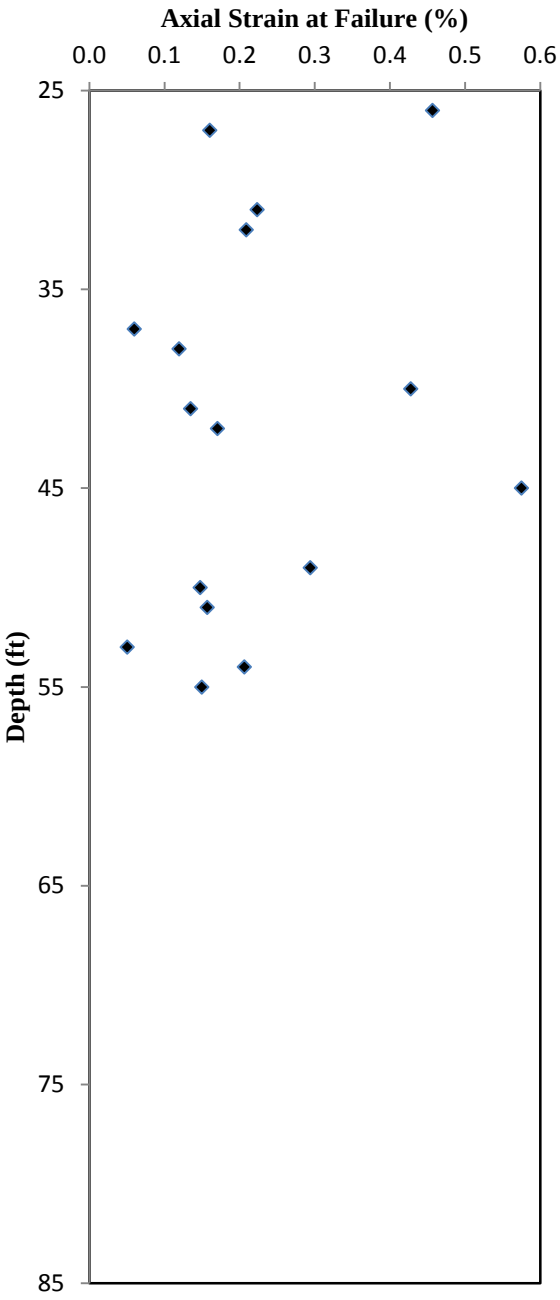

Figure 27: Axial Strain at Failure versus Depth

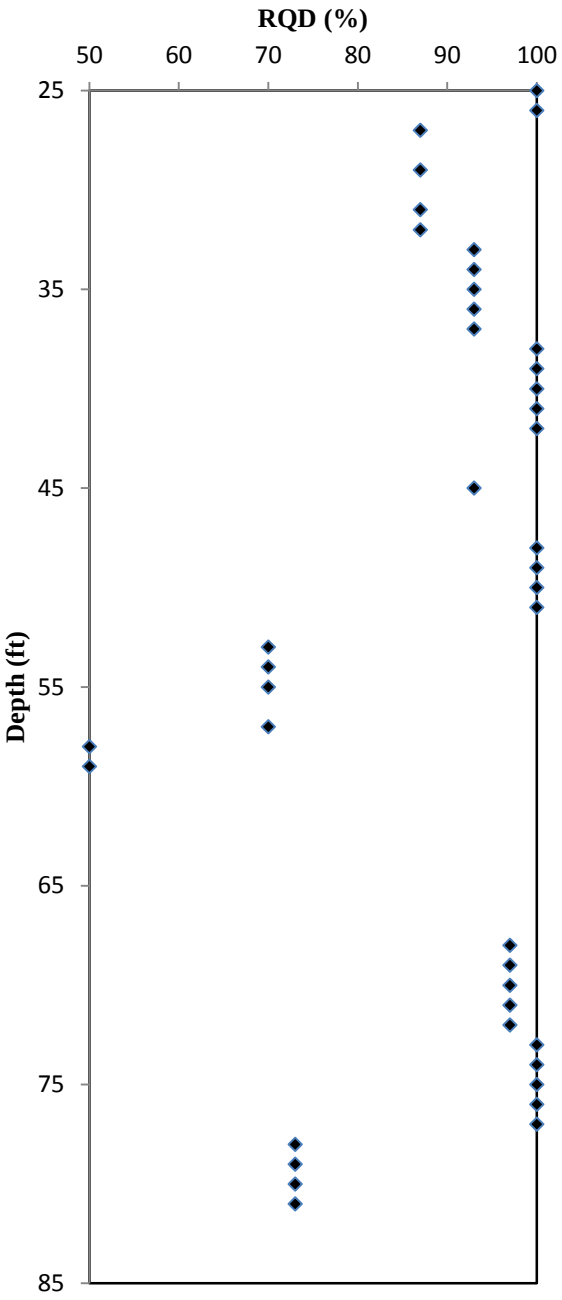

Figure 28: RQD versus Depth

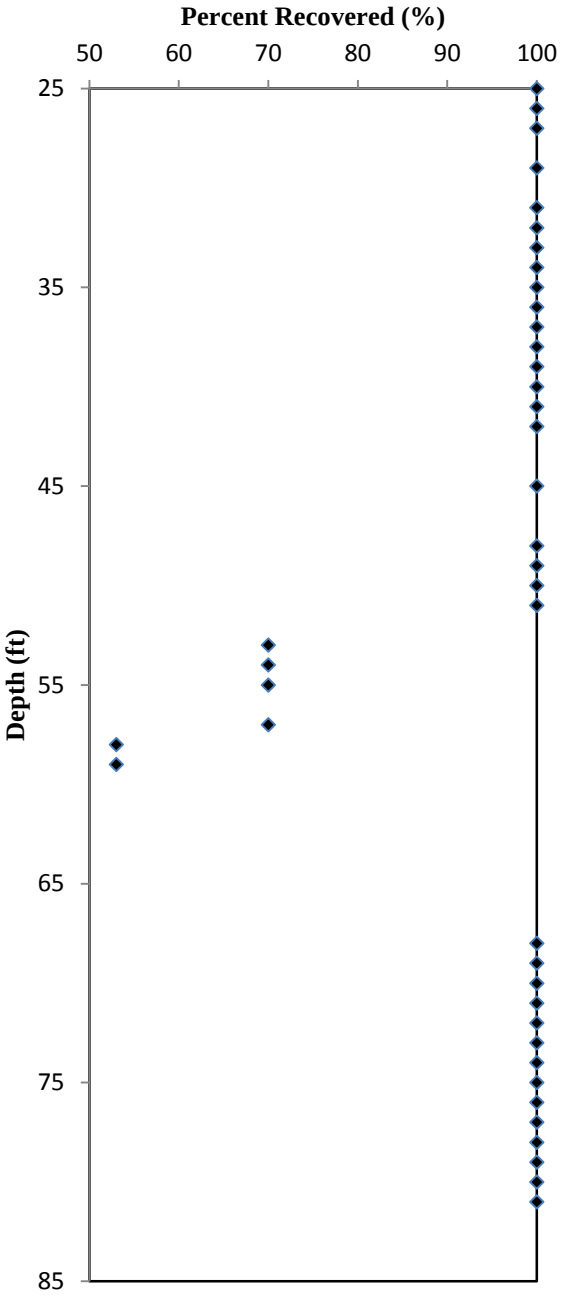

Figure 29: Percent Recovered versus Depth

3.3 Correlations among Parameters

As already mentioned, vertical trends suggest that there are at least some correlations worth exploring among index properties (unit weights, absorption, RQD, percent recovery) and parameters derived from the unconfined compression tests (strength, Young's modulus, axial strain). After considering all possible pairings, the following correlations are worth exploring. Included in the following discussion are the results from Brandes et al. (2011), who conducted similar tests also on Hawaiian basalt rock samples (although from the Big Island). He determined the unit weights and absorption of 22 samples, and performed triaxial tests and point load tests on seven of those samples, although the Young's modulus for one of these seven tests was not determined.

3.3.1 Absorption

Figures 30 through 33 compare the four unit weights determined in this study versus absorption. The test results show that all unit weights are inversely proportional to absorption but in a nonlinear manner. This makes sense intuitively. As absorption increases, the amount of voids increases and the bulk weight of rock specimens decreases.

The samples in this study have fairly high correlation coefficients, ranging between 0.87 and 0.97. The samples found in Brandes have lower values, between 0.70 and 0.78. The best correlation is observed with OD unit weight, although this is only marginally better than for the other types of unit weight. This was also noted in the study by Brandes et al. (2011). Correlation coefficients in that study were lower than in this one.

However, there are substantial differences between the values reported by Brandes et al. (2011) and this study. At unit weights less than about 150 pcf, absorption values by Brandes et al. (2011) are quite a bit lower. If absorption reflects porosity, then the solid rock mass of the specimens tested in this study would have a larger solid density. It should be pointed out that the specimens tested by Brandes et al. (2011) were surficial specimens and likely much younger than those from boring B4. Therefore rock mineralogy and degree of weathering may have been quite different. Differences between the two studies appear to decrease as unit weight increases past 160 pcf and absorption approaches 2% or less.

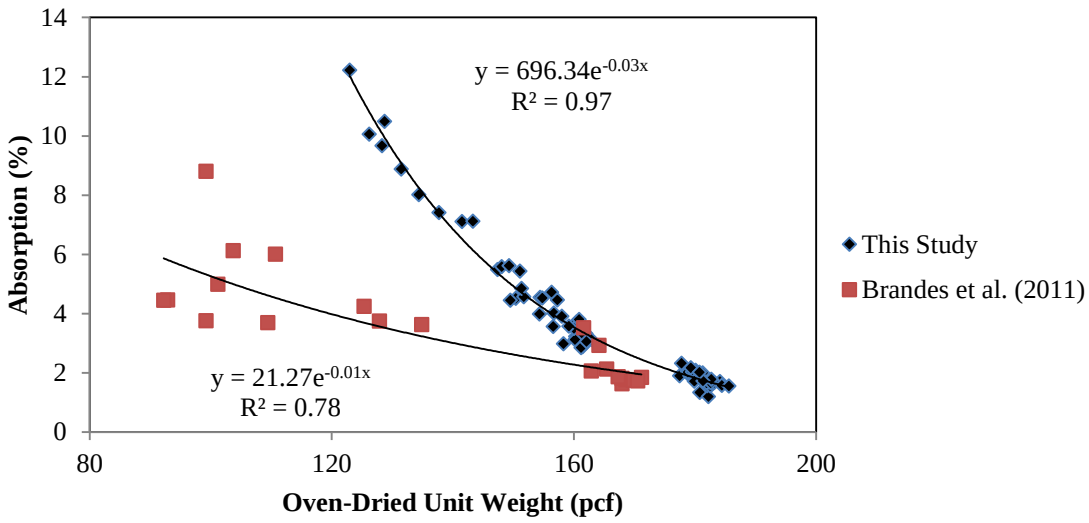

Figure 30: Oven-Dried Unit Weight versus Absorption

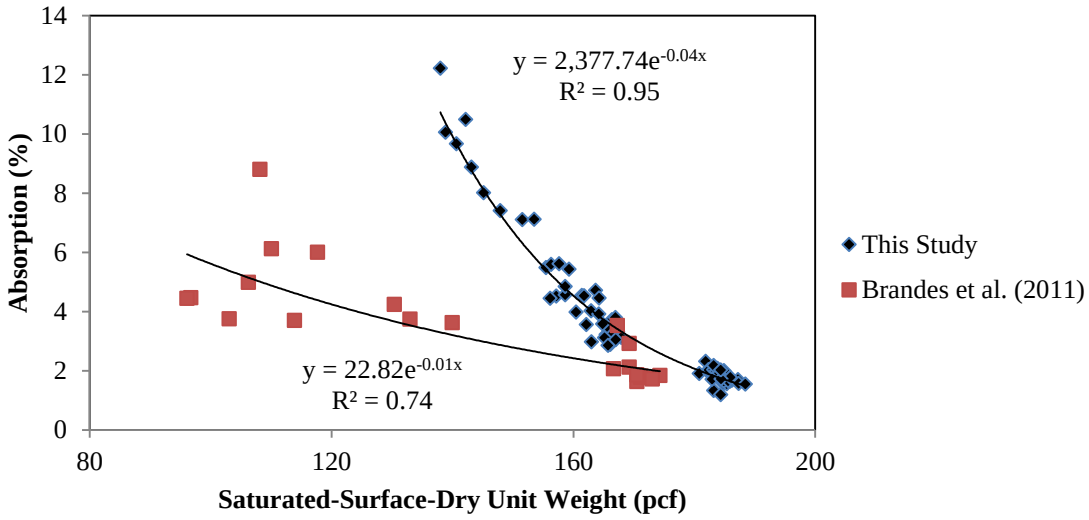

Figure 31: Saturated-Surface-Dry Unit Weight versus Absorption

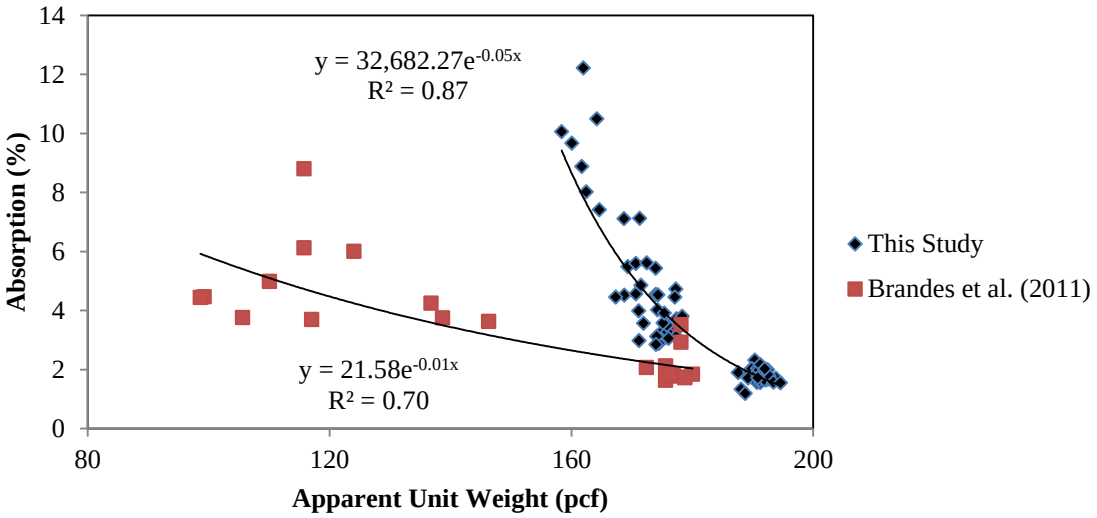

Figure 32: Apparent Unit Weight versus Absorption

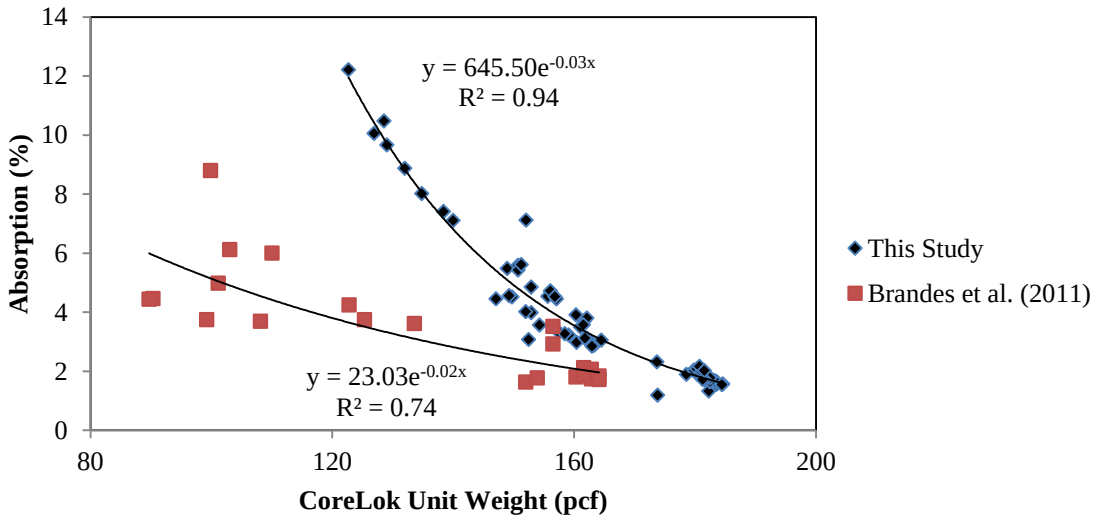

Figure 33: CoreLok Unit Weight versus Absorption

3.3.2 Unconfined Compressive Strength

Figures 34 through 37 compare all four unit weights versus unconfined compressive strength. Figure 38 shows absorption versus unconfined compressive. Based on the test results from this study and that by Brandes et al. (2011), all unit weights are proportional to unconfined compressive strength, while absorption is inversely proportional to unconfined compressive strength. The results again make sense intuitively. A rock with a high unit weight is expected to be stronger than a rock of the same type with a lower unit weight. A rock with lower absorption means the rock will have a higher unit weight as it has less voids, which results in higher strength.

The samples in this study have moderately high correlation coefficients for unit weights, ranging between 0.80 and 0.81, while the correlation coefficients for those from the Brandes et al. (2011) study ranged between 0.58 and 0.64. For absorption versus unconfined compressive strength, the correlation coefficient for this study was 0.77 which is slightly higher than in Brandes et al. (2011).

Similar to what was said in the previous section, for all four unit weight charts, there are many samples from Brandes et al. (2011) that are significantly different than the unit weights for the samples in this study. For example, the lowest oven-dried unit weight measured in this study was about 123 pcf, while four of the seven samples from Brandes et al. (2011) have a lower oven-dried unit weight than that. However the results from both tests are more similar for absorption versus unconfined compressive strength.

The unconfined compressive strength remains relatively constant up to a certain unit weight, between roughly 150 and 170 pcf depending on the exact unit weight, and then sharply increases. Similarly for absorption, the unconfined compressive strength is fairly constant for absorption higher than roughly 6 percent and then sharply increases as absorption decreases.

For Hawaiian basalt rocks as a whole, absorption appears to be a better indicator of unconfined compressive strength than unit weight. The absorption versus unconfined compressive strength plots from both studies overlap quite well, whereas the trendlines for unit weights versus unconfined compressive strength for both studies are quite different. This seems to indicate that the correlation between absorption and strength is less site-dependent than the correlation between unit weights and strength. For example, if a basalt rock from another site in Hawaii had its unit weights and absorption measured, it is more likely that its unconfined compressive strength could be more accurately determined with its absorption than its unit weight.

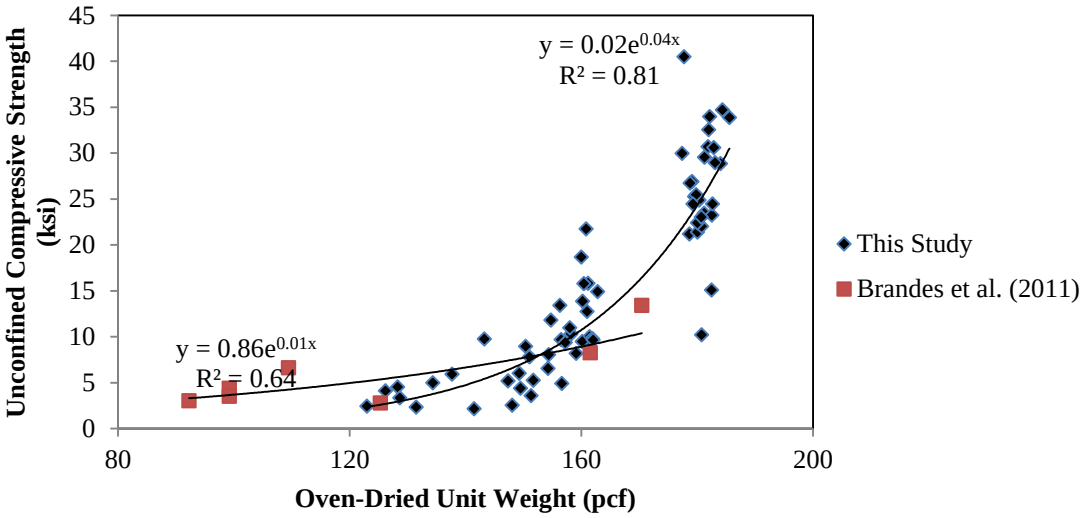

Figure 34: Oven-Dried Unit Weight versus Unconfined Compressive Strength

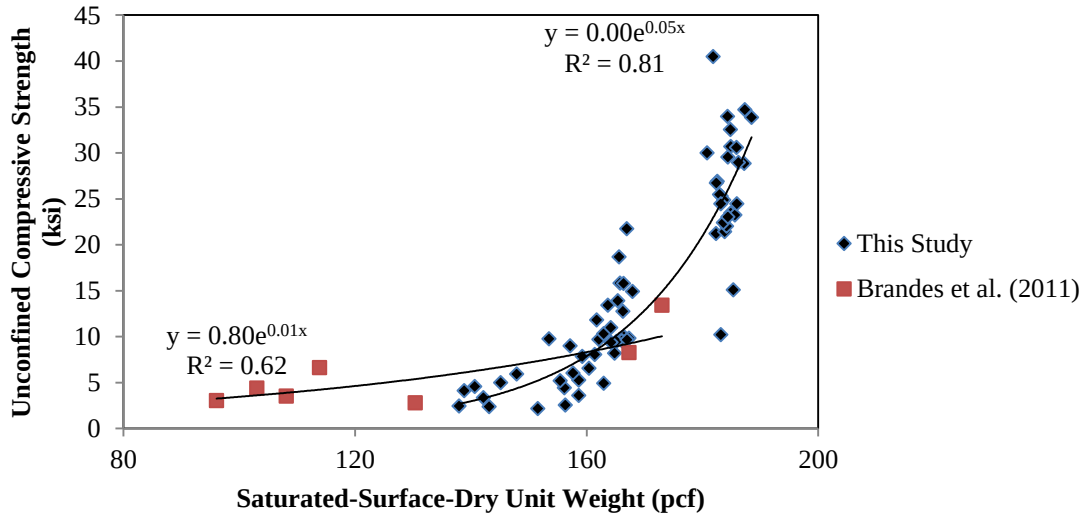

Figure 35: Saturated-Surface-Dry Unit Weight versus Unconfined Compressive Strength

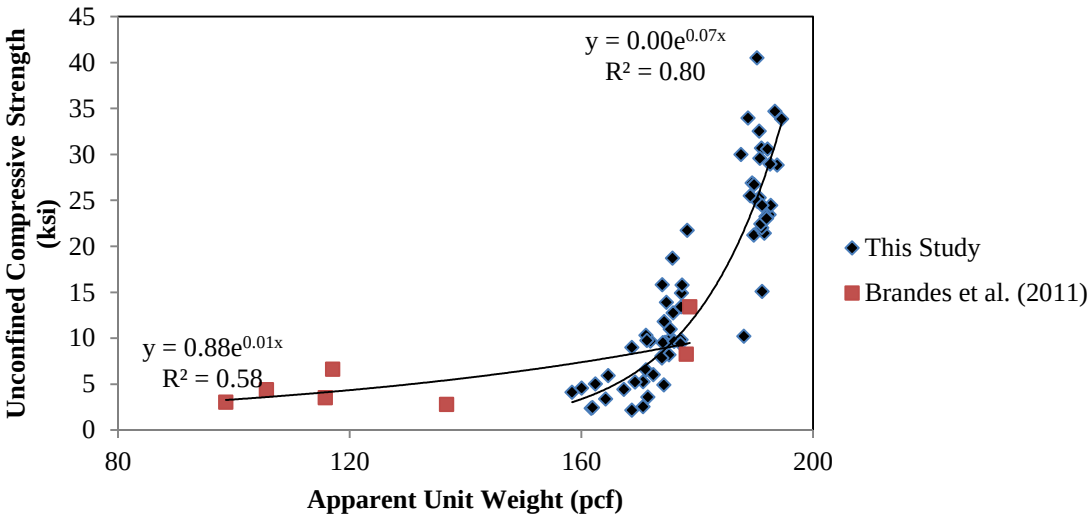

Figure 36: Apparent Unit Weight versus Unconfined Compressive Strength

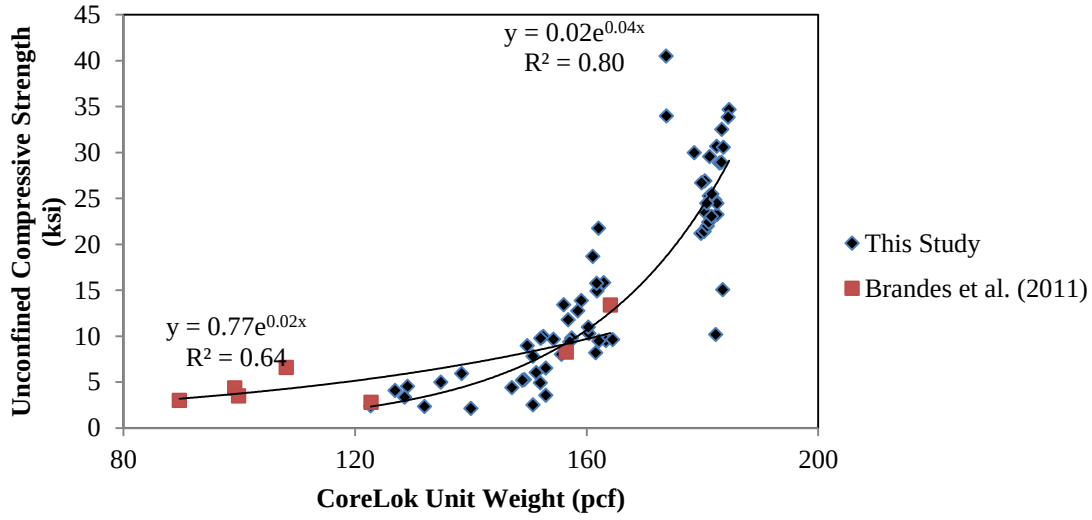

Figure 37: CoreLok Unit Weight versus Unconfined Compressive Strength

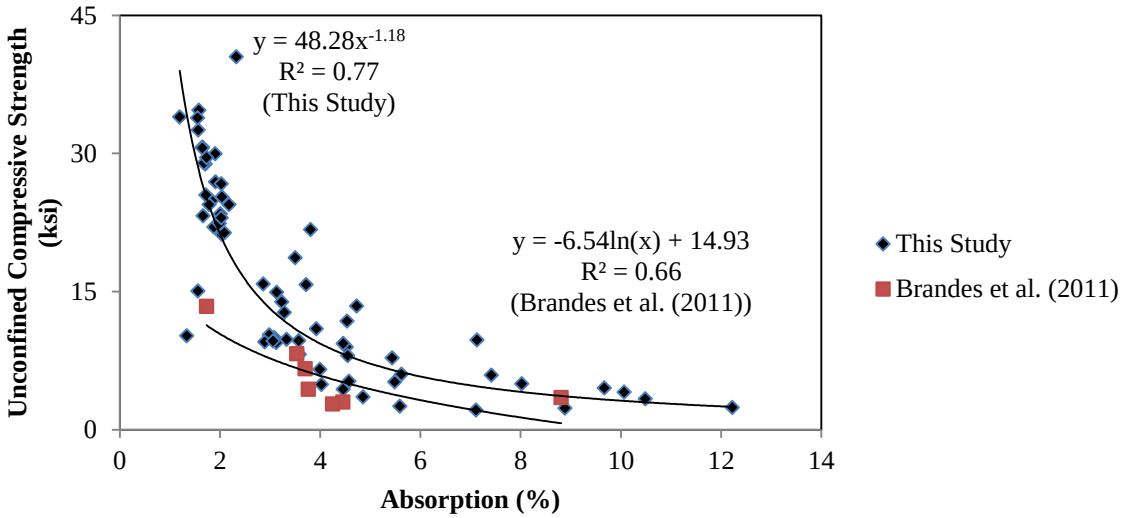

Figure 38: Absorption versus Unconfined Compressive Strength

3.3.3 Young's Modulus

Figures 39 through 42 depict unit weights versus Young's Modulus. Figure 43 compares absorption versus Young's Modulus and Figure 44 shows unconfined compressive strength versus Young's Modulus. The two studies show that unit weights and unconfined compressive strength are proportional to Young's Modulus, while absorption is inversely proportional to Young's Modulus. These results make sense intuitively as well. Rocks with a high Young's modulus typically are strong and have high unit weights and compressive strengths. Similarly, high absorption tends to indicate lower strengths and lower Young's moduli.

The correlation coefficients for unit weights versus Young's modulus were fairly high in this study, ranging between 0.77 and 0.80. However, the correlation coefficients in the Brandes et al. (2011) study ranged between 0.26 and 0.38. Such low values question whether there is any meaningful correlation at all in the Brandes et al. (2011) study. The trendlines are also very different from each other. For absorption versus Young's modulus, the correlation coefficients for both studies were high. For this study it was 0.81, while for Brandes et al. (2011) it was 0.90. The coefficient for unconfined compressive strength versus Young's modulus in this study was 0.86 and for Brandes et al. (2011) it was 0.68. The trendlines for both plots, in contrast with the trendlines for unit weights versus Young's modulus, almost overlap each other. The correlation coefficient for axial strain versus Young's modulus was 0.84, which is also high.

Similar observations as noted in the previous section apply here as well. Absorption and unconfined compressive strength appear to be stronger indicators of Young's modulus than unit

weight because the trendlines for both groups of samples have more overlap and similar slopes than the trendlines for the unit weights. The trendline for unconfined compressive strength versus Young's modulus are effectively identical for both studies as well, which makes sense as Young's modulus is based off of unconfined compressive strength.

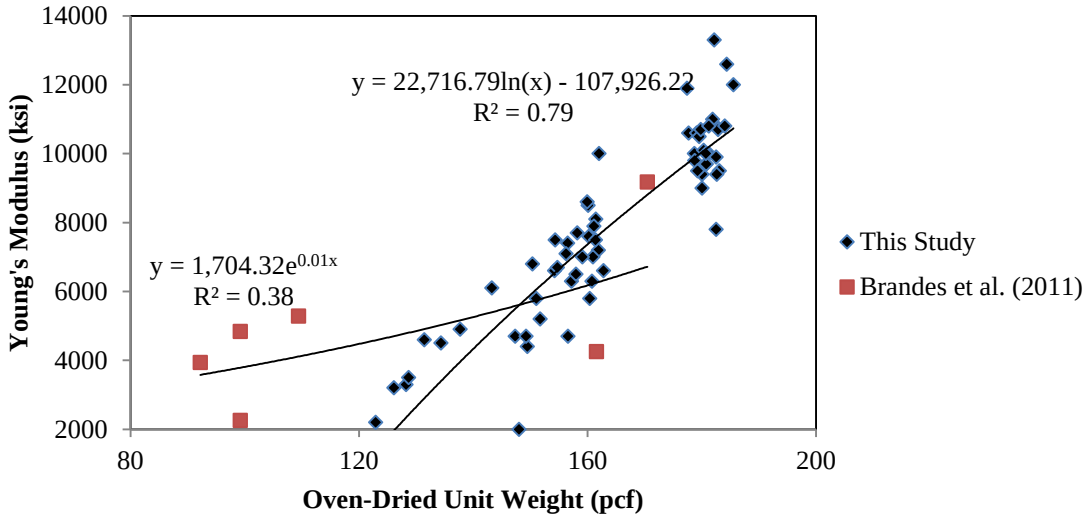

Figure 39: Oven-Dried Unit Weight versus Young's Modulus

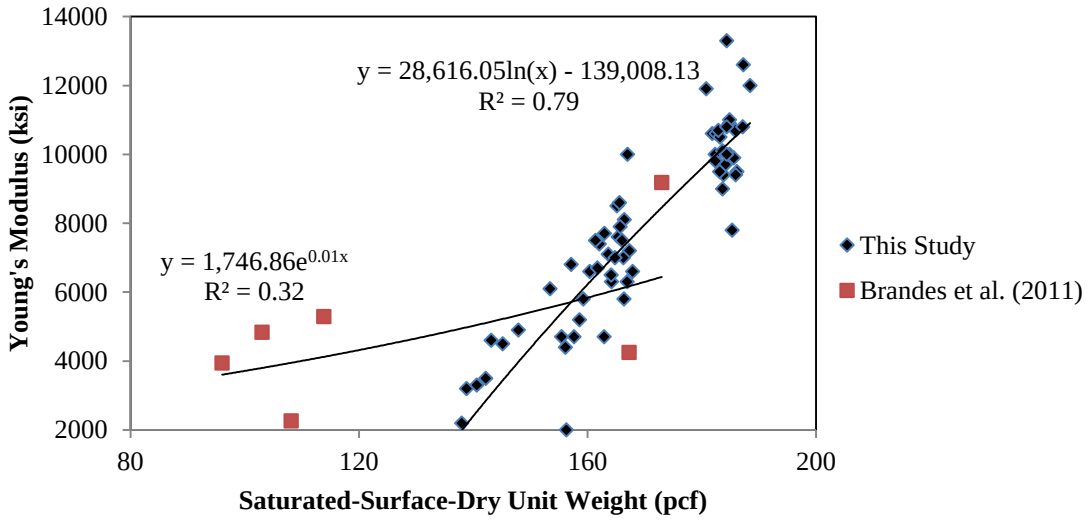

Figure 40: Saturated-Surface-Dry Unit Weight versus Young's Modulus

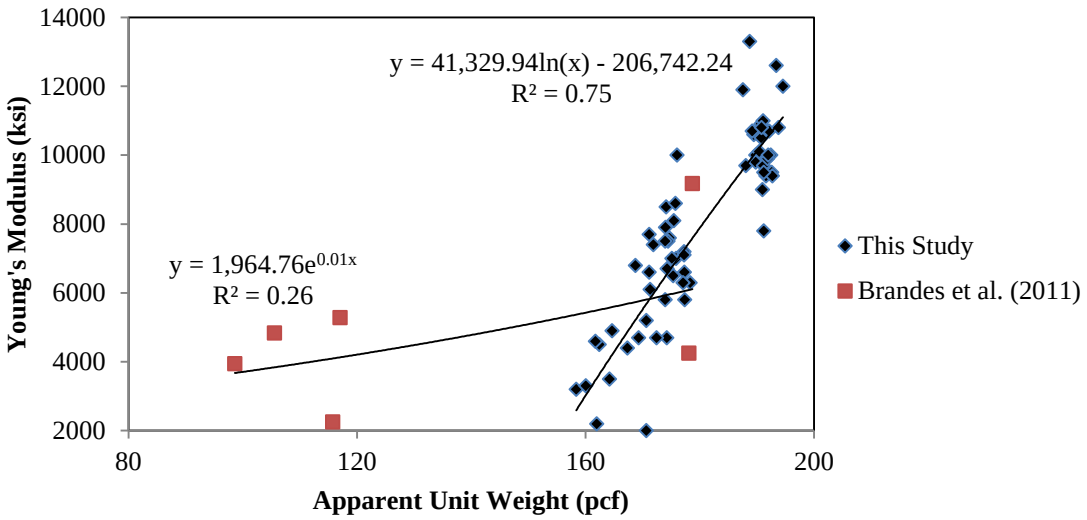

Figure 41: Apparent Unit Weight versus Young's Modulus

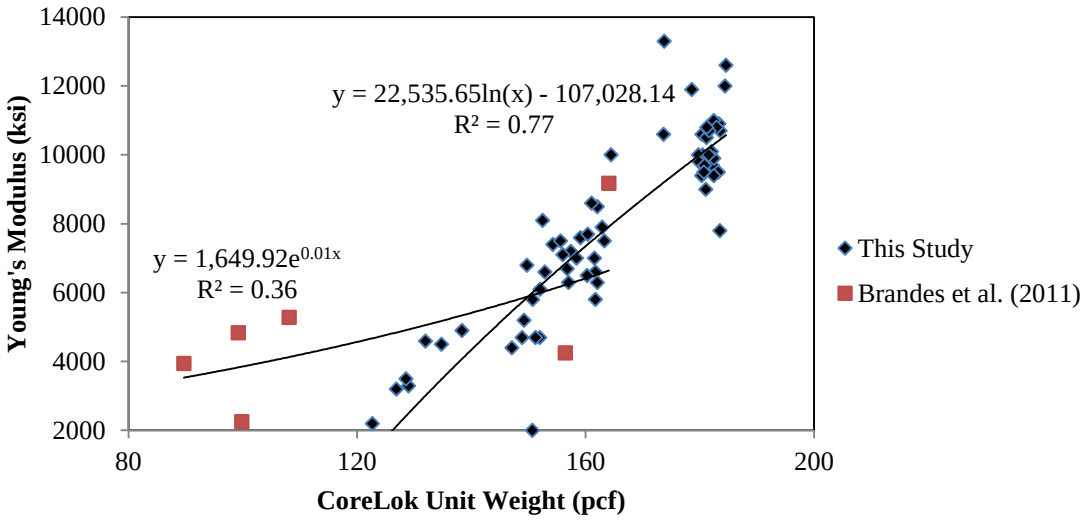

Figure 42: CoreLok Unit Weight versus Young's Modulus

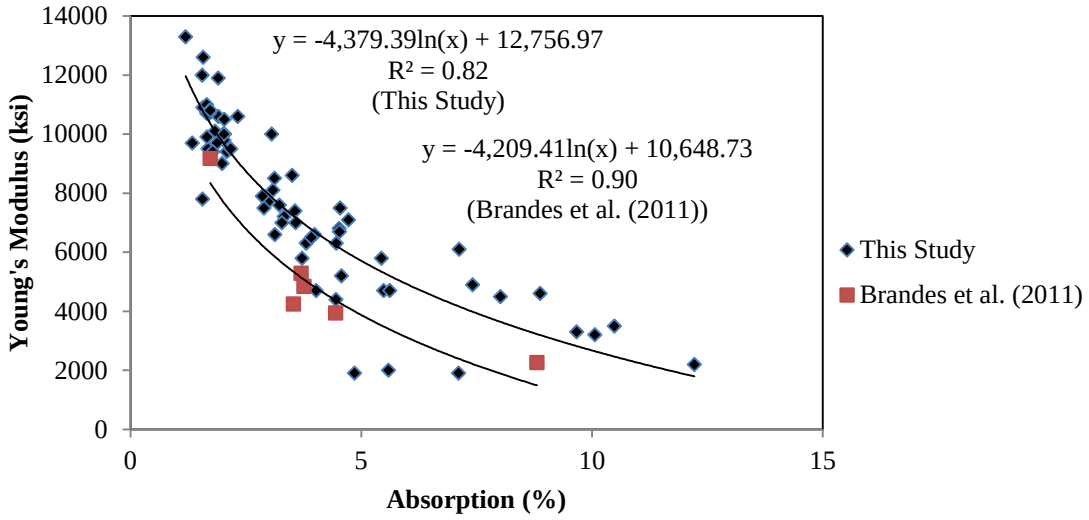

Figure 43: Absorption versus Young's Modulus

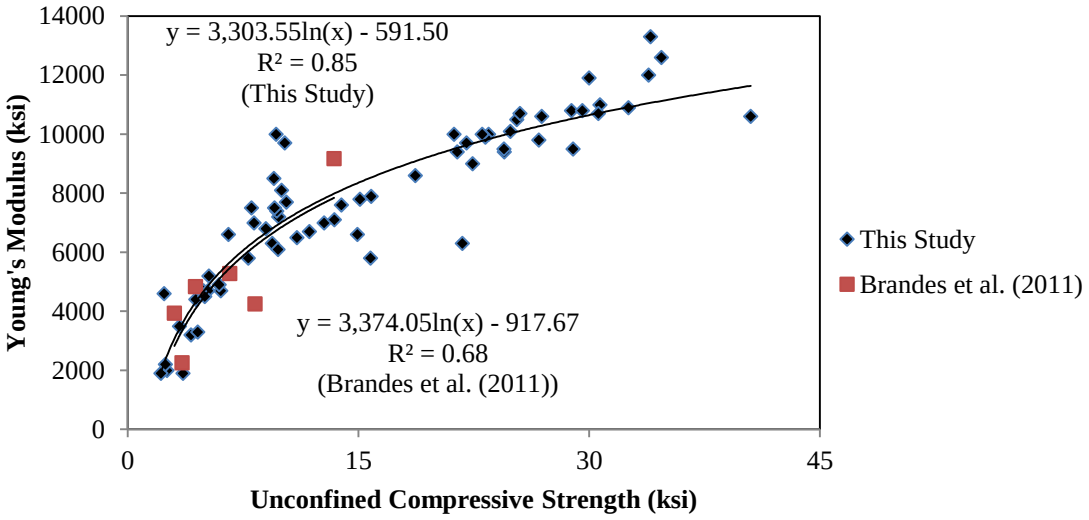

Figure 44: Unconfined Compressive Strength versus Young's Modulus

3.3.4 RQD, Percent Recovery, Axial Strain at Failure and Axial Strain at 50% Strength

Percent recovery displayed no discernible correlations to any of the index or strength parameters. Most of the boring log between 25 and 81 feet depth had 100 percent recovery, so a meaningful trendline could not be determined.

The same can be said about RQD. Out of the 66 samples, there were only seven unique values for RQD and no correlations with index or strength values could be determined.

Axial strain at failure versus any index or strength parameter yielded a widely scattered plot. No discernible trendline could be found and all attempted correlations yielded factors less than 0.1. Similarly, axial strain at 50% strength yielded compared to any index or strength parameter created scattered plots and coefficients of correlation less than 0.2.

3.4 Failure Patterns

Out of the 66 samples, 21 samples were determined to have a shatter-type failure mode (STF), 31 samples had a dominant-plane failure mode (DPF), and 13 samples had a multiple fracture failure mode (MFF). One sample was tested on the 50-kip machine but broke before it could be tested on the 300-kip machine, so its failure mode could not be determined. For the samples with a DPF mode, the angles the failure plane made to the horizontal ranged from 5 degrees to 90 degrees, but only two of the samples had an angle lower than 40 degrees.

Samples with a STF mode had an oven-dried unit weight between roughly 160 and 190 pcf, those with a DPF mode had a unit weight between about 120 and 185 pcf, and those with a MFF mode ranged between roughly 140 and 180 pcf (Figure 45). Samples with a STF mode in general have higher unit weights than those with a MFF mode. However, very little information can be derived from the samples with a DPF mode as they correspond to a wide range of oven-dried unit weight. Similar trends can be observed for the other unit weights (Figures 46 through 48).

Samples with a STF mode had an absorption between around 1 to 4 percent, while those with a DPF mode had an absorption between roughly 1 and 12.5 percent, and the samples with a MFF mode had an absorption between about 1 and 7.5 percent (Figure 49). This indicates that samples with a STF mode are due to a lower absorption than those with a MFF mode, which in turn can be expected to have a lower absorption than samples with a DPF mode.

Samples that shattered had an unconfined compressive strength between about 10 to 40 ksi, while those that had a dominant plane were between roughly 2 and 30 ksi, and those that had multiple fractures were between 2 and 22 ksi (Figure 50). This indicates that STF mode samples were generally stronger than DPF mode samples, which in turn were stronger than MFF mode samples.

When examining the Young's modulus, samples with a STF mode had a modulus between around 6,000 and 14,000 ksi (Figure 51). Those with a DPF mode had a modulus between roughly 2,000 and 12,000 ksi and those with a MFF mode were between about 2,000 and 10,000 ksi. This is a similar trend to unconfined compressive strength; i.e. samples with a STF mode had higher strength than those with a DPF mode, which in turn had a higher strength than those with a MFF mode.

In general, samples that shattered typically had high strength and unit weight and low absorption. In contrast, samples with a MFF mode had notably lower strength and unit weight and higher absorption. Samples with a DPF mode had a very wide range of unit weight, strength, and absorption. However, overall it appears that samples with a DPF mode are in between the other two failure modes when it comes to unit weight and strength. Interestingly enough, samples with a DPF mode had the highest absorption of the three failure types.

When failure types are considered with respect to depth, an interesting pattern can be observed (Figure 52). As discussed in section 3.2, the layer of rock between 55 feet and 81 feet depth is stronger than the layer of rock between 25 feet and 55 feet. Thus it makes sense that many of the samples in the lower and stronger rock layer had a STF mode while very few samples failed in one of the other two ways. In contrast, many of the samples in the upper weaker rock layer had a DPF or MFF mode while very few had a STF mode.

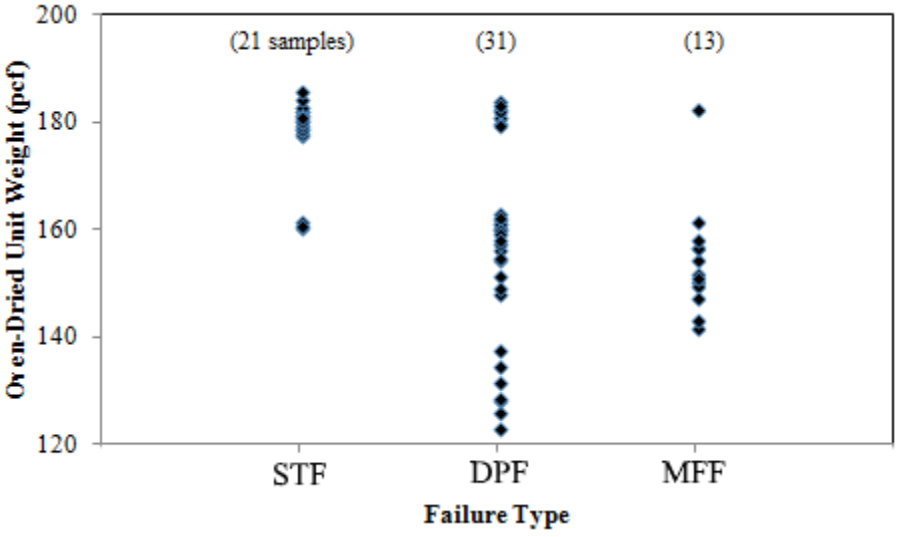

Figure 45: Failure Type versus Oven-Dried Unit Weight

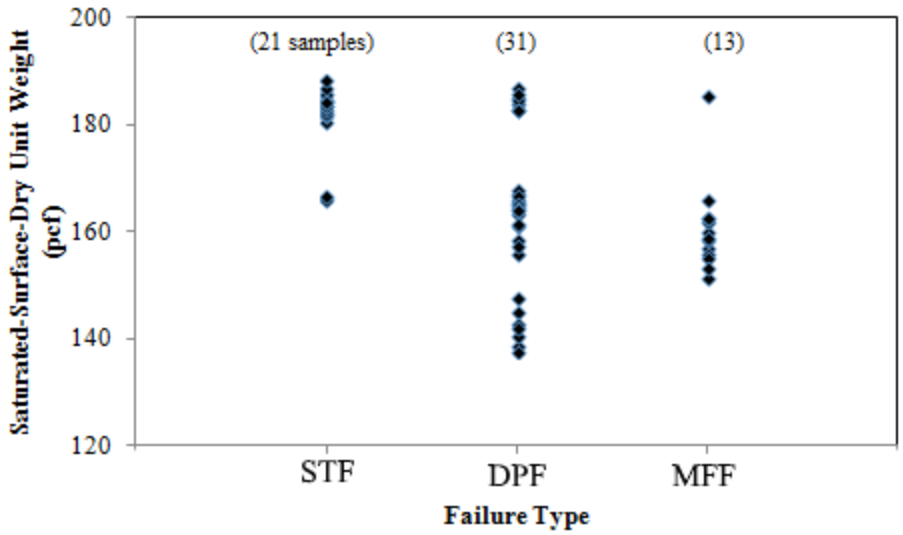

Figure 46: Failure Type versus Saturated-Surface-Dry Unit Weight

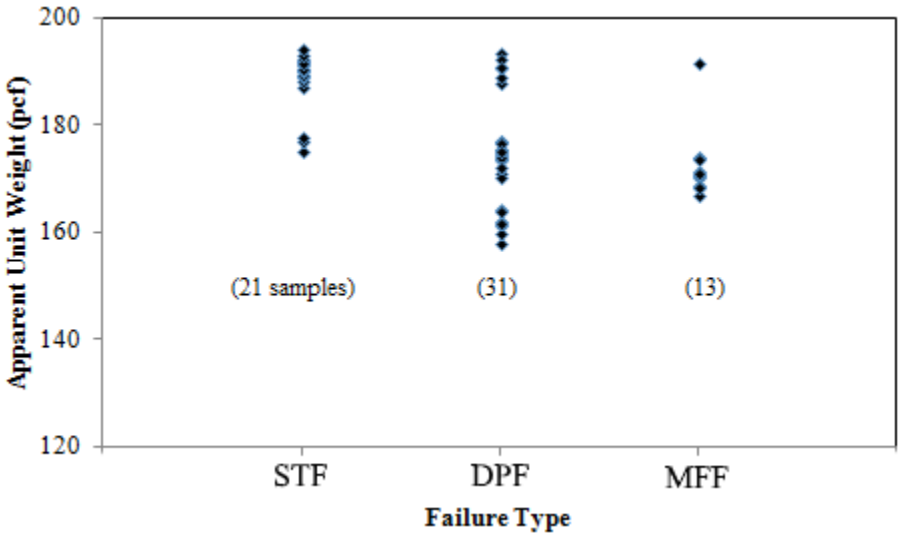

Figure 47: Failure Type versus Apparent Unit Weight

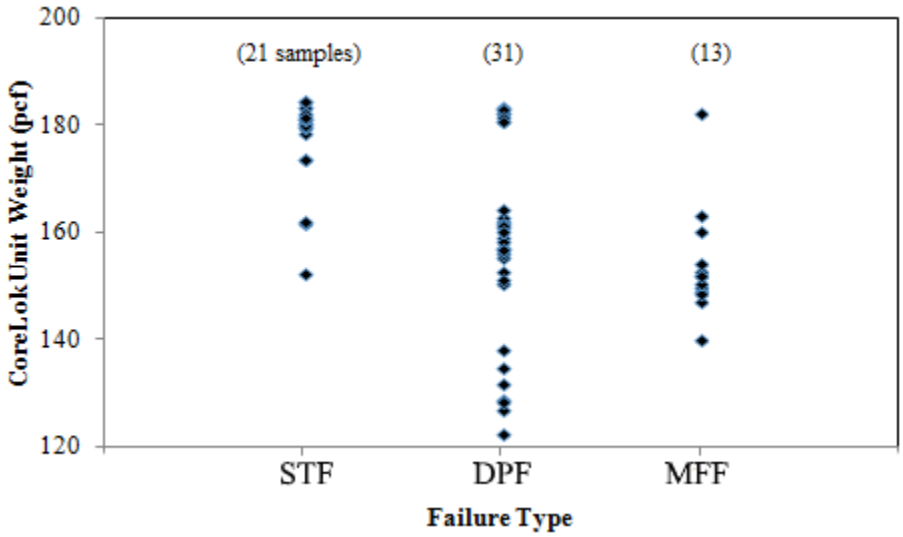

Figure 48: Failure Type versus CoreLok Unit Weight

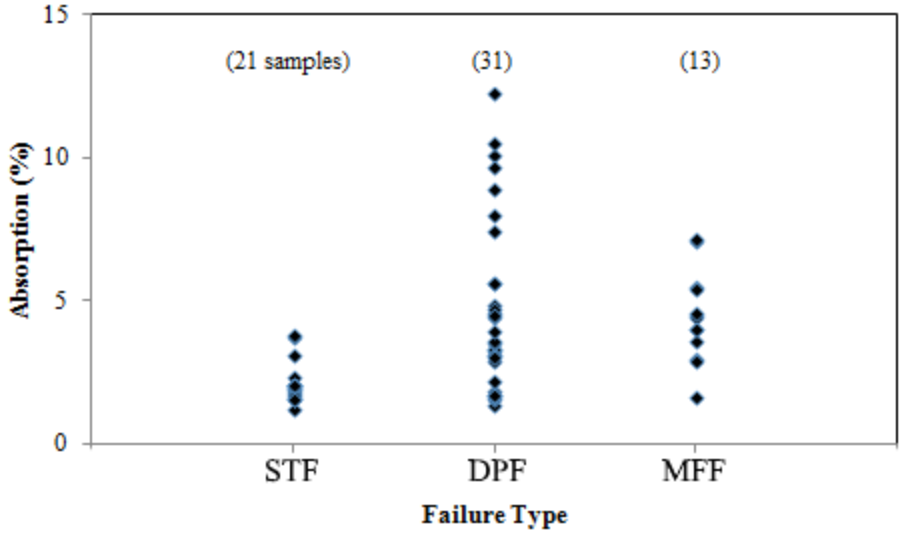

Figure 49: Failure Type versus Absorption

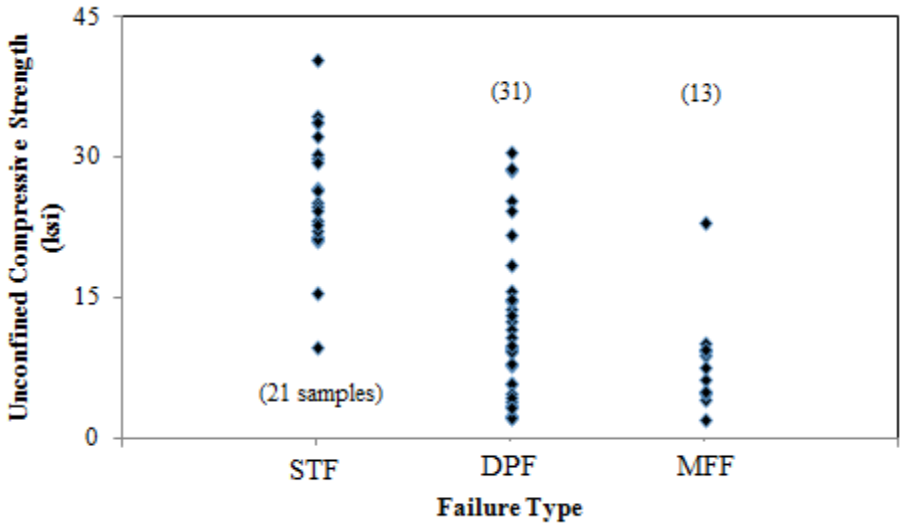

Figure 50: Failure Type versus Unconfined Compressive Strength

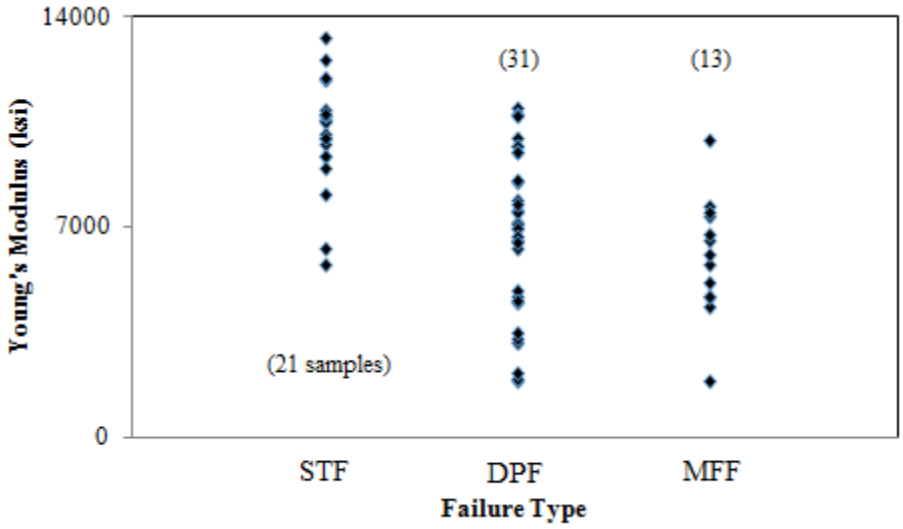

Figure 51: Failure Type versus Young's Modulus

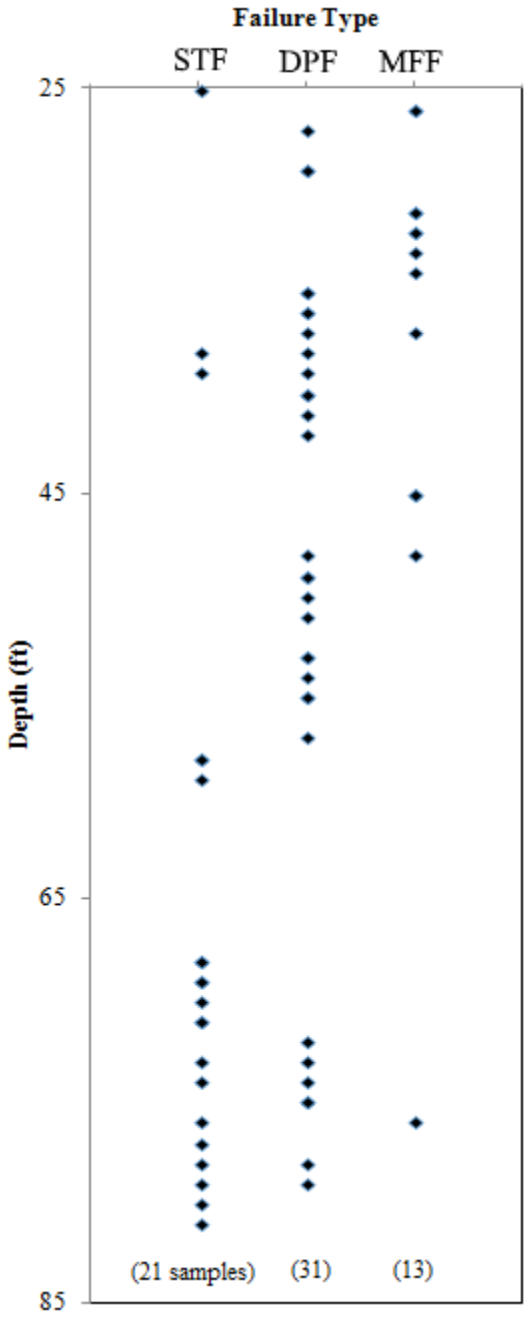

Figure 52: Failure Type versus Depth

4. CONCLUSIONS

A boring was drilled at the University of Hawaii at Manoa to a depth of 95 feet. From 17.5 feet depth to 81 feet depth, basalt rock was encountered and 66 samples were cut to undergo unconfined compression tests. The samples were first tested on a test frame with a maximum capacity of 50 kips and outfitted with an extensometer that measured axial strain. If the sample did not fail on that test frame, it was transferred to a test frame with a maximum capacity of 300 kips but without an extensometer. Parameters determined in this study included RQD, percent recovery, oven-dried unit weight, saturated-surface-dry unit weight, apparent unit weight, unit weight determined through a CoreLok machine, absorption, axial strain, unconfined compressive strength, Young's modulus, failure type and the failure plane angle to the horizontal. Trends with depth were determined, and the results from this study were compared to the results from Brandes et al. (2011), who tested basalt rock from the Big Island, to determine empirical correlations among the index and strength parameters.

In this study there was a clear pattern in depth trends some of for the index and strength parameters. Between 25 and 55 feet depth there is an upper layer of rock characterized by higher absorption and lower unit weights, strength, and stiffness, relative to the layer from 55 feet to 81 feet depth. It is likely that two different lava flows from the Honolulu Volcanic Series spread through the area where the boring was drilled. It seems likely that both flows correspond to the Sugarloaf eruption, or perhaps one of the flows erupted from the Tantalus vent, although this cannot be stated with certainty.

There were strong correlations when examining unit weights, absorption, unconfined compressive strength, and Young's modulus. Unit weights are inversely proportional to absorption, proportional to unconfined compressive strength and proportional to Young's modulus, in each case in a nonlinear manner. Absorption was inversely proportional to compressive strength and Young's modulus. Unconfined compressive strength was proportional to Young's modulus in a nonlinear manner.

RQD and percent recovery were not related to any of the index or strength parameters measured. Axial strain at failure and at 50% of the ultimate load had very weak correlation to index and strength parameters.

Of all the parameters measured in this study and in the one by Brandes et al. (2011), absorption appears to have the strongest correlation with Young's modulus and unconfined compressive strength. When comparing unit weight with Young's modulus or unconfined compressive strength, the trendlines from the two studies were notably different. However, the trendlines when comparing absorption to Young's modulus or unconfined compressive strength from both studies overlapped quite well. It is likely that these correlations are less site-dependent than the correlations between unit weight and Young's modulus or unconfined compressive strength. When considering basalt rock from other locations in Hawaii, if an estimation of the Young's

modulus or unconfined compressive strength is required, absorption will likely be the best predictor.

It is recommended that more testing on Hawaiian basalt rocks be performed. Test results from additional studies performed can be compared to the results from this study and from Brandes et al. (2011). In addition, the samples in this study and the one by Brandes et al. (2011) were largely unweathered. It would be interesting to see strength tests performed on weathered Hawaiian basalt rocks to see the effects of weathering.

5. REFERENCES

Al-Harthi, A. A., Al-Amri, R. M., and Shehata, W. M. (1999) "The Porosity and Engineering Properties of Vesicular Basalt in Saudi Arabia." *Engineering Geology 54,* pg 313-320.

Alemdag, S., Gurocak, Z., Solanki, P., and Zaman, M. (2007) "Estimation of Bearing Capacity of Basalts at the Atasu Dam Site, Turkey." *Bull Eng Geol Environ 67,* pg 79-85

Barton, N. R., Lien, R. and Lunde, J. (1974) *Rock Mech*, 6, pg 189-239.

Bieniawski, Z. T. (1974) *Proceedings of the 3rd International Congress on Rock Mechanics*, Denver, pg 27-32.

Birch, F. (1972) "Compressibility Elastic Constants." *American Institute of Physics Handbook, 3rd ed.*, New York; McGraw-Hill Book Company, pg 100-170.

Blair, B. E. (1955) "Physical Properties of Mine Rocks." (3), *U.S. Bureau of Mines, Rept Invest.*, 5130.

Blair, B. E. (1956) "Physical Properties of Mine Rocks." (4), *U.S. Bureau of Mines, Rept Invest.*, 5244.

Brady, B., & Brown, E. (2004) *Rock mechanics for underground mining* (3rd ed.). Dordrecht: Kluwer Academic.

Brandes, H. G., Robertson, I. N., and Johnson, G. P. (2011) "Soil and Rock Properties in a Young Volcanic Deposit on the Island of Hawaii." *American Society of Civil Engineers*, pg 597-610.

Coates, D. F. and Parsons, R. C. (1966) "Experimental Criteria for Classification of Rock Substances." *Int. F. Rock Mech. Min. Sci.*, 3, 181.

Cole, W. F. (1982) "The Performance of Deer Park Basalt in Triaxial Testing." *Proceedings of the Eleventh Australian Road Research Board Conference*. Melbourne, pg 52-59.

Deere, D. U., and R. P. Miller. (1966) *Engineering Classification and Index Properties for Intact Rock*. Ft. Belvoir: Defense Technical Information Center.

Dincer, I., Acar, A., Cobanoglu, I., and Uras, Y. (2004) "Correlation between Schmidt Hardness, Uniaxial Compressive Strength and Young's Modulus for Andesites, Basalts, and Tuffs." *Bull Eng Geol Environ 63,* pg 141-148.

Edelbro, Catrin. (2004) *Evaluation of Rock Mass Strength Criteria*. Licentiate Thesis. Lulea University of Technology, Sweden.

Engidasew, T. A. and Barbieri, G. (2013) "Geo-Engineering Evaluation of Termaber Basalt Rock Mass for Crushed Stone Aggregate and Building Stone from Central Ethiopia." *Journal of African Earth Sciences*, http://dx.doi.org/10.1016/j.jafrearsci.2013.11.020

Farmer, I. W. *Engineering Properties of Rocks*. London: Spon, 1968. Print.

Goel, R. K., Jethwa, J. L., and Paithankar, A. G. (1995) *Int. J. Rock Mech. Min.*, 33 (2), pg 179-181.

Griffith, A. A. (1937) *Physical Properties of Typical American Rocks.* Ames, Iowa: Iowa State College of Agriculture and Mechanical Arts, Iowa Engineering Experiment Station, Vol. 35, No. 19, pg 19-20.

Guidicini, G., Nieble, C. M., and Cornides, A. T. de. (1973) *Bulletin of the International Association of Engineering Geology*, Krefeld, pg 37-52.

Hoek, Evert, Peter K. Kaiser, and W. F. Bawden. (1995) *Support of Underground Excavations in Hard Rock*. Rotterdam, Netherlands: A.A. Balkema.

Hosking, J. R. (1955) "A Comparison of Tensile Strength, Crushing Strength, and Elastic Properties of Roadmaking Rocks", *Quarry Man. F.*, 39, 200.

Hunt, Roy E. (2005) *Geotechnical Engineering Investigation Handbook*. Boca Raton, FL: Taylor & Francis.

International Society for Rock Mechanics (ISRM). (1981) *Int. J. Rock Mech. Min.*, Abstr. 18, pg 85-110.

Jiang, Q., Feng, X., Hatzor, Y., Hao, X., and Li, S. (2014) "Mechanical Anisotropy of Columnar Jointed Basalts: An Example from the Baihetan Hydropower Station, China." *Engineering Geology 175*, pg 35-45.

Laubscher, D. H. and Taylor, H. W. (1976) *Proceedings of the Symposium on Exploration for Rock Engineering*, Johannesburg, A. A. Balkema, 1, pg 119-128.

Lauffer, H. (1953) "Classification for tunnel construction", *Geologie und Bauwesen.* 24(1), pg 46-51. [In German]

Johnson, A. M. (1970) *Physical Processes in Geology.* San Francisco, California; Freeman, Cooper and Company, pg 202.

Jumikis, Alfreds R. (1979) *Rock Mechanics*. 1st ed. Clausthal-Zellerfeld, Federal Republic of Germany: Trans Tech Publications.

Macdonald, G., & Abbott, A. (1979) *Volcanoes in the sea: The geology of Hawaii*. Honolulu, Hawaii: University of Hawaii Press.

Matula, M. and Holzer, R. (1978) *Proc. Of Felsnekanik Kolloquium*, Grudnlagen und Andwendung der Felsmekanik, Karlsruhe, Germany, pg 107-121.

Mendoza-Chavez, G., Martinez-Martinez, L. H., Delgado-Hernandez, D. J., Escobedo D., Alonso-Guzman, E. M., Martinez-Molina, W., Rocha-Arreygue, E., Chavez-Garcia, H. L., and Arteaga-Arcos, J. C. (2012) "Mechanical Properties of Rocks used for the Construction of Vehicular Bridges Supported by Pier Masonry." *Advanced Materials Research Vols 535-537*, pg 1881-1888.

Nicholls, H. R. (1961) "In-Situ Determination of the Dynamic Elastic Constants of Rock." *Int. Symp. Mining Res.* (ed. G. Clarke), Pergamon, Oxford.

Oliveira, P. C. and Zuquette, L. V. (2014) "Evaluation of Weathering of Basaltic Lithotypes based on pH, Electrical Conductivity, and Point-Load Strength Tests."*REM: R. Esc. Minas, Ouro Pretro, 67(1)*, pg 13-19.

Palmstrom, A. (1995) *A Rock Mass Characterisation System for Rock Engineering Purposes*, Ph. D thesis, University of Oslo, Norway.

Panek, L. A. and Fannon, T. A. (1992) "Size and Shape Effects in Point Load Tests of Irregular Rock Fragments." *Rock Mechanics and Rock Engineering 25*, Michigan Technological University, Houghton, Michigan, pg 109-140.

Rabcewicz, L. V. (1968) *New Austrian Tunnel Construction Method. I. Origin, Executions and Experiences. II. Static Forces and Design = Die Neue Österreichische Tunnelbauweise ; I. EEntstehung, Ausführungen Und Erfahrungen ; II. Statische Wirkungsweise Und Bermessung*. Denver, CO: U.S. Dept. of the Interior, Bureau of Reclamation.

Raj, K. and Pedram, R. (2015) "Correlations Between Direct and Indirect Strength Test Methods." *International Journal of Mining Science and Technology 25*.

Ramamurthy, T. and Aorra, V. K. (1993) *Geotechnical Engineering of Hard Soils – SoftRocks*, Anagnostopoulos et al., (Eds.), Balkema, Rotterdam. ISBN 90 5410 334 2

Romana, M. (1985) *Proceedings of the International Symposium on the Role of Rock Mechanics*, pg 49-53.

Stearns, H. (1966) *Geology of the State of Hawaii,*. Palo Alto, California: Pacific Books.

Stille, H., Groth, T. and Fredriksson, A. (1982) *FEM-Analysis of Rock Mechanical Problems with JOBFEM*, Stiftelsen Bergteknisk Korskning – BeFo, Stockholm, 307:1/82.

Stowe, Richard L. (1969) *Strength and Deformation Properties of Granite, Basalt, Limestone, and Tuff at Various Loading Rates*. Vicksburg, Miss.: Waterways Experiment Station.

Szechy, K. (1966) *The Art of Tunnelling.* Budapest: Akademiai Kiado, pg 76.

Terzaghi, K. (1946) *Rock Defects and Loads on Tunnel Supports*. Cambridge, MA: Harvard U, Graduate School of Engineering.

U.S. Bureau of Reclamation (1954). *Physical Properties of Typical Foundation Rocks*. Concrete Laboratory Report SP39.

Wickham, G.E., Tiedeman, H.R., and Skinner, E. H. (1972) *Proceedings of the North American Rapid Excavation & Tunnelling Conference*, American Society of Mechanical Engineers, New York, pg 43-64.

Williamson, D. A. (1984) *Bulletin of the Association of Engineering Geologists,* XXI (3), pg 345-354.

Windes, S. (1949) "Physical Properties of Mine Rock" *U.S. Bureau of Mines, Rept Invest.*, 4459.

Windes, S. (1950) "Physical Properties of Mine Rock (2)" *U.S. Bureau of Mines, Rept Invest.*, 4727.

Yan, F., Feng, X., Chen, R., Xia, K., and Jin, C. (2011) "Dynamic Tensile Failure of the Rock Interface Between Tuff and Basalt." *Rock Mech Rock Eng 45*, pg 341-348.

APPENDIX

Table A1: Tolerance Checks of Basalt Samples

Test Number	Depth ft	STRAIGHTNESS in		END FLATNESS in			PERPENDICULARITY in			
		DEV	pass	end 1	end 2	pass	end 1	end 2	H/230	pass
1	25	0.026	no	<.0015	0.012	no	0.059	0.154	0.022	no
2	26	0.010	yes	<.0015	0.021	no	0.045	0.040	0.022	no
3	26	0.020	no	0.004	0.002	no	0.067	0.072	0.022	no
4	27	0.022	no	0.002	0.002	no	0.035	0.031	0.021	no
5	29	0.016	yes	<.0015	0.008	no	0.038	0.183	0.022	no
6	29	0.006	yes	0.003	0.003	no	0.017	0.096	0.022	no
7	31	0.021	no	0.005	0.005	no	0.059	0.026	0.022	no
8	31	0.035	no	0.007	0.017	no	0.091	0.036	0.022	no
9	32	0.021	no	0.002	0.007	no	0.101	0.104	0.022	no
10	32	0.026	no	0.003	0.005	no	0.076	0.072	0.022	no
11	33	0.013	yes	0.006	0.003	no	0.026	0.050	0.022	no
12	34	0.008	yes	0.002	0.002	no	0.060	0.036	0.022	no
13	35	0.008	yes	0.007	0.030	no	0.051	0.090	0.022	no
14	35	0.008	yes	0.003	0.036	no	0.026	0.091	0.022	no
15	36	0.010	yes	0.003	0.003	no	0.041	0.087	0.022	no
16	36	0.010	yes	0.006	0.006	no	0.016	0.114	0.022	no
17	37	0.010	yes	0.007	0.004	no	0.042	0.095	0.022	no
18	37	0.020	no	0.007	0.003	no	0.051	0.091	0.022	no
19	38	0.016	yes	0.004	0.007	no	0.104	0.041	0.022	no
20	38	0.017	yes	0.005	0.006	no	0.023	0.115	0.022	no
21	39	0.005	yes	0.005	0.003	no	0.025	0.040	0.022	no
22	39	0.005	yes	0.006	0.006	no	0.041	0.066	0.022	no
23	40	0.020	no	0.006	0.004	no	0.052	0.082	0.022	no
24	40	0.013	yes	0.008	0.021	no	0.045	0.074	0.022	no
25	41	0.024	no	0.005	0.004	no	0.049	0.051	0.022	no
26	42	0.018	yes	0.005	0.019	no	0.052	0.072	0.022	no
27	45	0.021	no	0.006	0.009	no	0.061	0.025	0.022	no
28	45	0.043	no	0.006	0.004	no	0.075	0.051	0.022	no
29	48	0.004	yes	0.005	0.009	no	0.010	0.056	0.022	no
30	48	0.018	yes	0.005	0.008	no	0.050	0.055	0.022	no
31	49	0.015	yes	0.003	0.008	no	0.032	0.061	0.021	no
32	49	0.004	yes	0.006	0.007	no	0.027	0.109	0.022	no
33	50	0.022	no	0.004	0.004	no	0.035	0.073	0.022	no
34	51	0.005	yes	0.007	0.004	no	0.070	0.059	0.022	no
35	53	0.045	no	0.007	0.002	no	0.074	0.049	0.022	no
36	53	0.029	no	0.008	0.004	no	0.041	0.113	0.022	no
37	54	0.031	no	0.008	0.004	no	0.032	0.071	0.022	no
38	55	0.064	no	0.005	0.012	no	0.075	0.055	0.021	no

Table A1: Tolerance Checks of Basalt Samples (continued)

Test Number	Depth ft	STRAIGHTNESS in		END FLATNESS in			PERPENDICULARITY in			
		DEV	pass	end 1	end 2	pass	end 1	end 2	H/230	pass
39	55	0.050	no	0.006	0.007	no	0.059	0.116	0.022	no
40	57	0.013	yes	0.006	0.003	no	0.131	0.050	0.022	no
41	58	<.0015	no	0.014	0.013	no	0.075	0.086	0.022	no
42	58	0.004	yes	0.021	0.027	no	0.026	0.042	0.022	no
43	59	0.006	yes	0.004	0.006	no	0.040	0.075	0.022	no
44	68	<.0015	no	0.002	0.008	no	0.015	0.104	0.022	no
45	68	<.0015	no	0.016	0.027	no	0.072	0.052	0.022	no
46	69	0.003	yes	0.016	0.007	no	0.029	0.115	0.022	no
47	69	<.0015	yes	0.002	0.021	no	0.033	0.053	0.022	no
48	70	0.007	yes	0.003	0.006	no	0.032	0.094	0.022	no
49	71	<.0015	yes	0.003	0.009	no	0.038	0.070	0.022	no
50	71	0.002	yes	0.020	0.018	no	0.075	0.056	0.022	no
51	72	0.003	yes	0.003	0.003	no	0.030	0.115	0.022	no
52	73	<.0015	yes	0.026	0.004	no	0.042	0.008	0.022	no
53	73	<.0015	yes	0.004	0.004	no	0.025	0.021	0.022	no
54	74	<.0015	yes	0.012	0.003	no	0.030	0.033	0.022	no
55	74	<.0015	yes	0.018	0.009	no	0.040	0.050	0.022	no
56	75	<.0015	yes	0.006	0.015	no	0.072	0.026	0.022	no
57	75	<.0015	yes	0.005	0.015	no	0.028	0.087	0.022	no
58	76	<.0015	yes	0.009	0.005	no	0.030	0.072	0.022	no
59	76	<.0015	yes	0.006	0.025	no	0.024	0.047	0.022	no
60	77	<.0015	yes	0.006	0.007	no	0.041	0.073	0.022	no
61	78	0.025	no	0.006	0.023	no	0.050	0.109	0.022	no
62	78	<.0015	yes	0.007	0.011	no	0.072	0.051	0.022	no
63	79	<.0015	yes	0.005	0.025	no	0.049	0.126	0.022	no
64	79	0.009	yes	0.012	0.009	no	0.025	0.059	0.022	no
65	80	<.0015	yes	0.005	0.010	no	0.050	0.049	0.022	no
66	81	0.006	yes	0.005	0.014	no	0.046	0.165	0.022	no

Test No. 1: UH Boring B4, Sample Depth = 25 ft

A. Physical Properties

Oven-Dried Unit Weight	Saturated-Surface-Dry Unit Weight	Apparent Unit Weight	CoreLok Unit Weight	Absorption	RQD	Percent Recovered
(lb/ft^3)	(lb/ft^3)	(lb/ft^3)	(lb/ft^3)	(%)	(%)	
γ_{OD}	γ_{SSD}	γ_{APP}	γ_{CL}			
161.46	166.45	175.48	152.48	3.09	100	100

B. Stress-Strain Response

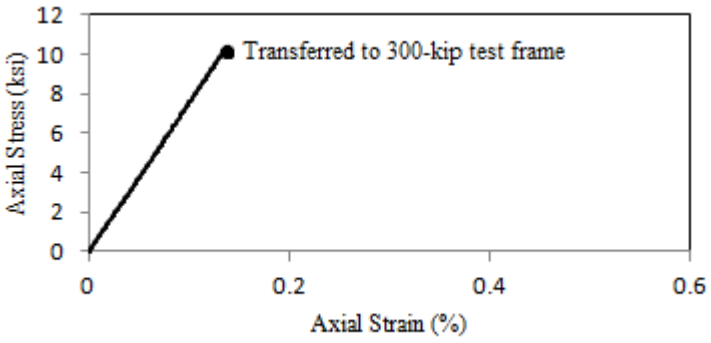

Sample Before Testing Sample at Failure

C. Strength and Stiffness Parameters

Unconfined Compressive Strength	Young's Modulus	Axial Strain at Failure	Axial Strain at 50% Strength	Failure Type	Failure Plane Angle to Horizontal
(ksi)	(ksi)	(%)	(%)		(Degrees)
q_u	E	ε_{af}	ε_{a50}		α
10.01	8100	N/D	0.07	STF	N/A

N/A – Not applicable N/D – Not determined See page 29

Test No. 2: UH Boring B4, Sample Depth = 26 ft

A. Physical Properties

Oven-Dried Unit Weight	Saturated-Surface-Dry Unit Weight	Apparent Unit Weight	CoreLok Unit Weight	Absorption	RQD	Percent Recovered
(lb/ft^3)	(lb/ft^3)	(lb/ft^3)	(lb/ft^3)	(%)	(%)	
γ_{OD}	γ_{SSD}	γ_{APP}	γ_{CL}			
154.27	160.42	171.15	152.93	3.99	100	100

B. Stress-Strain Response

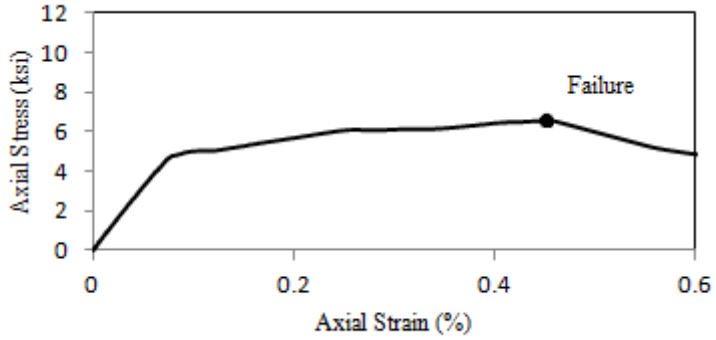

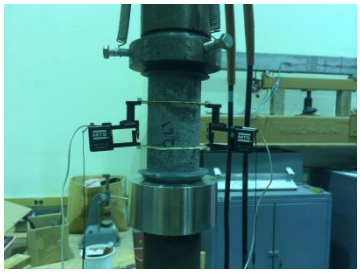

Sample Before Testing

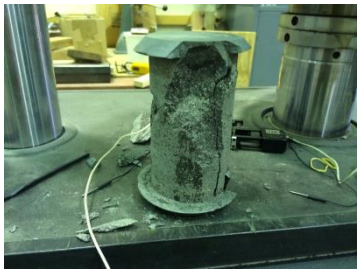

Sample at Failure

C. Strength and Stiffness Parameters

Unconfined Compressive Strength	Young's Modulus	Axial Strain at Failure	Axial Strain at 50% Strength	Failure Type	Failure Plane Angle to Horizontal
(ksi)	(ksi)	(%)	(%)		(Degrees)
q_u	E	ε_{af}	ε_{a50}		α
6.55	6600	0.46	0.05	MFF	N/A

N/A – Not applicable N/D – Not determined See page 29

Test No. 3: UH Boring B4, Sample Depth = 26 ft

A. Physical Properties

Oven-Dried Unit Weight	Saturated-Surface-Dry Unit Weight	Apparent Unit Weight	CoreLok Unit Weight	Absorption	RQD	Percent Recovered
(lb/ft^3)	(lb/ft^3)	(lb/ft^3)	(lb/ft^3)	(%)	(%)	
γ_{OD}	γ_{SSD}	γ_{APP}	γ_{CL}			
150.37	157.17	168.76	149.75	4.52	100	100

B. Stress-Strain Response

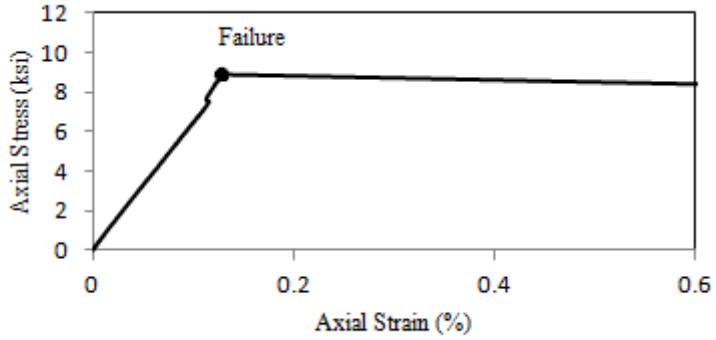

Sample Before Testing Sample at Failure

C. Strength and Stiffness Parameters

Unconfined Compressive Strength	Young's Modulus	Axial Strain at Failure	Axial Strain at 50% Strength	Failure Type	Failure Plane Angle to Horizontal
(ksi)	(ksi)	(%)	(%)		(Degrees)
q_u	E	ε_{af}	ε_{a50}		α
8.98	6800	0.13	0.07	MFF	N/A

N/A – Not applicable N/D – Not determined See page 29

Test No. 4: UH Boring B4, Sample Depth = 27 ft

A. Physical Properties

Oven-Dried Unit Weight	Saturated-Surface-Dry Unit Weight	Apparent Unit Weight	CoreLok Unit Weight	Absorption	RQD	Percent Recovered
(lb/ft^3)	(lb/ft^3)	(lb/ft^3)	(lb/ft^3)	(%)	(%)	
γ_{OD}	γ_{SSD}	γ_{APP}	γ_{CL}			
161.95	167.34	177.27	157.43	3.33	87	100

B. Stress-Strain Response

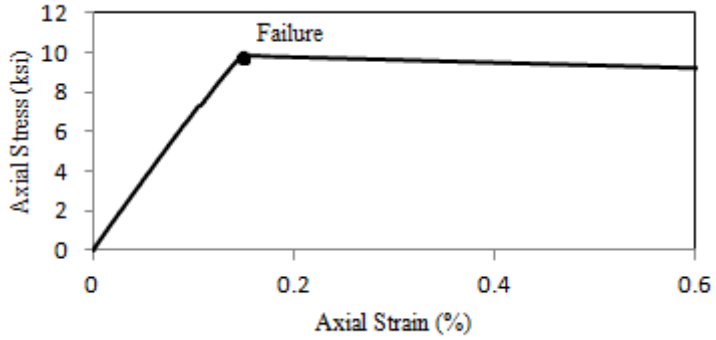

Sample Before Testing Sample at Failure

C. Strength and Stiffness Parameters

Unconfined Compressive Strength	Young's Modulus	Axial Strain at Failure	Axial Strain at 50% Strength	Failure Type	Failure Plane Angle to Horizontal
(ksi)	(ksi)	(%)	(%)		(Degrees)
q_u	E	ε_{af}	ε_{a50}		α
9.82	7200	0.16	0.07	DPF	75

N/A – Not applicable N/D – Not determined See page 29

Test No. 5: UH Boring B4, Sample Depth = 29 ft

A. Physical Properties

Oven-Dried Unit Weight	Saturated-Surface-Dry Unit Weight	Apparent Unit Weight	CoreLok Unit Weight	Absorption	RQD	Percent Recovered
(lb/ft^3)	(lb/ft^3)	(lb/ft^3)	(lb/ft^3)	(%)	(%)	
γ_{OD}	γ_{SSD}	γ_{APP}	γ_{CL}			
160.23	165.40	174.72	159.10	3.23	87	100

B. Stress-Strain Response

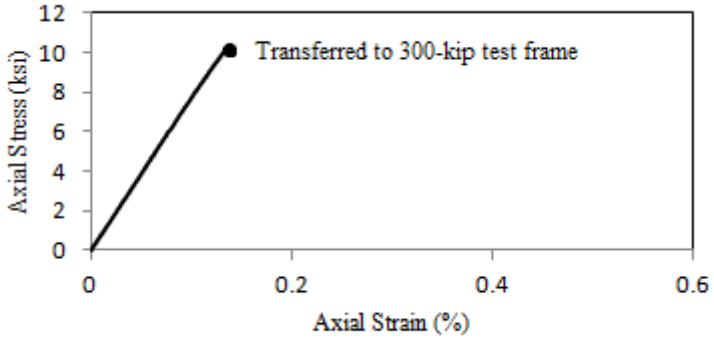

Sample Before Testing

Sample at Failure

C. Strength and Stiffness Parameters

Unconfined Compressive Strength	Young's Modulus	Axial Strain at Failure	Axial Strain at 50% Strength	Failure Type	Failure Plane Angle to Horizontal
(ksi)	(ksi)	(%)	(%)		(Degrees)
q_u	E	ε_{af}	ε_{a50}		α
13.89	7600	N/D	0.09	DPF	75

N/A – Not applicable N/D – Not determined See page 29

Test No. 6: UH Boring B4, Sample Depth = 29 ft

A. Physical Properties

Oven-Dried Unit Weight	Saturated-Surface-Dry Unit Weight	Apparent Unit Weight	CoreLok Unit Weight	Absorption	RQD	Percent Recovered
(lb/ft^3)	(lb/ft^3)	(lb/ft^3)	(lb/ft^3)	(%)	(%)	
γ_{OD}	γ_{SSD}	γ_{APP}	γ_{CL}			
160.99	166.27	175.88	158.46	3.28	87	100

B. Stress-Strain Response

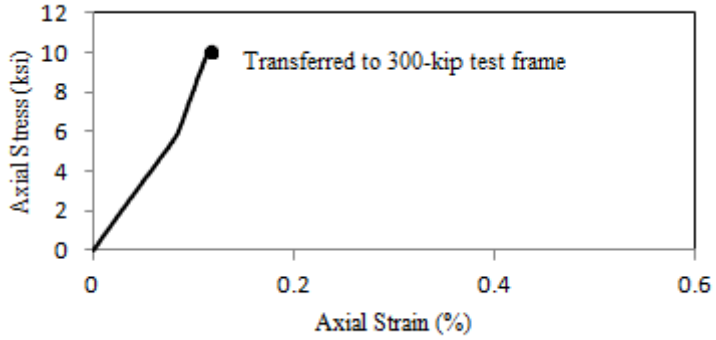

Sample Before Testing

Sample at Failure

C. Strength and Stiffness Parameters

Unconfined Compressive Strength	Young's Modulus	Axial Strain at Failure	Axial Strain at 50% Strength	Failure Type	Failure Plane Angle to Horizontal
(ksi)	(ksi)	(%)	(%)		(Degrees)
q_u	E	ε_{af}	ε_{a50}		α
12.77	7000	N/D	0.09	DPF	70

N/A – Not applicable N/D – Not determined See page 29

Test No. 7: UH Boring B4, Sample Depth = 31 ft

A. Physical Properties

Oven-Dried Unit Weight	Saturated-Surface-Dry Unit Weight	Apparent Unit Weight	CoreLok Unit Weight	Absorption	RQD	Percent Recovered
(lb/ft^3)	(lb/ft^3)	(lb/ft^3)	(lb/ft^3)	(%)	(%)	
γ_{OD}	γ_{SSD}	γ_{APP}	γ_{CL}			
149.48	156.14	167.34	147.11	4.46	87	100

B. Stress-Strain Response

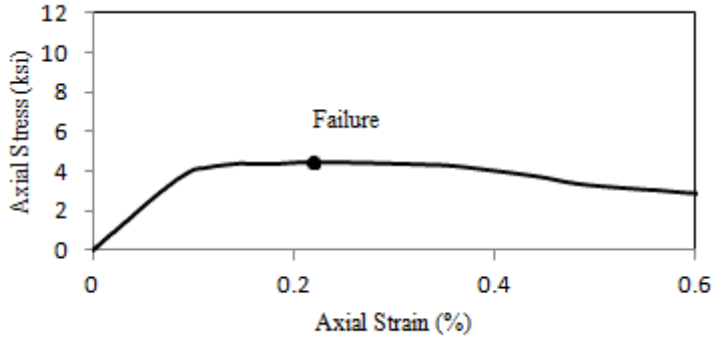

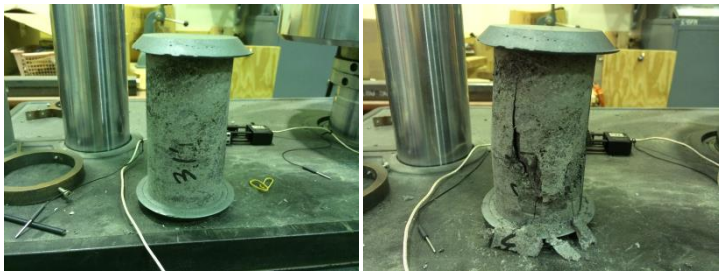

Sample Before Testing Sample at Failure

C. Strength and Stiffness Parameters

Unconfined Compressive Strength	Young's Modulus	Axial Strain at Failure	Axial Strain at 50% Strength	Failure Type	Failure Plane Angle to Horizontal
(ksi)	(ksi)	(%)	(%)		(Degrees)
q_u	E	ε_{af}	ε_{a50}		α
4.42	4400	0.22	0.05	MFF	N/A

N/A – Not applicable N/D – Not determined See page 29

Test No. 8: UH Boring B4, Sample Depth = 31 ft

A. Physical Properties

Oven-Dried Unit Weight	Saturated-Surface-Dry Unit Weight	Apparent Unit Weight	CoreLok Unit Weight	Absorption	RQD	Percent Recovered
(lb/ft^3)	(lb/ft^3)	(lb/ft^3)	(lb/ft^3)	(%)	(%)	
γ_{OD}	γ_{SSD}	γ_{APP}	γ_{CL}			
156.52	162.11	171.91	154.29	3.57	87	100

B. Stress-Strain Response

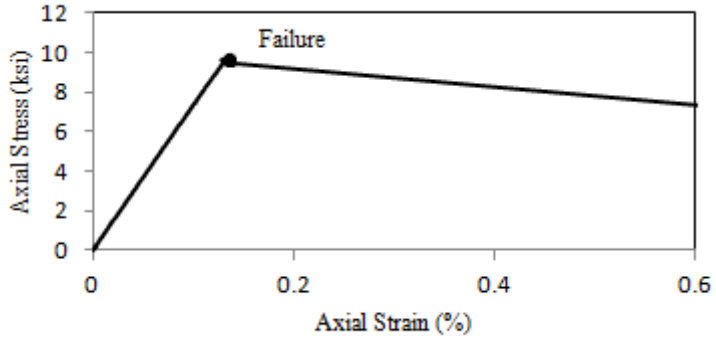

Sample Before Testing Sample at Failure

C. Strength and Stiffness Parameters

Unconfined Compressive Strength	Young's Modulus	Axial Strain at Failure	Axial Strain at 50% Strength	Failure Type	Failure Plane Angle to Horizontal
(ksi)	(ksi)	(%)	(%)		(Degrees)
q_u	E	ε_{af}	ε_{a50}		α
9.69	7400	0.13	0.07	MFF	N/A

N/A – Not applicable N/D – Not determined See page 29

Test No. 9: UH Boring B4, Sample Depth = 32 ft

A. Physical Properties

Oven-Dried Unit Weight	Saturated-Surface-Dry Unit Weight	Apparent Unit Weight	CoreLok Unit Weight	Absorption	RQD	Percent Recovered
(lb/ft^3)	(lb/ft^3)	(lb/ft^3)	(lb/ft^3)	(%)	(%)	
γ_{OD}	γ_{SSD}	γ_{APP}	γ_{CL}			
151.70	158.63	170.66	149.26	4.57	87	100

B. Stress-Strain Response

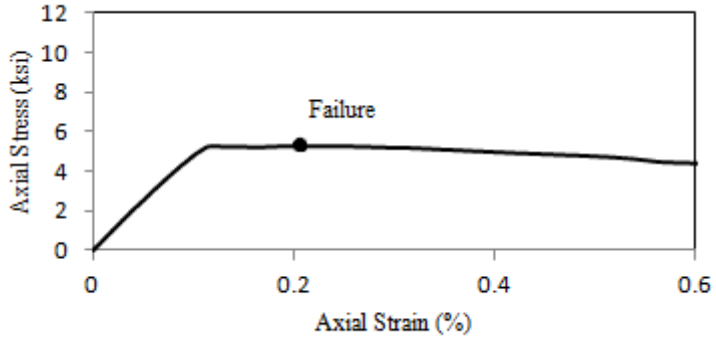

Sample Before Testing Sample at Failure

C. Strength and Stiffness Parameters

Unconfined Compressive Strength	Young's Modulus	Axial Strain at Failure	Axial Strain at 50% Strength	Failure Type	Failure Plane Angle to Horizontal
(ksi)	(ksi)	(%)	(%)		(Degrees)
q_u	E	ε_{af}	ε_{a50}		α
5.27	5200	0.21	0.05	MFF	N/A

N/A – Not applicable N/D – Not determined See page 29

Test No. 10: UH Boring B4, Sample Depth = 32 ft

A. Physical Properties

Oven-Dried Unit Weight	Saturated-Surface-Dry Unit Weight	Apparent Unit Weight	CoreLok Unit Weight	Absorption	RQD	Percent Recovered
(lb/ft^3)	(lb/ft^3)	(lb/ft^3)	(lb/ft^3)	(%)	(%)	
γ_{OD}	γ_{SSD}	γ_{APP}	γ_{CL}			
156.63	162.93	174.24	152.01	4.03	87	100

B. Stress-Strain Response

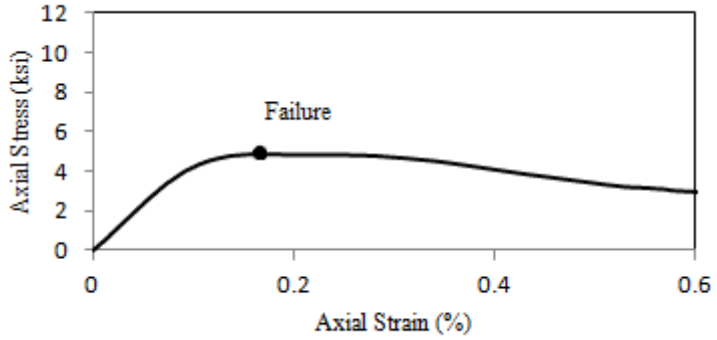

Sample Before Testing

Sample at Failure

C. Strength and Stiffness Parameters

Unconfined Compressive Strength	Young's Modulus	Axial Strain at Failure	Axial Strain at 50% Strength	Failure Type	Failure Plane Angle to Horizontal
(ksi)	(ksi)	(%)	(%)		(Degrees)
q_u	E	ε_{af}	ε_{a50}		α
4.92	4700	0.16	0.05	MFF	N/A

N/A – Not applicable N/D – Not determined See page 29

Test No. 11: UH Boring B4, Sample Depth = 33 ft

A. Physical Properties

Oven-Dried Unit Weight	Saturated-Surface-Dry Unit Weight	Apparent Unit Weight	CoreLok Unit Weight	Absorption	RQD	Percent Recovered
(lb/ft^3)	(lb/ft^3)	(lb/ft^3)	(lb/ft^3)	(%)	(%)	
γ_{OD}	γ_{SSD}	γ_{APP}	γ_{CL}			
158.24	162.96	171.19	160.43	2.98	93	100

B. Stress-Strain Response

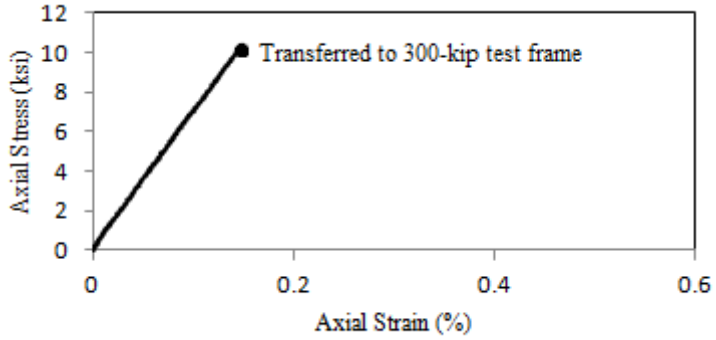

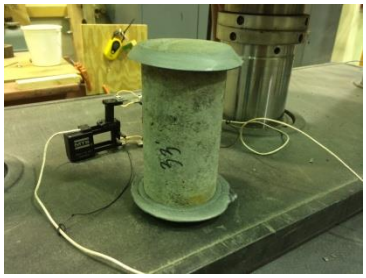

Sample Before Testing

Sample at Failure

C. Strength and Stiffness Parameters

Unconfined Compressive Strength	Young's Modulus	Axial Strain at Failure	Axial Strain at 50% Strength	Failure Type	Failure Plane Angle to Horizontal
(ksi)	(ksi)	(%)	(%)		(Degrees)
q_u	E	ε_{af}	ε_{a50}		α
10.32	7700	N/D	0.07	MFF	N/A

N/A – Not applicable N/D – Not determined See page 29

Test No. 12: UH Boring B4, Sample Depth = 34 ft

A. Physical Properties

Oven-Dried Unit Weight	Saturated-Surface-Dry Unit Weight	Apparent Unit Weight	CoreLok Unit Weight	Absorption	RQD	Percent Recovered
(lb/ft^3)	(lb/ft^3)	(lb/ft^3)	(lb/ft^3)	(%)	(%)	
γ_{OD}	γ_{SSD}	γ_{APP}	γ_{CL}			
161.41	166.08	174.47	163.31	2.89	93	100

B. Stress-Strain Response

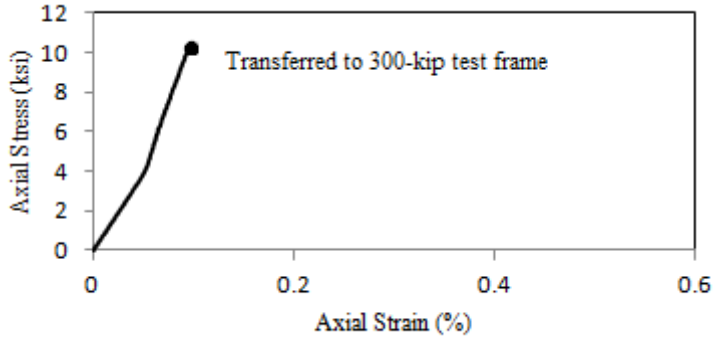

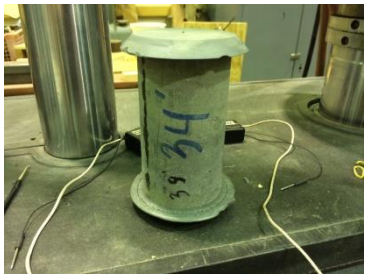

Sample Before Testing

Sample at Failure

C. Strength and Stiffness Parameters

Unconfined Compressive Strength	Young's Modulus	Axial Strain at Failure	Axial Strain at 50% Strength	Failure Type	Failure Plane Angle to Horizontal
(ksi)	(ksi)	(%)	(%)		(Degrees)
q_u	E	ε_{af}	ε_{a50}		α
9.55	7500	N/D	0.06	MFF	N/A

N/A – Not applicable N/D – Not determined See page 29

Test No. 13: UH Boring B4, Sample Depth = 35 ft

A. Physical Properties

Oven-Dried Unit Weight	Saturated-Surface-Dry Unit Weight	Apparent Unit Weight	CoreLok Unit Weight	Absorption	RQD	Percent Recovered
(lb/ft^3)	(lb/ft^3)	(lb/ft^3)	(lb/ft^3)	(%)	(%)	
γ_{OD}	γ_{SSD}	γ_{APP}	γ_{CL}			
160.15	165.15	174.11	162.11	3.12	93	100

B. Stress-Strain Response

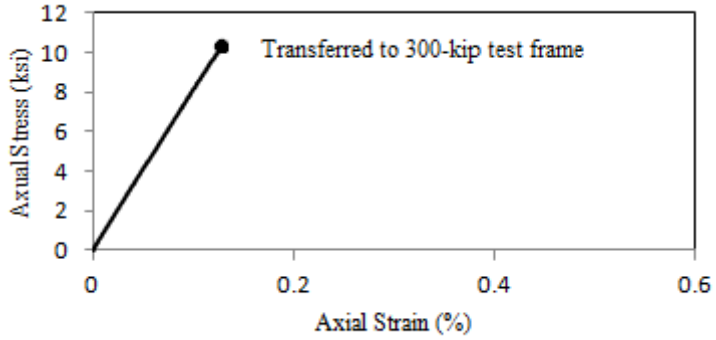

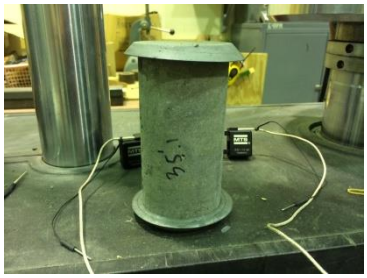

Sample Before Testing

Sample at Failure

C. Strength and Stiffness Parameters

Unconfined Compressive Strength	Young's Modulus	Axial Strain at Failure	Axial Strain at 50% Strength	Failure Type	Failure Plane Angle to Horizontal
(ksi)	(ksi)	(%)	(%)		(Degrees)
q_u	E	ε_{af}	ε_{a50}		α
9.50	8500	N/D	0.06	DPF	75

N/A – Not applicable N/D – Not determined See page 29

Test No. 14: UH Boring B4, Sample Depth = 35 ft

A. Physical Properties

Oven-Dried Unit Weight	Saturated-Surface-Dry Unit Weight	Apparent Unit Weight	CoreLok Unit Weight	Absorption	RQD	Percent Recovered
(lb/ft^3)	(lb/ft^3)	(lb/ft^3)	(lb/ft^3)	(%)	(%)	
γ_{OD}	γ_{SSD}	γ_{APP}	γ_{CL}			
161.14	165.75	173.99	162.95	2.86	93	100

B. Stress-Strain Response

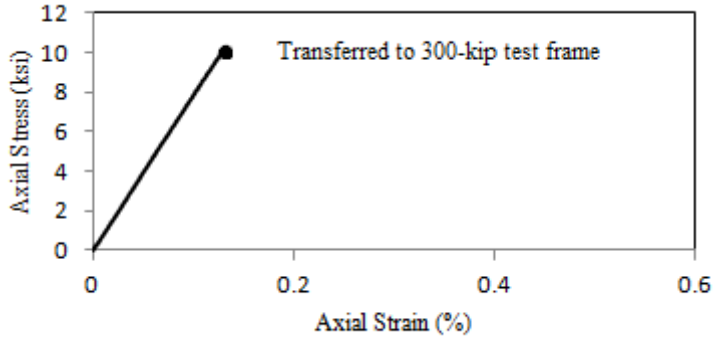

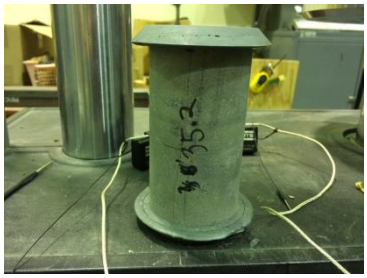

Sample Before Testing

Sample at Failure

C. Strength and Stiffness Parameters

Unconfined Compressive Strength	Young's Modulus	Axial Strain at Failure	Axial Strain at 50% Strength	Failure Type	Failure Plane Angle to Horizontal
(ksi)	(ksi)	(%)	(%)		(Degrees)
q_u	E	ε_{af}	ε_{a50}		α
15.84	7900	N/D	0.10	DPF	70

N/A – Not applicable N/D – Not determined See page 29

Test No. 15: UH Boring B4, Sample Depth = 36 ft

A. Physical Properties

Oven-Dried Unit Weight	Saturated-Surface-Dry Unit Weight	Apparent Unit Weight	CoreLok Unit Weight	Absorption	RQD	Percent Recovered
(lb/ft^3)	(lb/ft^3)	(lb/ft^3)	(lb/ft^3)	(%)	(%)	
γ_{OD}	γ_{SSD}	γ_{APP}	γ_{CL}			
162.82	167.92	177.31	161.77	3.13	93	100

B. Stress-Strain Response

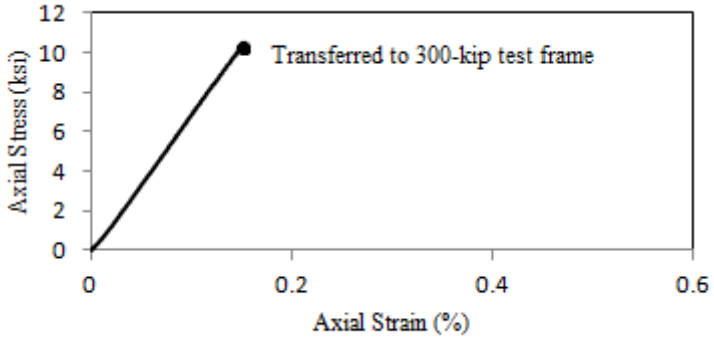

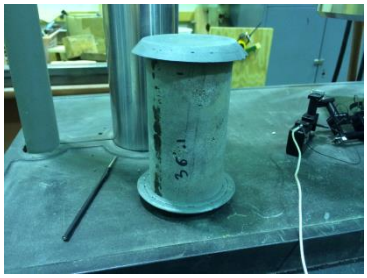

Sample Before Testing

Sample at Failure

C. Strength and Stiffness Parameters

Unconfined Compressive Strength	Young's Modulus	Axial Strain at Failure	Axial Strain at 50% Strength	Failure Type	Failure Plane Angle to Horizontal
(ksi)	(ksi)	(%)	(%)		(Degrees)
q_u	E	ε_{af}	ε_{a50}		α
14.92	6600	N/D	0.11	DPF	65

N/A – Not applicable N/D – Not determined See page 29

Test No. 16: UH Boring B4, Sample Depth = 36 ft

A. Physical Properties

Oven-Dried Unit Weight	Saturated-Surface-Dry Unit Weight	Apparent Unit Weight	CoreLok Unit Weight	Absorption	RQD	Percent Recovered
(lb/ft^3)	(lb/ft^3)	(lb/ft^3)	(lb/ft^3)	(%)	(%)	
γ_{OD}	γ_{SSD}	γ_{APP}	γ_{CL}			
151.30	158.65	171.49	152.92	4.86	93	100

B. Stress-Strain Response

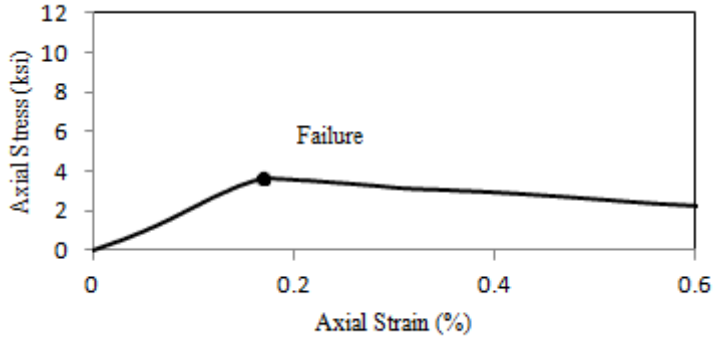

Sample Before Testing

Sample at Failure

C. Strength and Stiffness Parameters

Unconfined Compressive Strength	Young's Modulus	Axial Strain at Failure	Axial Strain at 50% Strength	Failure Type	Failure Plane Angle to Horizontal
(ksi)	(ksi)	(%)	(%)		(Degrees)
q_u	E	ε_{af}	ε_{a50}		α
3.59	1900	0.18	0.09	DPF	10

N/A – Not applicable N/D – Not determined See page 29

Test No. 17: UH Boring B4, Sample Depth = 37 ft

A. Physical Properties

Oven-Dried Unit Weight	Saturated-Surface-Dry Unit Weight	Apparent Unit Weight	CoreLok Unit Weight	Absorption	RQD	Percent Recovered
(lb/ft^3)	(lb/ft^3)	(lb/ft^3)	(lb/ft^3)	(%)	(%)	
γ_{OD}	γ_{SSD}	γ_{APP}	γ_{CL}			
154.37	161.39	173.94	155.65	4.55	93	100

B. Stress-Strain Response

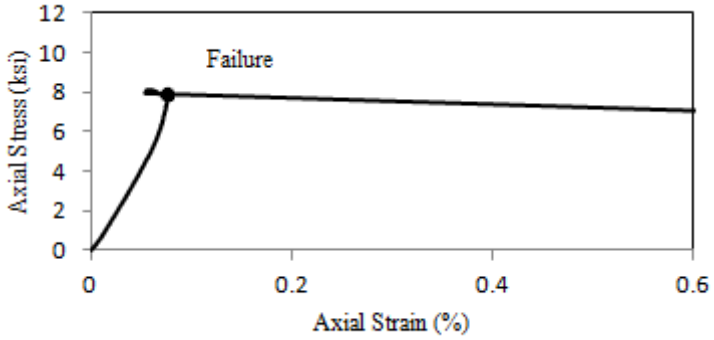

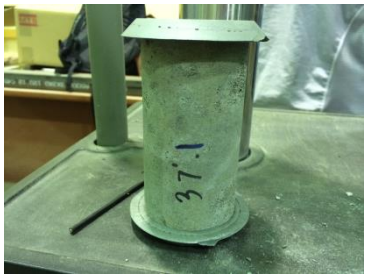

Sample Before Testing

Sample at Failure

C. Strength and Stiffness Parameters

Unconfined Compressive Strength	Young's Modulus	Axial Strain at Failure	Axial Strain at 50% Strength	Failure Type	Failure Plane Angle to Horizontal
(ksi)	(ksi)	(%)	(%)		(Degrees)
q_u	E	ε_{af}	ε_{a50}		α
8.05	7500	0.06	0.05	DPF	70

N/A – Not applicable N/D – Not determined See page 29

Test No. 18: UH Boring B4, Sample Depth = 37 ft

A. Physical Properties

Oven-Dried Unit Weight	Saturated-Surface-Dry Unit Weight	Apparent Unit Weight	CoreLok Unit Weight	Absorption	RQD	Percent Recovered
(lb/ft^3)	(lb/ft^3)	(lb/ft^3)	(lb/ft^3)	(%)	(%)	
γ_{OD}	γ_{SSD}	γ_{APP}	γ_{CL}			
147.36	155.45	169.31	148.92	5.49	93	100

B. Stress-Strain Response

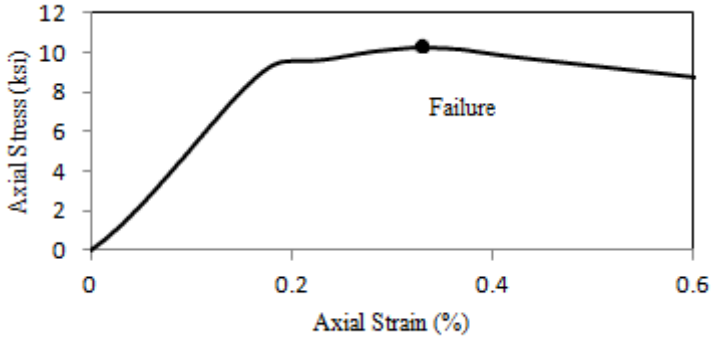

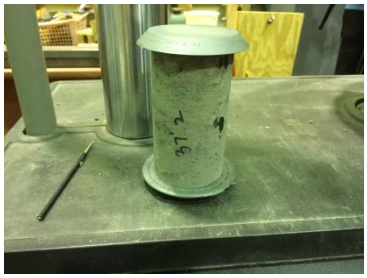

Sample Before Testing

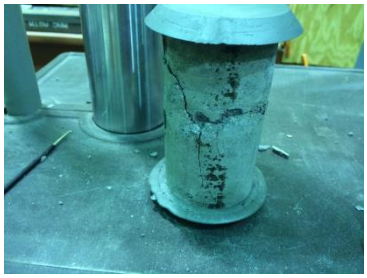

Sample at Failure

C. Strength and Stiffness Parameters

Unconfined Compressive Strength	Young's Modulus	Axial Strain at Failure	Axial Strain at 50% Strength	Failure Type	Failure Plane Angle to Horizontal
(ksi)	(ksi)	(%)	(%)		(Degrees)
q_u	E	ε_{af}	ε_{a50}		α
5.22	4700	0.33	0.10	MFF	N/A

N/A – Not applicable N/D – Not determined See page 29

Test No. 19: UH Boring B4, Sample Depth = 38 ft

A. Physical Properties

Oven-Dried Unit Weight	Saturated-Surface-Dry Unit Weight	Apparent Unit Weight	CoreLok Unit Weight	Absorption	RQD	Percent Recovered
(lb/ft^3)	(lb/ft^3)	(lb/ft^3)	(lb/ft^3)	(%)	(%)	
γ_{OD}	γ_{SSD}	γ_{APP}	γ_{CL}			
162.05	167.00	176.03	164.48	3.06	100	100

B. Stress-Strain Response

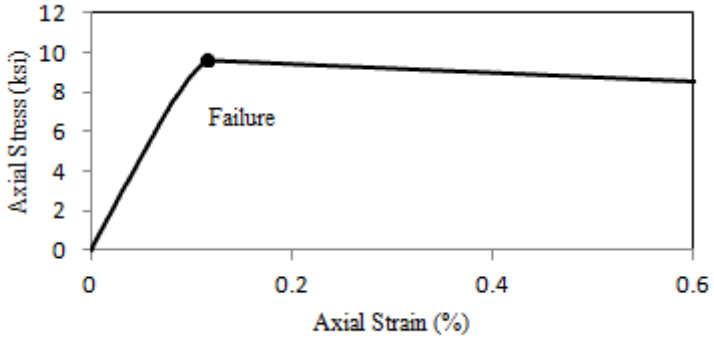

Sample Before Testing

Sample at Failure

C. Strength and Stiffness Parameters

Unconfined Compressive Strength	Young's Modulus	Axial Strain at Failure	Axial Strain at 50% Strength	Failure Type	Failure Plane Angle to Horizontal
(ksi)	(ksi)	(%)	(%)		(Degrees)
q_u	E	ε_{af}	ε_{a50}		α
9.65	10000	0.12	0.05	DPF	70

N/A – Not applicable N/D – Not determined See page 29

Test No. 20: UH Boring B4, Sample Depth = 38 ft

A. Physical Properties

Oven-Dried Unit Weight	Saturated-Surface-Dry Unit Weight	Apparent Unit Weight	CoreLok Unit Weight	Absorption	RQD	Percent Recovered
(lb/ft^3)	(lb/ft^3)	(lb/ft^3)	(lb/ft^3)	(%)	(%)	
γ_{OD}	γ_{SSD}	γ_{APP}	γ_{CL}			
160.42	166.38	177.38	161.74	3.72	100	100

B. Stress-Strain Response

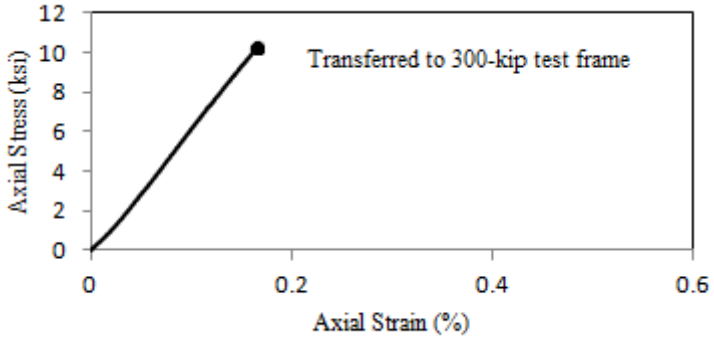

Sample Before Testing

Sample at Failure

C. Strength and Stiffness Parameters

Unconfined Compressive Strength	Young's Modulus	Axial Strain at Failure	Axial Strain at 50% Strength	Failure Type	Failure Plane Angle to Horizontal
(ksi)	(ksi)	(%)	(%)		(Degrees)
q_u	E	ε_{af}	ε_{a50}		α
15.78	5800	N/D	0.13	STF	N/A

N/A – Not applicable N/D – Not determined See page 29

Test No. 21: UH Boring B4, Sample Depth = 39 ft

A. Physical Properties

Oven-Dried Unit Weight	Saturated-Surface-Dry Unit Weight	Apparent Unit Weight	CoreLok Unit Weight	Absorption	RQD	Percent Recovered
(lb/ft^3)	(lb/ft^3)	(lb/ft^3)	(lb/ft^3)	(%)	(%)	
γ_{OD}	γ_{SSD}	γ_{APP}	γ_{CL}			
160.82	166.94	178.31	162.09	3.81	100	100

B. Stress-Strain Response

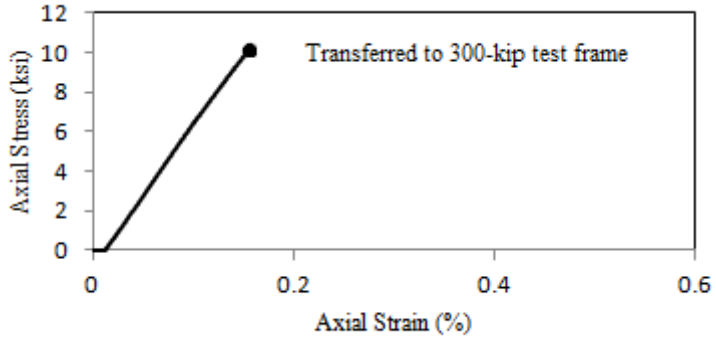

Sample Before Testing

Sample at Failure

C. Strength and Stiffness Parameters

Unconfined Compressive Strength	Young's Modulus	Axial Strain at Failure	Axial Strain at 50% Strength	Failure Type	Failure Plane Angle to Horizontal
(ksi)	(ksi)	(%)	(%)		(Degrees)
q_u	E	ε_{af}	ε_{a50}		α
21.75	6300	N/D	N/D	STF	N/A

N/A – Not applicable N/D – Not determined See page 29

Test No. 22: UH Boring B4, Sample Depth = 39 ft

A. Physical Properties

Oven-Dried Unit Weight	Saturated-Surface-Dry Unit Weight	Apparent Unit Weight	CoreLok Unit Weight	Absorption	RQD	Percent Recovered
(lb/ft^3)	(lb/ft^3)	(lb/ft^3)	(lb/ft^3)	(%)	(%)	
γ_{OD}	γ_{SSD}	γ_{APP}	γ_{CL}			
156.28	163.67	177.27	156.06	4.73	100	100

B. Stress-Strain Response

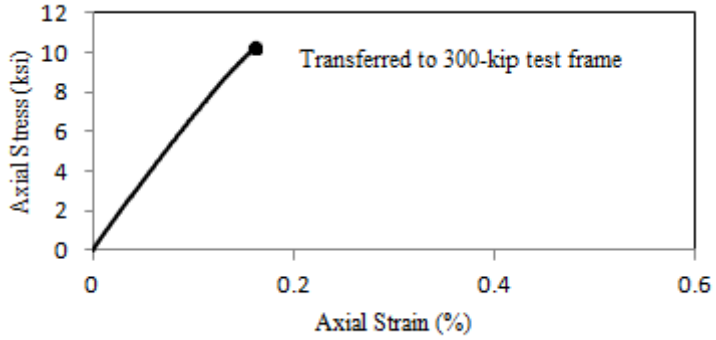

Sample Before Testing

Sample at Failure

C. Strength and Stiffness Parameters

Unconfined Compressive Strength	Young's Modulus	Axial Strain at Failure	Axial Strain at 50% Strength	Failure Type	Failure Plane Angle to Horizontal
(ksi)	(ksi)	(%)	(%)		(Degrees)
q_u	E	ε_{af}	ε_{a50}		α
13.43	7100	N/D	0.10	DPF	90

N/A – Not applicable N/D – Not determined See page 29

Test No. 23: UH Boring B4, Sample Depth = 40 ft

A. Physical Properties

Oven-Dried Unit Weight	Saturated-Surface-Dry Unit Weight	Apparent Unit Weight	CoreLok Unit Weight	Absorption	RQD	Percent Recovered
(lb/ft^3)	(lb/ft^3)	(lb/ft^3)	(lb/ft^3)	(%)	(%)	
γ_{OD}	γ_{SSD}	γ_{APP}	γ_{CL}			
148.04	156.31	170.68	150.73	5.59	100	100

B. Stress-Strain Response

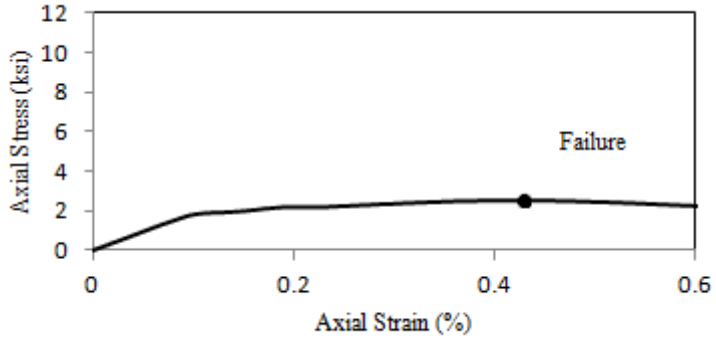

Sample Before Testing

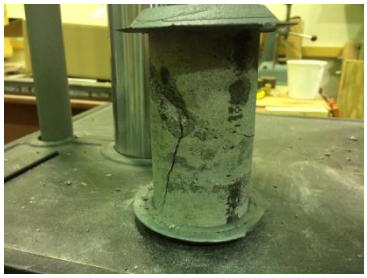

Sample at Failure

C. Strength and Stiffness Parameters

Unconfined Compressive Strength	Young's Modulus	Axial Strain at Failure	Axial Strain at 50% Strength	Failure Type	Failure Plane Angle to Horizontal
(ksi)	(ksi)	(%)	(%)		(Degrees)
q_u	E	ε_{af}	ε_{a50}		α
2.55	2000	0.43	0.07	DPF	40

N/A – Not applicable N/D – Not determined See page 29

Test No. 24: UH Boring B4, Sample Depth = 40 ft

A. Physical Properties

Oven-Dried Unit Weight	Saturated-Surface-Dry Unit Weight	Apparent Unit Weight	CoreLok Unit Weight	Absorption	RQD	Percent Recovered
(lb/ft^3)	(lb/ft^3)	(lb/ft^3)	(lb/ft^3)	(%)	(%)	
γ_{OD}	γ_{SSD}	γ_{APP}	γ_{CL}			
159.99	165.59	175.77	161.08	3.50	100	100

B. Stress-Strain Response

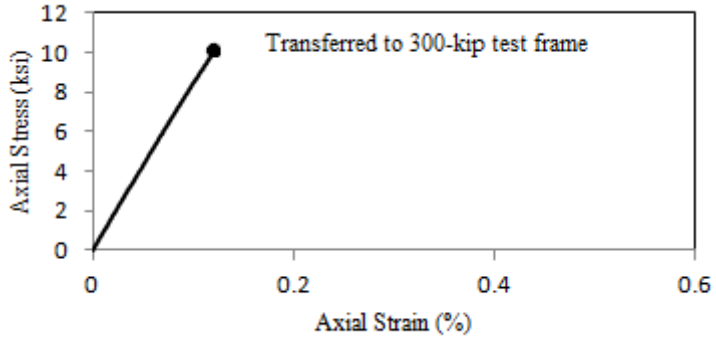

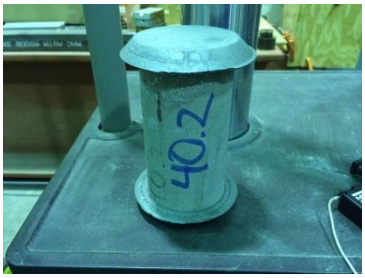

Sample Before Testing

Sample at Failure

C. Strength and Stiffness Parameters

Unconfined Compressive Strength	Young's Modulus	Axial Strain at Failure	Axial Strain at 50% Strength	Failure Type	Failure Plane Angle to Horizontal
(ksi)	(ksi)	(%)	(%)		(Degrees)
q_u	E	ε_{af}	ε_{a50}		α
18.70	8600	N/D	0.11	DPF	90

N/A – Not applicable N/D – Not determined See page 29

Test No. 25: UH Boring B4, Sample Depth = 41 ft

A. Physical Properties

Oven-Dried Unit Weight	Saturated-Surface-Dry Unit Weight	Apparent Unit Weight	CoreLok Unit Weight	Absorption	RQD	Percent Recovered
(lb/ft^3)	(lb/ft^3)	(lb/ft^3)	(lb/ft^3)	(%)	(%)	
γ_{OD}	γ_{SSD}	γ_{APP}	γ_{CL}			
159.13	164.83	175.13	161.56	3.58	100	100

B. Stress-Strain Response

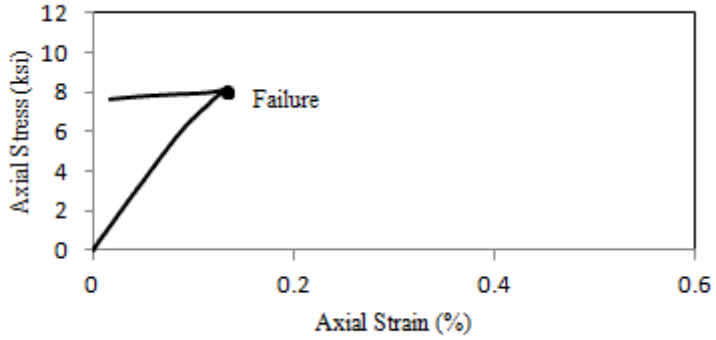

Sample Before Testing

Sample at Failure

C. Strength and Stiffness Parameters

Unconfined Compressive Strength	Young's Modulus	Axial Strain at Failure	Axial Strain at 50% Strength	Failure Type	Failure Plane Angle to Horizontal
(ksi)	(ksi)	(%)	(%)		(Degrees)
q_u	E	ε_{af}	ε_{a50}		α
8.21	7000	0.13	0.06	DPF	70

N/A – Not applicable N/D – Not determined See page 29

Test No. 26: UH Boring B4, Sample Depth = 42 ft

A. Physical Properties

Oven-Dried Unit Weight	Saturated-Surface-Dry Unit Weight	Apparent Unit Weight	CoreLok Unit Weight	Absorption	RQD	Percent Recovered
(lb/ft^3)	(lb/ft^3)	(lb/ft^3)	(lb/ft^3)	(%)	(%)	
γ_{OD}	γ_{SSD}	γ_{APP}	γ_{CL}			
157.22	164.23	177.12	157.07	4.46	100	100

B. Stress-Strain Response

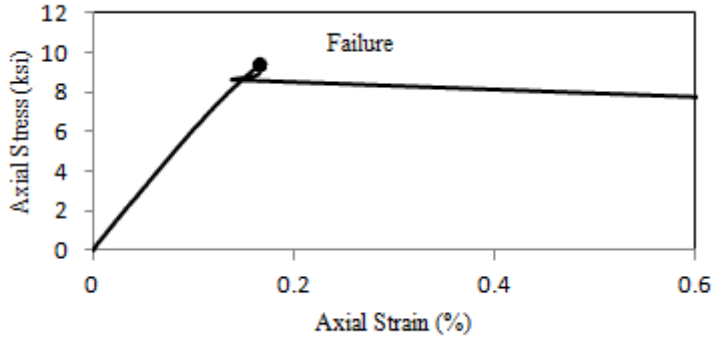

Sample Before Testing Sample at Failure

C. Strength and Stiffness Parameters

Unconfined Compressive Strength	Young's Modulus	Axial Strain at Failure	Axial Strain at 50% Strength	Failure Type	Failure Plane Angle to Horizontal
(ksi)	(ksi)	(%)	(%)		(Degrees)
q_u	E	ε_{af}	ε_{a50}		α
9.40	6300	0.17	0.08	DPF	60

N/A – Not applicable N/D – Not determined See page 29

Test No. 27: UH Boring B4, Sample Depth = 45 ft

A. Physical Properties

Oven-Dried Unit Weight	Saturated-Surface-Dry Unit Weight	Apparent Unit Weight	CoreLok Unit Weight	Absorption	RQD	Percent Recovered
(lb/ft^3)	(lb/ft^3)	(lb/ft^3)	(lb/ft^3)	(%)	(%)	
γ_{OD}	γ_{SSD}	γ_{APP}	γ_{CL}			
151.06	159.27	173.95	150.76	5.44	93	100

B. Stress-Strain Response

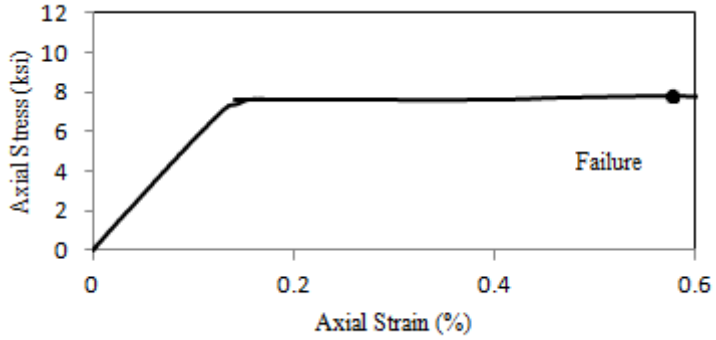

Sample Before Testing

Sample at Failure

C. Strength and Stiffness Parameters

Unconfined Compressive Strength	Young's Modulus	Axial Strain at Failure	Axial Strain at 50% Strength	Failure Type	Failure Plane Angle to Horizontal
(ksi)	(ksi)	(%)	(%)		(Degrees)
q_u	E	ε_{af}	ε_{a50}		α
7.83	5800	0.58	0.07	MFF	N/A

N/A – Not applicable N/D – Not determined See page 29

Test No. 28: UH Boring B4, Sample Depth = 45 ft

A. Physical Properties

Oven-Dried Unit Weight	Saturated-Surface-Dry Unit Weight	Apparent Unit Weight	CoreLok Unit Weight	Absorption	RQD	Percent Recovered
(lb/ft^3)	(lb/ft^3)	(lb/ft^3)	(lb/ft^3)	(%)	(%)	
γ_{OD}	γ_{SSD}	γ_{APP}	γ_{CL}			
141.50	151.56	168.71	140.00	7.11	93	100

B. Stress-Strain Response

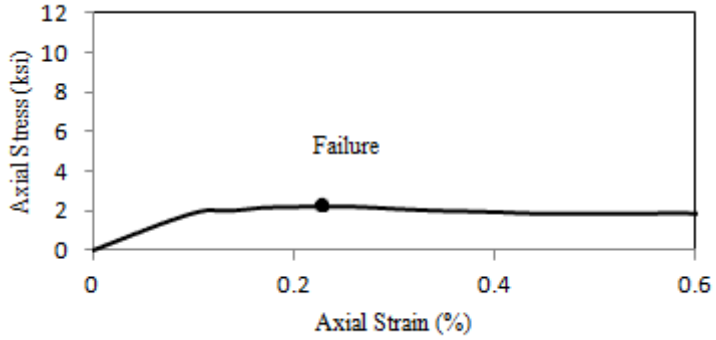

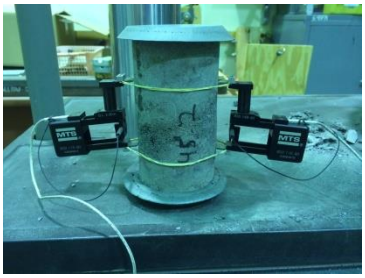

Sample Before Testing

Sample at Failure

C. Strength and Stiffness Parameters

Unconfined Compressive Strength	Young's Modulus	Axial Strain at Failure	Axial Strain at 50% Strength	Failure Type	Failure Plane Angle to Horizontal
(ksi)	(ksi)	(%)	(%)		(Degrees)
q_u	E	ε_{af}	ε_{a50}		α
2.16	1900	0.23	0.06	MFF	N/A

N/A – Not applicable N/D – Not determined See page 29

Test No. 29: UH Boring B4, Sample Depth = 48 ft

A. Physical Properties

Oven-Dried Unit Weight	Saturated-Surface-Dry Unit Weight	Apparent Unit Weight	CoreLok Unit Weight	Absorption	RQD	Percent Recovered
(lb/ft^3)	(lb/ft^3)	(lb/ft^3)	(lb/ft^3)	(%)	(%)	
γ_{OD}	γ_{SSD}	γ_{APP}	γ_{CL}			
154.73	161.74	174.32	156.80	4.53	100	100

B. Stress-Strain Response

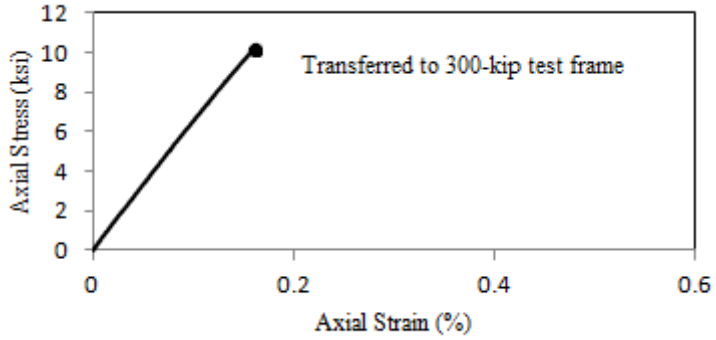

Sample Before Testing

Sample at Failure

C. Strength and Stiffness Parameters

Unconfined Compressive Strength	Young's Modulus	Axial Strain at Failure	Axial Strain at 50% Strength	Failure Type	Failure Plane Angle to Horizontal
(ksi)	(ksi)	(%)	(%)		(Degrees)
q_u	E	ε_{af}	ε_{a50}		α
11.81	6700	N/D	0.09	DPF	80

N/A – Not applicable N/D – Not determined See page 29

Test No. 30: UH Boring B4, Sample Depth = 48 ft

A. Physical Properties

Oven-Dried Unit Weight	Saturated-Surface-Dry Unit Weight	Apparent Unit Weight	CoreLok Unit Weight	Absorption	RQD	Percent Recovered
(lb/ft^3)	(lb/ft^3)	(lb/ft^3)	(lb/ft^3)	(%)	(%)	
γ_{OD}	γ_{SSD}	γ_{APP}	γ_{CL}			
143.27	153.48	171.31	152.07	7.13	100	100

B. Stress-Strain Response

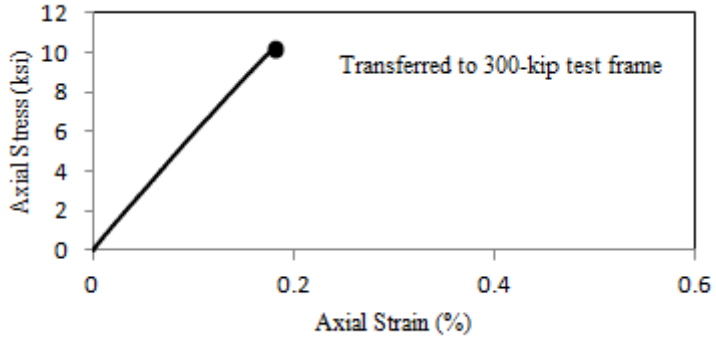

Sample Before Testing

Sample at Failure

C. Strength and Stiffness Parameters

Unconfined Compressive Strength	Young's Modulus	Axial Strain at Failure	Axial Strain at 50% Strength	Failure Type	Failure Plane Angle to Horizontal
(ksi)	(ksi)	(%)	(%)		(Degrees)
q_u	E	ε_{af}	ε_{a50}		α
9.77	6100	N/D	0.08	MFF	N/A

N/A – Not applicable N/D – Not determined See page 29

Test No. 31: UH Boring B4, Sample Depth = 49 ft

A. Physical Properties

Oven-Dried Unit Weight	Saturated-Surface-Dry Unit Weight	Apparent Unit Weight	CoreLok Unit Weight	Absorption	RQD	Percent Recovered
(lb/ft^3)	(lb/ft^3)	(lb/ft^3)	(lb/ft^3)	(%)	(%)	
γ_{OD}	γ_{SSD}	γ_{APP}	γ_{CL}			
149.25	157.64	172.43	151.28	5.62	100	100

B. Stress-Strain Response

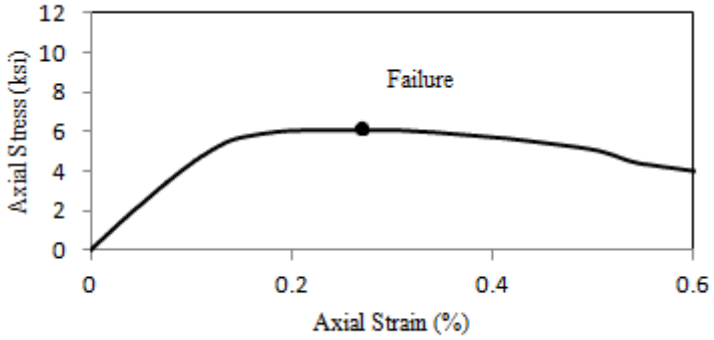

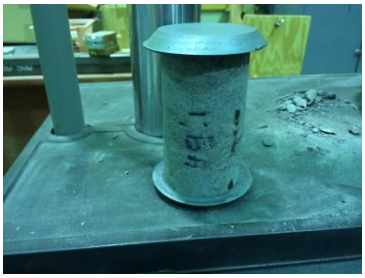

Sample Before Testing

Sample at Failure

C. Strength and Stiffness Parameters

Unconfined Compressive Strength	Young's Modulus	Axial Strain at Failure	Axial Strain at 50% Strength	Failure Type	Failure Plane Angle to Horizontal
(ksi)	(ksi)	(%)	(%)		(Degrees)
q_u	E	ε_{af}	ε_{a50}		α
6.05	4700	0.29	0.07	DPF	60

N/A – Not applicable N/D – Not determined See page 29

Test No. 32: UH Boring B4, Sample Depth = 49 ft

A. Physical Properties

Oven-Dried Unit Weight	Saturated-Surface-Dry Unit Weight	Apparent Unit Weight	CoreLok Unit Weight	Absorption	RQD	Percent Recovered
(lb/ft^3)	(lb/ft^3)	(lb/ft^3)	(lb/ft^3)	(%)	(%)	
γ_{OD}	γ_{SSD}	γ_{APP}	γ_{CL}			
157.98	164.18	175.39	160.30	3.92	100	100

B. Stress-Strain Response

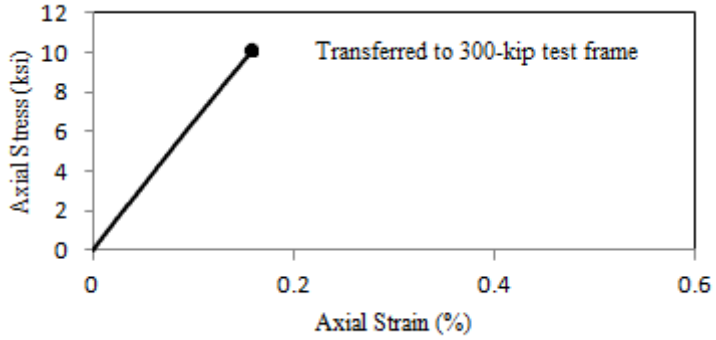

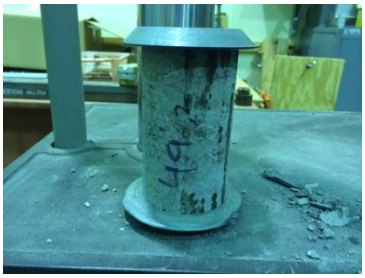

Sample Before Testing

Sample at Failure

C. Strength and Stiffness Parameters

Unconfined Compressive Strength	Young's Modulus	Axial Strain at Failure	Axial Strain at 50% Strength	Failure Type	Failure Plane Angle to Horizontal
(ksi)	(ksi)	(%)	(%)		(Degrees)
q_u	E	ε_{af}	ε_{a50}		α
10.99	6500	N/D	0.09	DPF	80

N/A – Not applicable N/D – Not determined See page 29

Test No. 33: UH Boring B4, Sample Depth = 50 ft

A. Physical Properties

Oven-Dried Unit Weight	Saturated-Surface-Dry Unit Weight	Apparent Unit Weight	CoreLok Unit Weight	Absorption	RQD	Percent Recovered
(lb/ft^3)	(lb/ft^3)	(lb/ft^3)	(lb/ft^3)	(%)	(%)	
γ_{OD}	γ_{SSD}	γ_{APP}	γ_{CL}			
137.69	147.91	164.64	138.38	7.42	100	100

B. Stress-Strain Response

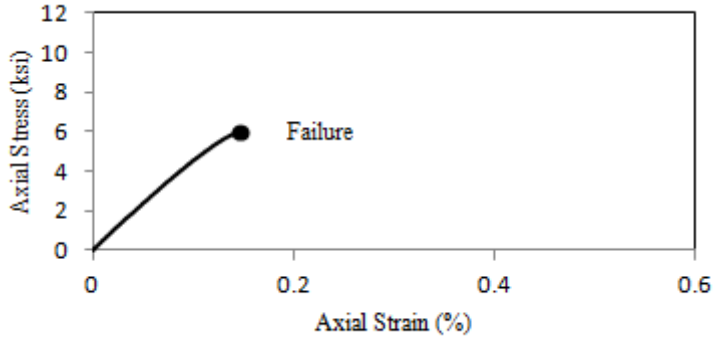

Sample Before Testing

Sample at Failure

C. Strength and Stiffness Parameters

Unconfined Compressive Strength	Young's Modulus	Axial Strain at Failure	Axial Strain at 50% Strength	Failure Type	Failure Plane Angle to Horizontal
(ksi)	(ksi)	(%)	(%)		(Degrees)
q_u	E	ε_{af}	ε_{a50}		α
5.94	4900	0.15	0.06	DPF	80

N/A – Not applicable N/D – Not determined See page 29

Test No. 34: UH Boring B4, Sample Depth = 51 ft

A. Physical Properties

Oven-Dried Unit Weight	Saturated-Surface-Dry Unit Weight	Apparent Unit Weight	CoreLok Unit Weight	Absorption	RQD	Percent Recovered
(lb/ft^3)	(lb/ft^3)	(lb/ft^3)	(lb/ft^3)	(%)	(%)	
γ_{OD}	γ_{SSD}	γ_{APP}	γ_{CL}			
134.37	145.15	162.43	134.82	8.02	100	100

B. Stress-Strain Response

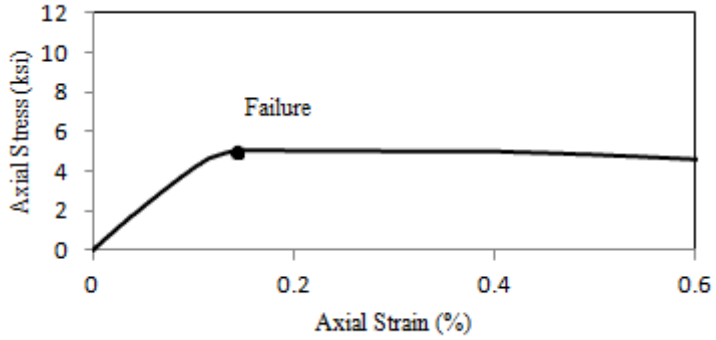

Sample Before Testing

Sample at Failure

C. Strength and Stiffness Parameters

Unconfined Compressive Strength	Young's Modulus	Axial Strain at Failure	Axial Strain at 50% Strength	Failure Type	Failure Plane Angle to Horizontal
(ksi)	(ksi)	(%)	(%)		(Degrees)
q_u	E	ε_{af}	ε_{a50}		α
5.00	4500	0.16	0.06	DPF	50

N/A – Not applicable N/D – Not determined See page 29

Test No. 35: UH Boring B4, Sample Depth = 53 ft

A. Physical Properties

Oven-Dried Unit Weight	Saturated-Surface-Dry Unit Weight	Apparent Unit Weight	CoreLok Unit Weight	Absorption	RQD	Percent Recovered
(lb/ft^3)	(lb/ft^3)	(lb/ft^3)	(lb/ft^3)	(%)	(%)	
γ_{OD}	γ_{SSD}	γ_{APP}	γ_{CL}			
131.47	143.14	161.73	132.00	8.88	70	70

B. Stress-Strain Response

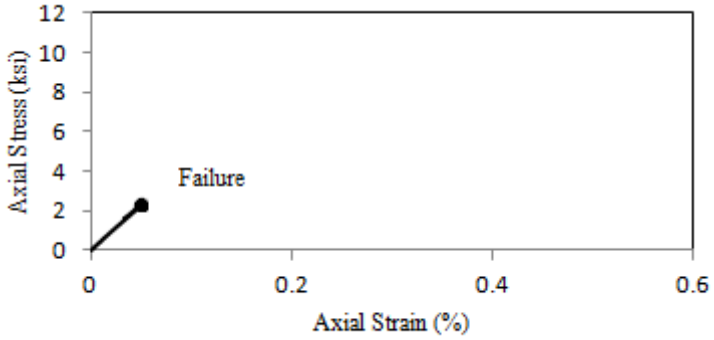

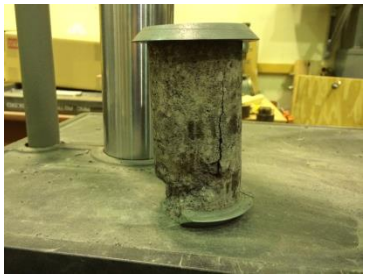

Sample at Failure

*Picture of sample before testing was not taken

C. Strength and Stiffness Parameters

Unconfined Compressive Strength	Young's Modulus	Axial Strain at Failure	Axial Strain at 50% Strength	Failure Type	Failure Plane Angle to Horizontal
(ksi)	(ksi)	(%)	(%)		(Degrees)
q_u	E	ε_{af}	ε_{a50}		α
2.36	4600	0.05	0.03	DPF	5

N/A – Not applicable N/D – Not determined See page 29

Test No. 36: UH Boring B4, Sample Depth = 53 ft

A. Physical Properties

Oven-Dried Unit Weight	Saturated-Surface-Dry Unit Weight	Apparent Unit Weight	CoreLok Unit Weight	Absorption	RQD	Percent Recovered
(lb/ft^3)	(lb/ft^3)	(lb/ft^3)	(lb/ft^3)	(%)	(%)	
γ_{OD}	γ_{SSD}	γ_{APP}	γ_{CL}			
126.15	138.85	158.38	126.91	10.06	70	70

B. Stress-Strain Response

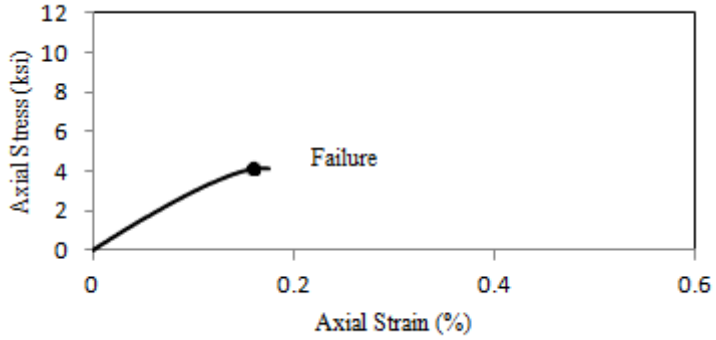

Sample Before Testing

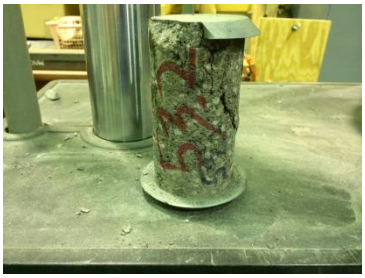

Sample at Failure

C. Strength and Stiffness Parameters

Unconfined Compressive Strength	Young's Modulus	Axial Strain at Failure	Axial Strain at 50% Strength	Failure Type	Failure Plane Angle to Horizontal
(ksi)	(ksi)	(%)	(%)		(Degrees)
q_u	E	ε_{af}	ε_{a50}		α
4.11	3200	0.17	0.07	DPF	55

N/A – Not applicable N/D – Not determined See page 29

Test No. 37: UH Boring B4, Sample Depth = 54 ft

A. Physical Properties

Oven-Dried Unit Weight	Saturated-Surface-Dry Unit Weight	Apparent Unit Weight	CoreLok Unit Weight	Absorption	RQD	Percent Recovered
(lb/ft^3)	(lb/ft^3)	(lb/ft^3)	(lb/ft^3)	(%)	(%)	
γ_{OD}	γ_{SSD}	γ_{APP}	γ_{CL}			
128.25	140.66	160.07	129.05	9.67	70	70

B. Stress-Strain Response

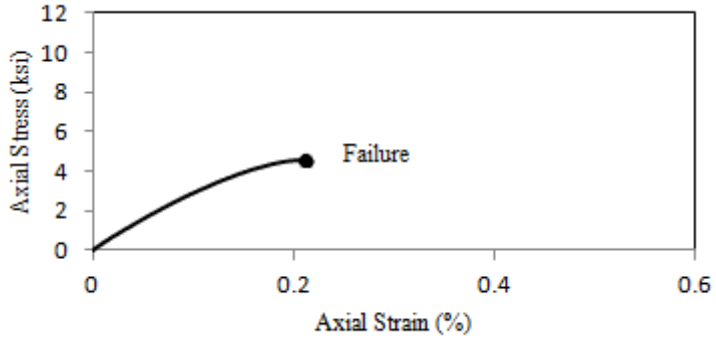

Sample Before Testing

Sample at Failure

C. Strength and Stiffness Parameters

Unconfined Compressive Strength	Young's Modulus	Axial Strain at Failure	Axial Strain at 50% Strength	Failure Type	Failure Plane Angle to Horizontal
(ksi)	(ksi)	(%)	(%)		(Degrees)
q_u	E	ε_{af}	ε_{a50}		α
4.55	3300	0.21	0.07	DPF	70

N/A – Not applicable N/D – Not determined See page 29

Test No. 38: UH Boring B4, Sample Depth = 55 ft

A. Physical Properties

Oven-Dried Unit Weight	Saturated-Surface-Dry Unit Weight	Apparent Unit Weight	CoreLok Unit Weight	Absorption	RQD	Percent Recovered
(lb/ft^3)	(lb/ft^3)	(lb/ft^3)	(lb/ft^3)	(%)	(%)	
γ_{OD}	γ_{SSD}	γ_{APP}	γ_{CL}			
122.95	137.98	161.95	122.70	12.22	70	70

B. Stress-Strain Response

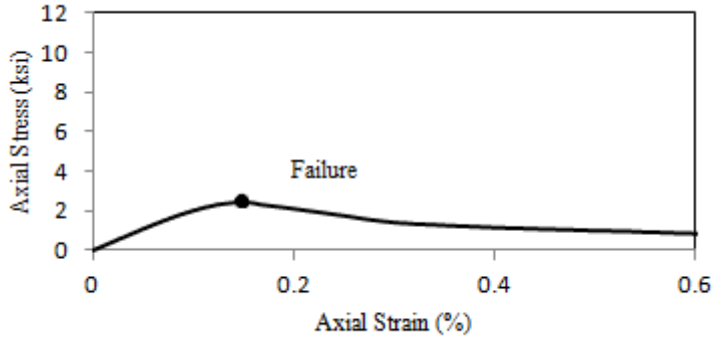

Sample Before Testing Sample at Failure

C. Strength and Stiffness Parameters

Unconfined Compressive Strength	Young's Modulus	Axial Strain at Failure	Axial Strain at 50% Strength	Failure Type	Failure Plane Angle to Horizontal
(ksi)	(ksi)	(%)	(%)		(Degrees)
q_u	E	ε_{af}	ε_{a50}		α
2.44	2200	0.15	0.06	DPF	70

N/A – Not applicable N/D – Not determined See page 29

Test No. 39: UH Boring B4, Sample Depth = 55 ft

A. Physical Properties

Oven-Dried Unit Weight	Saturated-Surface-Dry Unit Weight	Apparent Unit Weight	CoreLok Unit Weight	Absorption	RQD	Percent Recovered
(lb/ft^3)	(lb/ft^3)	(lb/ft^3)	(lb/ft^3)	(%)	(%)	
γ_{OD}	γ_{SSD}	γ_{APP}	γ_{CL}			
128.69	142.19	164.22	128.56	10.49	70	70

B. Stress-Strain Response

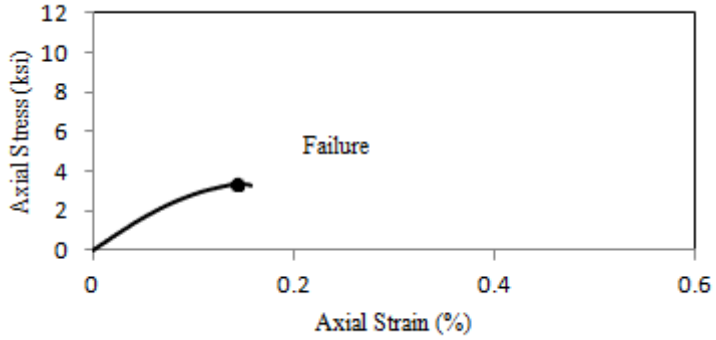

Sample Before Testing

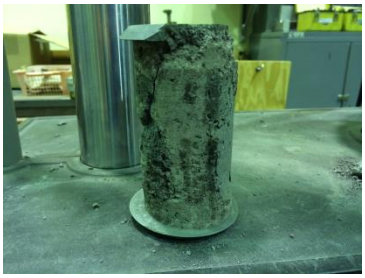

Sample at Failure

C. Strength and Stiffness Parameters

Unconfined Compressive Strength	Young's Modulus	Axial Strain at Failure	Axial Strain at 50% Strength	Failure Type	Failure Plane Angle to Horizontal
(ksi)	(ksi)	(%)	(%)		(Degrees)
q_u	E	ε_{af}	ε_{a50}		α
3.37	3500	0.15	0.05	DPF	60

N/A – Not applicable N/D – Not determined See page 29

Test No. 40: UH Boring B4, Sample Depth = 57 ft

A. Physical Properties

Oven-Dried Unit Weight	Saturated-Surface-Dry Unit Weight	Apparent Unit Weight	CoreLok Unit Weight	Absorption	RQD	Percent Recovered
(lb/ft^3)	(lb/ft^3)	(lb/ft^3)	(lb/ft^3)	(%)	(%)	
γ_{OD}	γ_{SSD}	γ_{APP}	γ_{CL}			
180.77	183.19	188.06	182.27	1.34	70	70

B. Stress-Strain Response

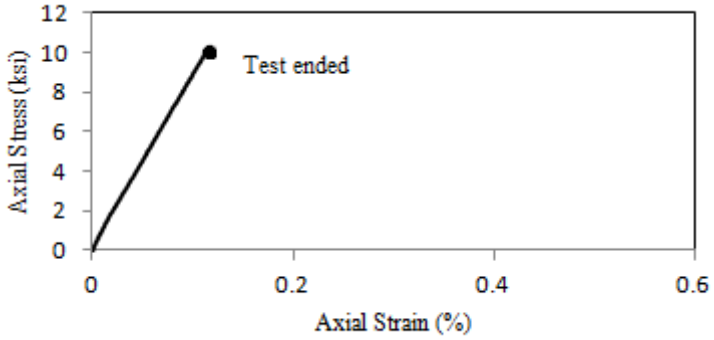

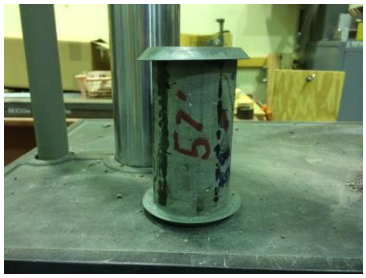

Sample Before Testing

Sample was destroyed before it could be tested on the 300-kip test frame

C. Strength and Stiffness Parameters

Unconfined Compressive Strength	Young's Modulus	Axial Strain at Failure	Axial Strain at 50% Strength	Failure Type	Failure Plane Angle to Horizontal
(ksi)	(ksi)	(%)	(%)		(Degrees)
q_u	E	ε_{af}	ε_{a50}		α
10.20	9700	N/D	0.06	N/A	N/A

N/A – Not applicable N/D – Not determined See page 29

Test No. 41: UH Boring B4, Sample Depth = 58 ft

A. Physical Properties

Oven-Dried Unit Weight	Saturated-Surface-Dry Unit Weight	Apparent Unit Weight	CoreLok Unit Weight	Absorption	RQD	Percent Recovered
(lb/ft^3)	(lb/ft^3)	(lb/ft^3)	(lb/ft^3)	(%)	(%)	
γ_{OD}	γ_{SSD}	γ_{APP}	γ_{CL}			
177.43	180.81	187.59	178.60	1.91	50	53

B. Stress-Strain Response

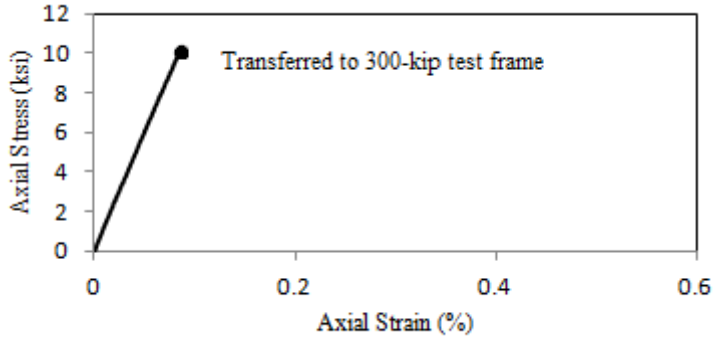

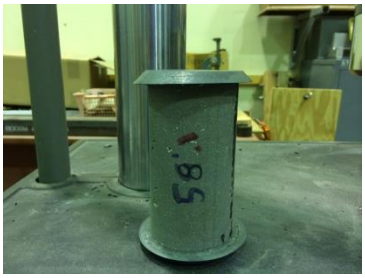

Sample Before Testing

Sample at Failure

C. Strength and Stiffness Parameters

Unconfined Compressive Strength	Young's Modulus	Axial Strain at Failure	Axial Strain at 50% Strength	Failure Type	Failure Plane Angle to Horizontal
(ksi)	(ksi)	(%)	(%)		(Degrees)
q_u	E	ε_{af}	ε_{a50}		α
29.99	11900	N/D	N/D	STF	N/A

N/A – Not applicable N/D – Not determined See page 29

Test No. 42: UH Boring B4, Sample Depth = 58 ft

A. Physical Properties

Oven-Dried Unit Weight	Saturated-Surface-Dry Unit Weight	Apparent Unit Weight	CoreLok Unit Weight	Absorption	RQD	Percent Recovered
(lb/ft^3)	(lb/ft^3)	(lb/ft^3)	(lb/ft^3)	(%)	(%)	
γ_{OD}	γ_{SSD}	γ_{APP}	γ_{CL}			
177.73	181.86	190.33	173.71	2.32	50	53

B. Stress-Strain Response

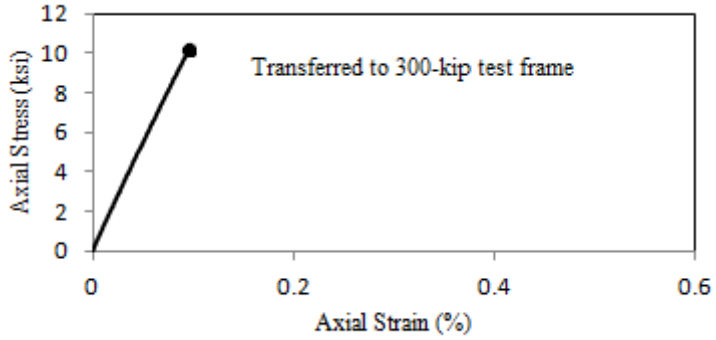

Sample Before Testing

Sample at Failure

C. Strength and Stiffness Parameters

Unconfined Compressive Strength	Young's Modulus	Axial Strain at Failure	Axial Strain at 50% Strength	Failure Type	Failure Plane Angle to Horizontal
(ksi)	(ksi)	(%)	(%)		(Degrees)
q_u	E	ε_{af}	ε_{a50}		α
40.50	10600	N/D	N/D	STF	N/A

N/A – Not applicable N/D – Not determined See page 29

Test No. 43: UH Boring B4, Sample Depth = 59 ft

A. Physical Properties

Oven-Dried Unit Weight	Saturated-Surface-Dry Unit Weight	Apparent Unit Weight	CoreLok Unit Weight	Absorption	RQD	Percent Recovered
(lb/ft^3)	(lb/ft^3)	(lb/ft^3)	(lb/ft^3)	(%)	(%)	
γ_{OD}	γ_{SSD}	γ_{APP}	γ_{CL}			
182.18	184.36	188.78	173.81	1.20	50	53

B. Stress-Strain Response

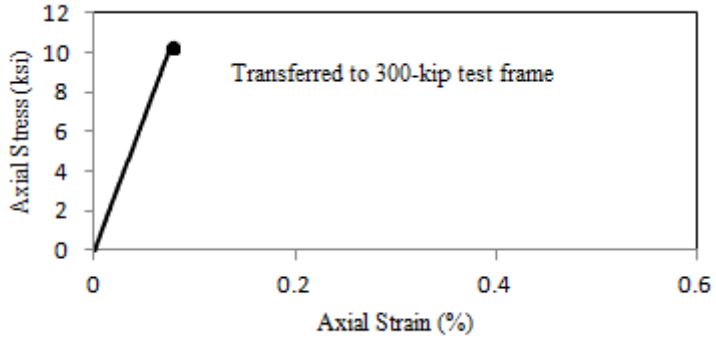

Sample Before Testing

Sample at Failure

C. Strength and Stiffness Parameters

Unconfined Compressive Strength	Young's Modulus	Axial Strain at Failure	Axial Strain at 50% Strength	Failure Type	Failure Plane Angle to Horizontal
(ksi)	(ksi)	(%)	(%)		(Degrees)
q_u	E	ε_{af}	ε_{a50}		α
33.98	13300	N/D	N/D	STF	N/A

N/A – Not applicable N/D – Not determined See page 29

Test No. 44: UH Boring B4, Sample Depth = 68 ft

A. Physical Properties

Oven-Dried Unit Weight	Saturated-Surface-Dry Unit Weight	Apparent Unit Weight	CoreLok Unit Weight	Absorption	RQD	Percent Recovered
(lb/ft^3)	(lb/ft^3)	(lb/ft^3)	(lb/ft^3)	(%)	(%)	
γ_{OD}	γ_{SSD}	γ_{APP}	γ_{CL}			
181.25	184.88	192.45	180.50	2.00	97	100

B. Stress-Strain Response

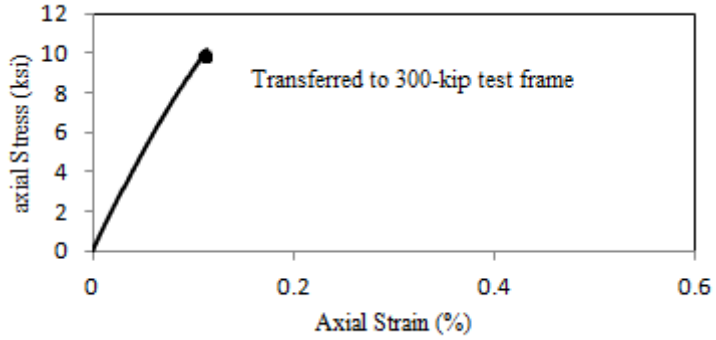

Sample Before Testing

Sample at Failure

C. Strength and Stiffness Parameters

Unconfined Compressive Strength	Young's Modulus	Axial Strain at Failure	Axial Strain at 50% Strength	Failure Type	Failure Plane Angle to Horizontal
(ksi)	(ksi)	(%)	(%)		(Degrees)
q_u	E	ε_{af}	ε_{a50}		α
23.47	10000	N/D	N/D	STF	N/A

N/A – Not applicable N/D – Not determined See page 29

Test No. 45: UH Boring B4, Sample Depth = 68 ft

A. Physical Properties

Oven-Dried Unit Weight	Saturated-Surface-Dry Unit Weight	Apparent Unit Weight	CoreLok Unit Weight	Absorption	RQD	Percent Recovered
(lb/ft^3)	(lb/ft^3)	(lb/ft^3)	(lb/ft^3)	(%)	(%)	
γ_{OD}	γ_{SSD}	γ_{APP}	γ_{CL}			
179.12	182.54	189.51	180.40	1.91	97	100

B. Stress-Strain Response

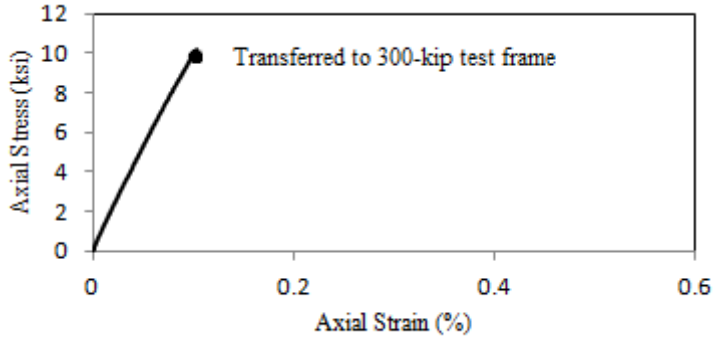

Sample Before Testing

Sample at Failure

C. Strength and Stiffness Parameters

Unconfined Compressive Strength	Young's Modulus	Axial Strain at Failure	Axial Strain at 50% Strength	Failure Type	Failure Plane Angle to Horizontal
(ksi)	(ksi)	(%)	(%)		(Degrees)
q_u	E	ε_{af}	ε_{a50}		α
26.91	10600	N/D	N/D	STF	N/A

N/A – Not applicable N/D – Not determined See page 29

Test No. 46: UH Boring B4, Sample Depth = 69 ft

A. Physical Properties

Oven-Dried Unit Weight	Saturated-Surface-Dry Unit Weight	Apparent Unit Weight	CoreLok Unit Weight	Absorption	RQD	Percent Recovered
(lb/ft^3)	(lb/ft^3)	(lb/ft^3)	(lb/ft^3)	(%)	(%)	
γ_{OD}	γ_{SSD}	γ_{APP}	γ_{CL}			
178.70	182.35	189.79	179.77	2.04	97	100

B. Stress-Strain Response

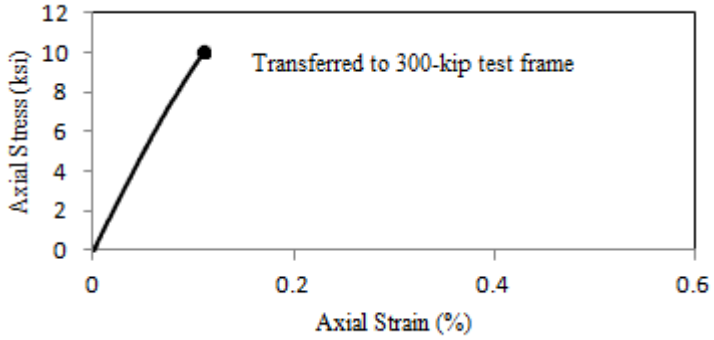

Sample Before Testing

Sample at Failure

C. Strength and Stiffness Parameters

Unconfined Compressive Strength	Young's Modulus	Axial Strain at Failure	Axial Strain at 50% Strength	Failure Type	Failure Plane Angle to Horizontal
(ksi)	(ksi)	(%)	(%)		(Degrees)
q_u	E	ε_{af}	ε_{a50}		α
21.21	10000	N/D	N/D	STF	N/A

N/A – Not applicable N/D – Not determined See page 29

Test No. 47: UH Boring B4, Sample Depth = 69 ft

A. Physical Properties

Oven-Dried Unit Weight	Saturated-Surface-Dry Unit Weight	Apparent Unit Weight	CoreLok Unit Weight	Absorption	RQD	Percent Recovered
(lb/ft^3)	(lb/ft^3)	(lb/ft^3)	(lb/ft^3)	(%)	(%)	
γ_{OD}	γ_{SSD}	γ_{APP}	γ_{CL}			
178.79	182.42	189.82	179.88	2.03	97	100

B. Stress-Strain Response

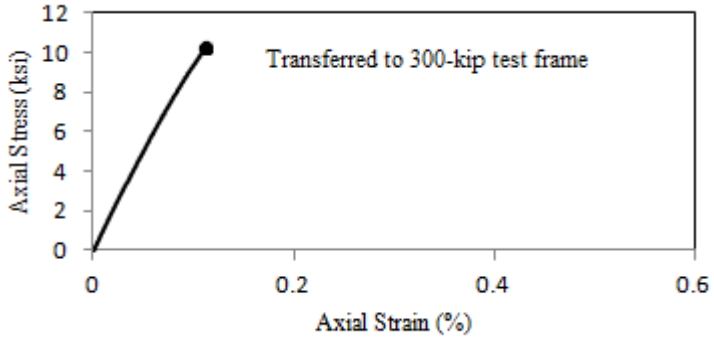

Sample Before Testing

Sample at Failure

C. Strength and Stiffness Parameters

Unconfined Compressive Strength	Young's Modulus	Axial Strain at Failure	Axial Strain at 50% Strength	Failure Type	Failure Plane Angle to Horizontal
(ksi)	(ksi)	(%)	(%)		(Degrees)
q_u	E	ε_{af}	ε_{a50}		α
26.72	9800	N/D	N/D	STF	N/A

N/A – Not applicable N/D – Not determined See page 29

Test No. 48: UH Boring B4, Sample Depth = 70 ft

A. Physical Properties

Oven-Dried Unit Weight	Saturated-Surface-Dry Unit Weight	Apparent Unit Weight	CoreLok Unit Weight	Absorption	RQD	Percent Recovered
(lb/ft^3)	(lb/ft^3)	(lb/ft^3)	(lb/ft^3)	(%)	(%)	
γ_{OD}	γ_{SSD}	γ_{APP}	γ_{CL}			
181.98	184.84	190.71	183.36	1.57	97	100

B. Stress-Strain Response

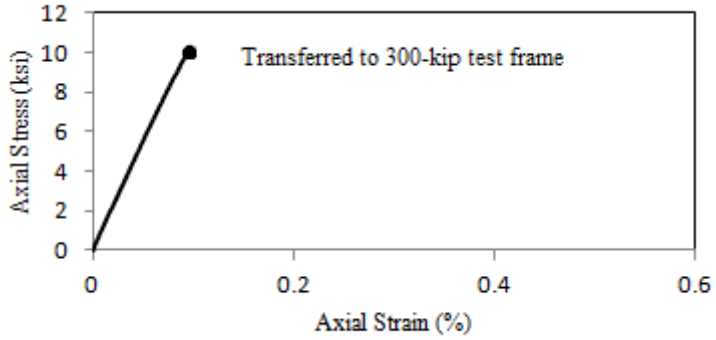

Sample Before Testing

Sample at Failure

C. Strength and Stiffness Parameters

Unconfined Compressive Strength	Young's Modulus	Axial Strain at Failure	Axial Strain at 50% Strength	Failure Type	Failure Plane Angle to Horizontal
(ksi)	(ksi)	(%)	(%)		(Degrees)
q_u	E	ε_{af}	ε_{a50}		α
32.55	10900	N/D	N/D	STF	N/A

N/A – Not applicable N/D – Not determined See page 29

Test No. 49: UH Boring B4, Sample Depth = 71 ft

A. Physical Properties

Oven-Dried Unit Weight	Saturated-Surface-Dry Unit Weight	Apparent Unit Weight	CoreLok Unit Weight	Absorption	RQD	Percent Recovered
(lb/ft^3)	(lb/ft^3)	(lb/ft^3)	(lb/ft^3)	(%)	(%)	
γ_{OD}	γ_{SSD}	γ_{APP}	γ_{CL}			
179.56	183.22	190.74	181.18	2.04	97	100

B. Stress-Strain Response

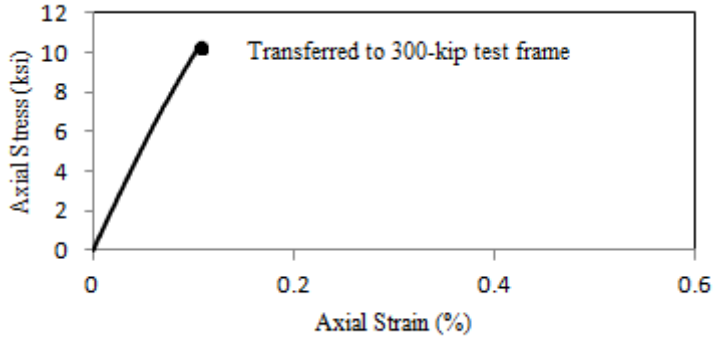

Sample Before Testing

Sample at Failure

C. Strength and Stiffness Parameters

Unconfined Compressive Strength	Young's Modulus	Axial Strain at Failure	Axial Strain at 50% Strength	Failure Type	Failure Plane Angle to Horizontal
(ksi)	(ksi)	(%)	(%)		(Degrees)
q_u	E	ε_{af}	ε_{a50}		α
25.29	10500	N/D	N/D	STF	N/A

N/A – Not applicable N/D – Not determined See page 29

Test No. 50: UH Boring B4, Sample Depth = 71 ft

A. Physical Properties

Oven-Dried Unit Weight	Saturated-Surface-Dry Unit Weight	Apparent Unit Weight	CoreLok Unit Weight	Absorption	RQD	Percent Recovered
(lb/ft^3)	(lb/ft^3)	(lb/ft^3)	(lb/ft^3)	(%)	(%)	
γ_{OD}	γ_{SSD}	γ_{APP}	γ_{CL}			
180.08	183.85	191.63	180.32	2.09	97	100

B. Stress-Strain Response

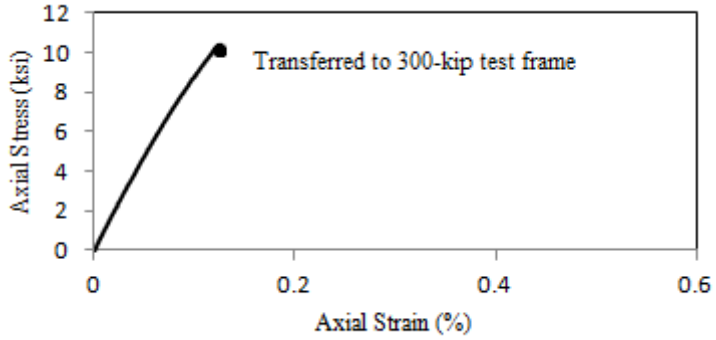

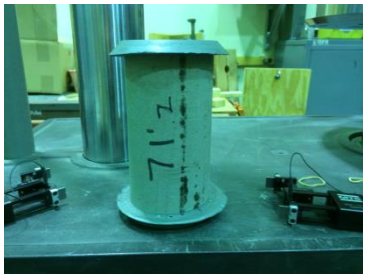

Sample Before Testing

Sample at Failure

C. Strength and Stiffness Parameters

Unconfined Compressive Strength	Young's Modulus	Axial Strain at Failure	Axial Strain at 50% Strength	Failure Type	Failure Plane Angle to Horizontal
(ksi)	(ksi)	(%)	(%)		(Degrees)
q_u	E	ε_{af}	ε_{a50}		α
21.42	9400	N/D	N/D	STF	N/A

N/A – Not applicable N/D – Not determined See page 29

Test No. 51: UH Boring B4, Sample Depth = 72 ft

A. Physical Properties

Oven-Dried Unit Weight	Saturated-Surface-Dry Unit Weight	Apparent Unit Weight	CoreLok Unit Weight	Absorption	RQD	Percent Recovered
(lb/ft^3)	(lb/ft^3)	(lb/ft^3)	(lb/ft^3)	(%)	(%)	
γ_{OD}	γ_{SSD}	γ_{APP}	γ_{CL}			
182.51	185.36	191.24	183.53	1.56	97	100

B. Stress-Strain Response

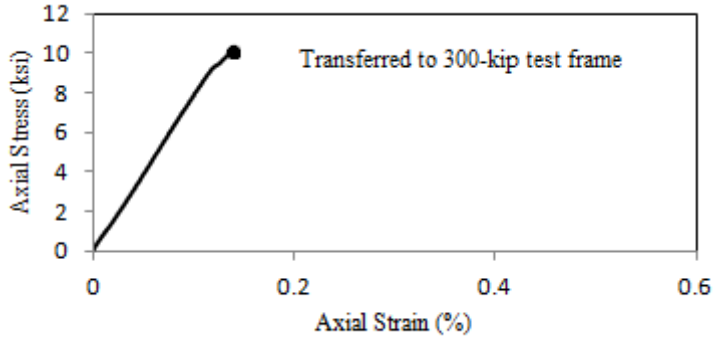

Sample Before Testing

Sample at Failure

C. Strength and Stiffness Parameters

Unconfined Compressive Strength	Young's Modulus	Axial Strain at Failure	Axial Strain at 50% Strength	Failure Type	Failure Plane Angle to Horizontal
(ksi)	(ksi)	(%)	(%)		(Degrees)
q_u	E	ε_{af}	ε_{a50}		α
15.09	7800	N/D	0.10	DPF	90

N/A – Not applicable N/D – Not determined See page 29

Test No. 52: UH Boring B4, Sample Depth = 73 ft

A. Physical Properties

Oven-Dried Unit Weight	Saturated-Surface-Dry Unit Weight	Apparent Unit Weight	CoreLok Unit Weight	Absorption	RQD	Percent Recovered
(lb/ft^3)	(lb/ft^3)	(lb/ft^3)	(lb/ft^3)	(%)	(%)	
γ_{OD}	γ_{SSD}	γ_{APP}	γ_{CL}			
180.77	184.16	191.16	180.84	1.88	100	100

B. Stress-Strain Response

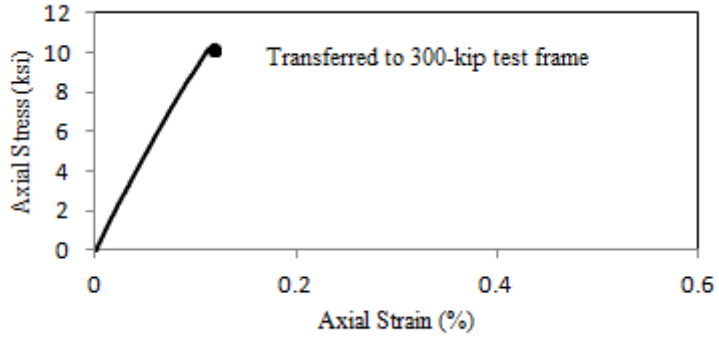

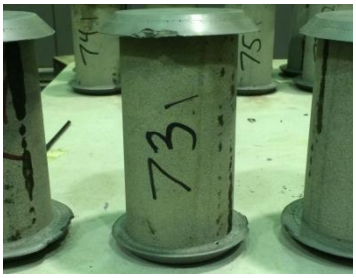

Sample Before Testing

Sample at Failure

C. Strength and Stiffness Parameters

Unconfined Compressive Strength	Young's Modulus	Axial Strain at Failure	Axial Strain at 50% Strength	Failure Type	Failure Plane Angle to Horizontal
(ksi)	(ksi)	(%)	(%)		(Degrees)
q_u	E	ε_{af}	ε_{a50}		α
22.02	9700	N/D	N/D	DPF	75

N/A – Not applicable N/D – Not determined See page 29

Test No. 53: UH Boring B4, Sample Depth = 73 ft

A. Physical Properties

Oven-Dried Unit Weight	Saturated-Surface-Dry Unit Weight	Apparent Unit Weight	CoreLok Unit Weight	Absorption	RQD	Percent Recovered
(lb/ft^3)	(lb/ft^3)	(lb/ft^3)	(lb/ft^3)	(%)	(%)	
γ_{OD}	γ_{SSD}	γ_{APP}	γ_{CL}			
180.34	183.65	190.45	182.10	1.84	100	100

B. Stress-Strain Response

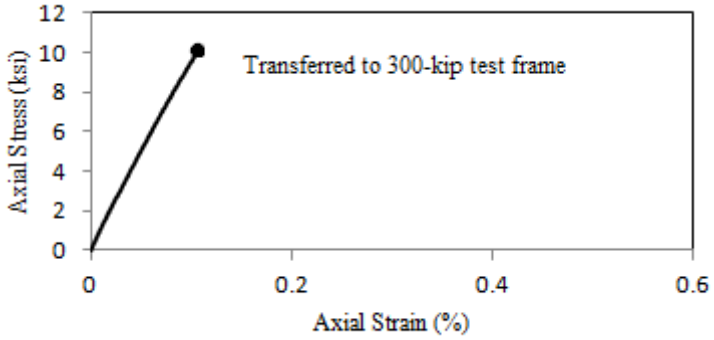

Sample Before Testing Sample at Failure

C. Strength and Stiffness Parameters

Unconfined Compressive Strength	Young's Modulus	Axial Strain at Failure	Axial Strain at 50% Strength	Failure Type	Failure Plane Angle to Horizontal
(ksi)	(ksi)	(%)	(%)		(Degrees)
q_u	E	ε_{af}	ε_{a50}		α
24.88	10100	N/D	N/D	STF	N/A

N/A – Not applicable N/D – Not determined See page 29

Test No. 54: UH Boring B4, Sample Depth = 74 ft

A. Physical Properties

Oven-Dried Unit Weight	Saturated-Surface-Dry Unit Weight	Apparent Unit Weight	CoreLok Unit Weight	Absorption	RQD	Percent Recovered
(lb/ft^3)	(lb/ft^3)	(lb/ft^3)	(lb/ft^3)	(%)	(%)	
γ_{OD}	γ_{SSD}	γ_{APP}	γ_{CL}			
181.89	184.90	191.09	182.46	1.65	100	100

B. Stress-Strain Response

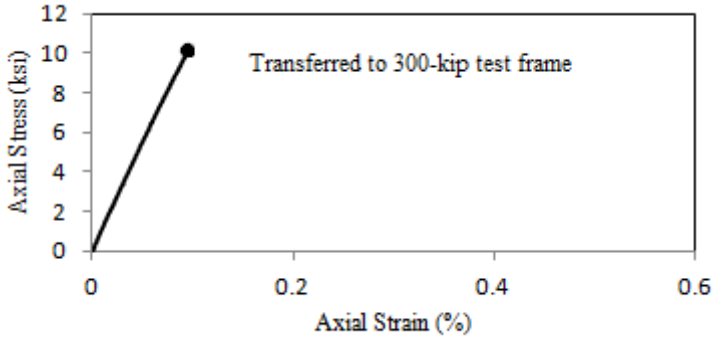

Sample Before Testing Sample at Failure

C. Strength and Stiffness Parameters

Unconfined Compressive Strength	Young's Modulus	Axial Strain at Failure	Axial Strain at 50% Strength	Failure Type	Failure Plane Angle to Horizontal
(ksi)	(ksi)	(%)	(%)		(Degrees)
q_u	E	ε_{af}	ε_{a50}		α
30.70	11000	N/D	N/D	DPF	60

N/A – Not applicable N/D – Not determined See page 29

Test No. 55: UH Boring B4, Sample Depth = 74 ft

A. Physical Properties

Oven-Dried Unit Weight	Saturated-Surface-Dry Unit Weight	Apparent Unit Weight	CoreLok Unit Weight	Absorption	RQD	Percent Recovered
(lb/ft^3)	(lb/ft^3)	(lb/ft^3)	(lb/ft^3)	(%)	(%)	
γ_{OD}	γ_{SSD}	γ_{APP}	γ_{CL}			
182.88	185.90	192.18	183.60	1.65	100	100

B. Stress-Strain Response

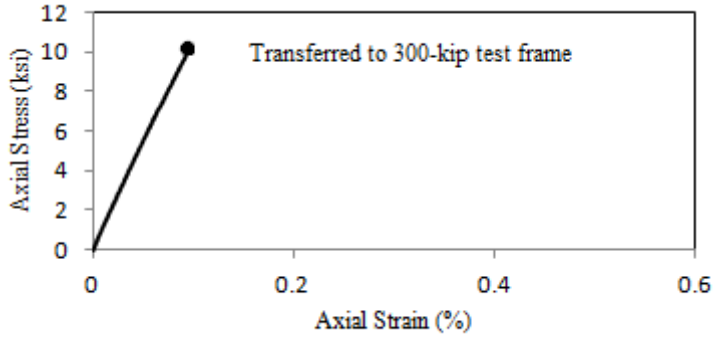

Sample Before Testing

Sample at Failure

C. Strength and Stiffness Parameters

Unconfined Compressive Strength	Young's Modulus	Axial Strain at Failure	Axial Strain at 50% Strength	Failure Type	Failure Plane Angle to Horizontal
(ksi)	(ksi)	(%)	(%)		(Degrees)
q_u	E	ε_{af}	ε_{a50}		α
30.59	10700	N/D	N/D	STF	N/A

N/A – Not applicable N/D – Not determined See page 29

Test No. 56: UH Boring B4, Sample Depth = 75 ft

A. Physical Properties

Oven-Dried Unit Weight	Saturated-Surface-Dry Unit Weight	Apparent Unit Weight	CoreLok Unit Weight	Absorption	RQD	Percent Recovered
(lb/ft^3)	(lb/ft^3)	(lb/ft^3)	(lb/ft^3)	(%)	(%)	
γ_{OD}	γ_{SSD}	γ_{APP}	γ_{CL}			
184.06	187.20	193.82	182.97	1.71	100	100

B. Stress-Strain Response

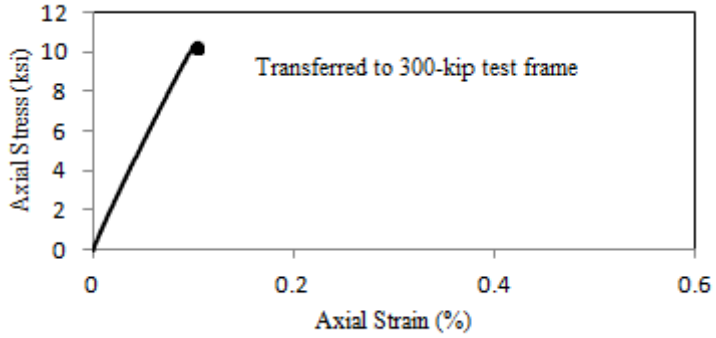

Sample Before Testing

Sample at Failure

C. Strength and Stiffness Parameters

Unconfined Compressive Strength	Young's Modulus	Axial Strain at Failure	Axial Strain at 50% Strength	Failure Type	Failure Plane Angle to Horizontal
(ksi)	(ksi)	(%)	(%)		(Degrees)
q_u	E	ε_{af}	ε_{a50}		α
28.85	10800	N/D	N/D	DPF	60

N/A – Not applicable N/D – Not determined See page 29

Test No. 57: UH Boring B4, Sample Depth = 75 ft

A. Physical Properties

Oven-Dried Unit Weight	Saturated-Surface-Dry Unit Weight	Apparent Unit Weight	CoreLok Unit Weight	Absorption	RQD	Percent Recovered
(lb/ft^3)	(lb/ft^3)	(lb/ft^3)	(lb/ft^3)	(%)	(%)	
γ_{OD}	γ_{SSD}	γ_{APP}	γ_{CL}			
183.12	186.20	192.62	183.28	1.68	100	100

B. Stress-Strain Response

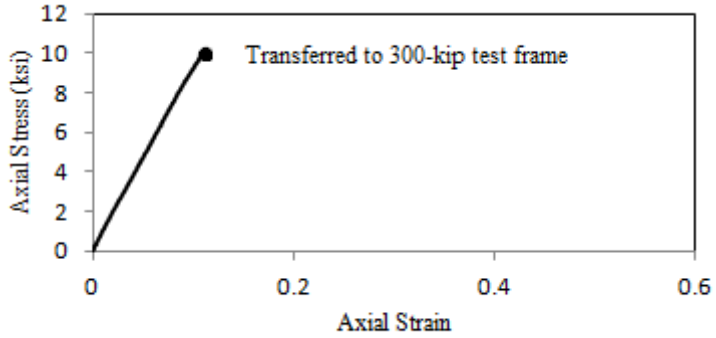

Sample Before Testing Sample at Failure

C. Strength and Stiffness Parameters

Unconfined Compressive Strength	Young's Modulus	Axial Strain at Failure	Axial Strain at 50% Strength	Failure Type	Failure Plane Angle to Horizontal
(ksi)	(ksi)	(%)	(%)		(Degrees)
q_u	E	ε_{af}	ε_{a50}		α
28.96	9500	N/D	N/D	DPF	60

N/A – Not applicable N/D – Not determined See page 29

Test No. 58: UH Boring B4, Sample Depth = 76 ft

A. Physical Properties

Oven-Dried Unit Weight	Saturated-Surface-Dry Unit Weight	Apparent Unit Weight	CoreLok Unit Weight	Absorption	RQD	Percent Recovered
(lb/ft^3)	(lb/ft^3)	(lb/ft^3)	(lb/ft^3)	(%)	(%)	
γ_{OD}	γ_{SSD}	γ_{APP}	γ_{CL}			
182.56	185.59	191.89	182.50	1.66	100	100

B. Stress-Strain Response

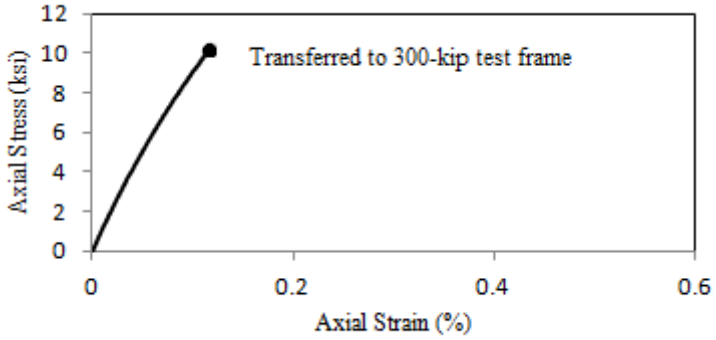

Sample Before Testing Sample at Failure

C. Strength and Stiffness Parameters

Unconfined Compressive Strength	Young's Modulus	Axial Strain at Failure	Axial Strain at 50% Strength	Failure Type	Failure Plane Angle to Horizontal
(ksi)	(ksi)	(%)	(%)		(Degrees)
q_u	E	ε_{af}	ε_{a50}		α
23.25	9900	N/D	N/D	MFF	N/A

N/A – Not applicable N/D – Not determined See page 29

Test No. 59: UH Boring B4, Sample Depth = 76 ft

A. Physical Properties

Oven-Dried Unit Weight	Saturated-Surface-Dry Unit Weight	Apparent Unit Weight	CoreLok Unit Weight	Absorption	RQD	Percent Recovered
(lb/ft^3)	(lb/ft^3)	(lb/ft^3)	(lb/ft^3)	(%)	(%)	
γ_{OD}	γ_{SSD}	γ_{APP}	γ_{CL}			
182.67	185.93	192.73	182.50	1.78	100	100

B. Stress-Strain Response

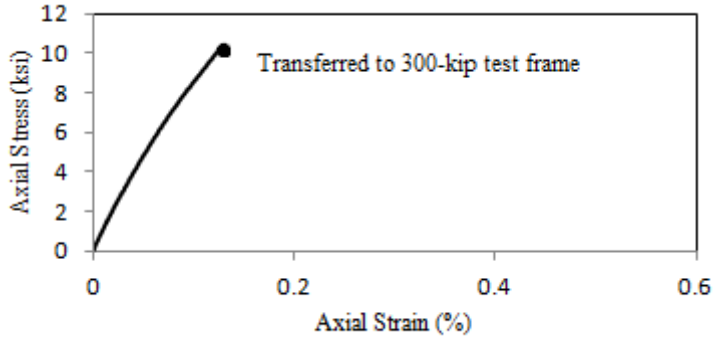

Sample Before Testing Sample at Failure

C. Strength and Stiffness Parameters

Unconfined Compressive Strength	Young's Modulus	Axial Strain at Failure	Axial Strain at 50% Strength	Failure Type	Failure Plane Angle to Horizontal
(ksi)	(ksi)	(%)	(%)		(Degrees)
q_u	E	ε_{af}	ε_{a50}		α
24.47	9400	N/D	N/D	STF	N/A

N/A – Not applicable N/D – Not determined See page 29

Test No. 60: UH Boring B4, Sample Depth = 77 ft

A. Physical Properties

Oven-Dried Unit Weight	Saturated-Surface-Dry Unit Weight	Apparent Unit Weight	CoreLok Unit Weight	Absorption	RQD	Percent Recovered
(lb/ft^3)	(lb/ft^3)	(lb/ft^3)	(lb/ft^3)	(%)	(%)	
γ_{OD}	γ_{SSD}	γ_{APP}	γ_{CL}			
180.06	183.64	191.01	181.09	1.99	100	100

B. Stress-Strain Response

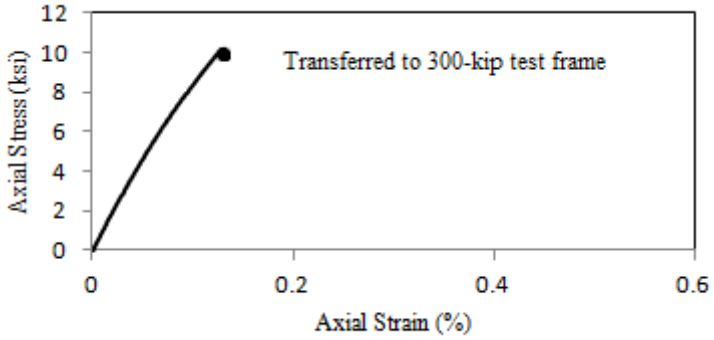

Sample Before Testing Sample at Failure

C. Strength and Stiffness Parameters

Unconfined Compressive Strength	Young's Modulus	Axial Strain at Failure	Axial Strain at 50% Strength	Failure Type	Failure Plane Angle to Horizontal
(ksi)	(ksi)	(%)	(%)		(Degrees)
q_u	E	ε_{af}	ε_{a50}		α
22.42	9000	N/D	N/D	STF	N/A

N/A – Not applicable N/D – Not determined See page 29

Test No. 61: UH Boring B4, Sample Depth = 78 ft

A. Physical Properties

Oven-Dried Unit Weight	Saturated-Surface-Dry Unit Weight	Apparent Unit Weight	CoreLok Unit Weight	Absorption	RQD	Percent Recovered
(lb/ft^3)	(lb/ft^3)	(lb/ft^3)	(lb/ft^3)	(%)	(%)	
γ_{OD}	γ_{SSD}	γ_{APP}	γ_{CL}			
179.84	182.93	189.21	181.63	1.72	73	100

B. Stress-Strain Response

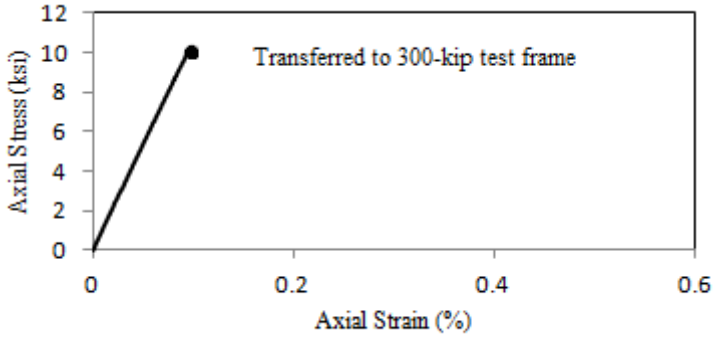

Sample Before Testing Sample at Failure

C. Strength and Stiffness Parameters

Unconfined Compressive Strength	Young's Modulus	Axial Strain at Failure	Axial Strain at 50% Strength	Failure Type	Failure Plane Angle to Horizontal
(ksi)	(ksi)	(%)	(%)		(Degrees)
q_u	E	ε_{af}	ε_{a50}		α
25.49	10700	N/D	N/D	DPF	75

N/A – Not applicable N/D – Not determined See page 29

Test No. 62: UH Boring B4, Sample Depth = 78 ft

A. Physical Properties

Oven-Dried Unit Weight	Saturated-Surface-Dry Unit Weight	Apparent Unit Weight	CoreLok Unit Weight	Absorption	RQD	Percent Recovered
(lb/ft^3)	(lb/ft^3)	(lb/ft^3)	(lb/ft^3)	(%)	(%)	
γ_{OD}	γ_{SSD}	γ_{APP}	γ_{CL}			
181.25	184.39	190.84	181.26	1.73	73	100

B. Stress-Strain Response

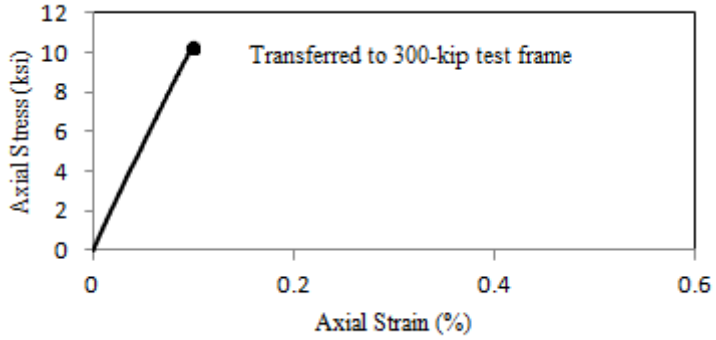

Sample Before Testing Sample at Failure

C. Strength and Stiffness Parameters

Unconfined Compressive Strength	Young's Modulus	Axial Strain at Failure	Axial Strain at 50% Strength	Failure Type	Failure Plane Angle to Horizontal
(ksi)	(ksi)	(%)	(%)		(Degrees)
q_u	E	ε_{af}	ε_{a50}		α
29.56	10800	N/D	N/D	STF	N/A

N/A – Not applicable N/D – Not determined See page 29

Test No. 63: UH Boring B4, Sample Depth = 79 ft

A. Physical Properties

Oven-Dried Unit Weight	Saturated-Surface-Dry Unit Weight	Apparent Unit Weight	CoreLok Unit Weight	Absorption	RQD	Percent Recovered
(lb/ft^3)	(lb/ft^3)	(lb/ft^3)	(lb/ft^3)	(%)	(%)	
γ_{OD}	γ_{SSD}	γ_{APP}	γ_{CL}			
179.28	183.18	191.23	180.73	2.18	73	100

B. Stress-Strain Response

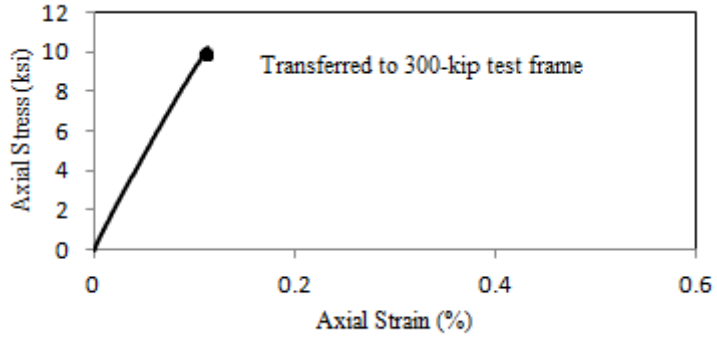

Sample Before Testing

Sample at Failure

C. Strength and Stiffness Parameters

Unconfined Compressive Strength	Young's Modulus	Axial Strain at Failure	Axial Strain at 50% Strength	Failure Type	Failure Plane Angle to Horizontal
(ksi)	(ksi)	(%)	(%)		(Degrees)
q_u	E	ε_{af}	ε_{a50}		α
24.47	9500	N/D	N/D	DPF	60

N/A – Not applicable N/D – Not determined See page 29

Test No. 64: UH Boring B4, Sample Depth = 79 ft

A. Physical Properties

Oven-Dried Unit Weight	Saturated-Surface-Dry Unit Weight	Apparent Unit Weight	CoreLok Unit Weight	Absorption	RQD	Percent Recovered
(lb/ft^3)	(lb/ft^3)	(lb/ft^3)	(lb/ft^3)	(%)	(%)	
γ_{OD}	γ_{SSD}	γ_{APP}	γ_{CL}			
180.72	184.38	191.99	181.56	2.03	73	100

B. Stress-Strain Response

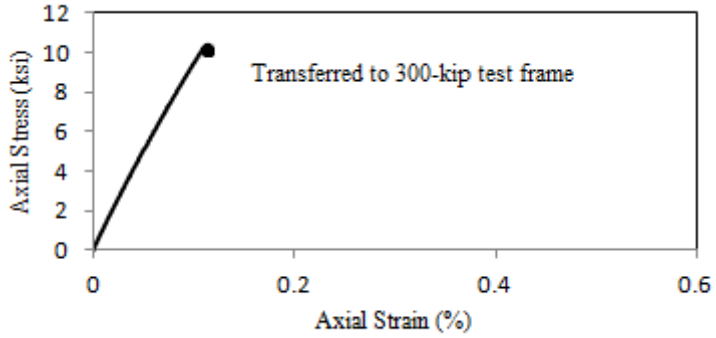

Sample Before Testing Sample at Failure

C. Strength and Stiffness Parameters

Unconfined Compressive Strength	Young's Modulus	Axial Strain at Failure	Axial Strain at 50% Strength	Failure Type	Failure Plane Angle to Horizontal
(ksi)	(ksi)	(%)	(%)		(Degrees)
q_u	E	ε_{af}	ε_{a50}		α
23.04	10000	N/D	N/D	STF	N/A

N/A – Not applicable N/D – Not determined See page 29

Test No. 65: UH Boring B4, Sample Depth = 80 ft

A. Physical Properties

Oven-Dried Unit Weight	Saturated-Surface-Dry Unit Weight	Apparent Unit Weight	CoreLok Unit Weight	Absorption	RQD	Percent Recovered
(lb/ft^3)	(lb/ft^3)	(lb/ft^3)	(lb/ft^3)	(%)	(%)	
γ_{OD}	γ_{SSD}	γ_{APP}	γ_{CL}			
184.40	187.31	193.42	184.63	1.58	73	100

B. Stress-Strain Response

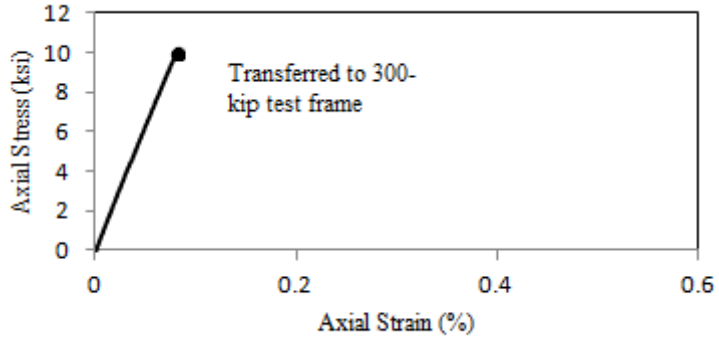

Sample Before Testing

Sample at Failure

C. Strength and Stiffness Parameters

Unconfined Compressive Strength	Young's Modulus	Axial Strain at Failure	Axial Strain at 50% Strength	Failure Type	Failure Plane Angle to Horizontal
(ksi)	(ksi)	(%)	(%)		(Degrees)
q_u	E	ε_{af}	ε_{a50}		α
34.69	12600	N/D	N/D	STF	N/A

N/A – Not applicable N/D – Not determined See page 29

Test No. 66: UH Boring B4, Sample Depth = 81 ft

A. Physical Properties

Oven-Dried Unit Weight	Saturated-Surface-Dry Unit Weight	Apparent Unit Weight	CoreLok Unit Weight	Absorption	RQD	Percent Recovered
(lb/ft^3)	(lb/ft^3)	(lb/ft^3)	(lb/ft^3)	(%)	(%)	
γ_{OD}	γ_{SSD}	γ_{APP}	γ_{CL}			
185.57	188.46	194.57	184.44	1.56	73	100

B. Stress-Strain Response

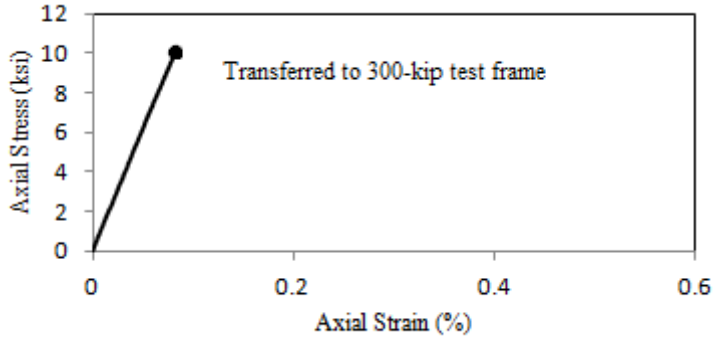

Sample Before Testing Sample at Failure

C. Strength and Stiffness Parameters

Unconfined Compressive Strength	Young's Modulus	Axial Strain at Failure	Axial Strain at 50% Strength	Failure Type	Failure Plane Angle to Horizontal
(ksi)	(ksi)	(%)	(%)		(Degrees)
q_u	E	ε_{af}	ε_{a50}		α
33.86	12000	N/D	N/D	STF	N/A

N/A – Not applicable N/D – Not determined See page 29